8th Croatian-Hungarian and 19th Hungarian geomathematical congress

Geomathematics - present and future of geological modelling

Editors:

Marko Cvetković, Kristina Novak Zelenika, Janina Horváth and István Gábor Hatvani

ISBN 978-953-59036-1-1

Trakošćan, 26-28 May, 2016

Impressum

Publisher: Croatian Geological Society, 2016

For publisher: Lilit Cota, president of the Croatian Geological Society

Editors: Marko Cvetković, Kristina Novak Zelenika, Janina Horváth and István Gábor Hatvani

Circulation: 50 copies

Copy and distribution: Denona d.o.o., Zagreb

ISBN 978-953-59036-1-1

Note

The content of proceedings has not been passed English proof reading by native speaker, and that is why solely the authors are responsible for the quality of language usage.

Organizers

Croatian Geological Society (Hrvatsko geološko društvo)
http://www.geologija.hr
Geomathematical Section (Geomatematički odsjek)
http://www.geologija.hr/geomat.php

Hungarian Geological Society (Magyarhoni Földtani Társulat)
http://www.foldtan.hu/
Geomathematical Section (Geomatematikai Szakosztály)
https://www.smartportal.hu/

Faculty of Mining, Geology and Petroleum Engineering (Rudarsko-geološko-naftni fakultet)
http://www.rgn.hr

RGNF

SPONSORS

MOL

Committees

Organizing Committee

Ph.D. Marko Cvetković, Assistant Professor (chairman, University of Zagreb, HR)

PhD. Janina Horváth (Univ. Szeged, HU)

PhD. Kristina Novak Zelenika (INA, HR)

Scientific Committee

Ph.D. Janos Geiger (chairman, Univ. Szeged, HU)

Ph.D. Marko Cvetković, Assistant Professor (chairman, University of Zagreb, HR)

Ph.D. Janina Horváth (Univ. Szeged, HU)

Ph.D. Kristina Novak Zelenika (INA, HR)

Ph.D. István Gábor Hatvani (MTA Research Centre for Astronomy and Earth Sciences, HU)

CONTENTS

FOREWORD

It has been almost a year passed by since the last HR-HU geomathematical congress, and almost two years since such congress was held in Croatia. This year Hungarian and Croatian geomathematician will gather in Trakošćan, a small place in Hrvatsko zagorje region.

Geostatistics is very important topic in modern time. It is included in almost every segment of geoscience. Today, it is just about impossible to create any map or predict any distribution without using geostatistical methods. This is why it is very important to discuss such methods, results and some recent innovations in geostatistical investigations.

Since the excellent cooperation between Hungarian and Croatian colleagues continues, many good and quality papers appeared in this year's congress. Topics of the congress are widely spread and they range from the theory to the applications of different geostatistical methods, especially in reservoir modelling. This volume contains full overview of 17 presentations. Authors of the papers came from different institutions. Some of them are employees of major oil industries such as INA-Oil industry from Croatia and GEOCHEM from Hungary while others are representatives of the Universities (University of Zagreb, University of Szeged and University of Pannonia) or other Esteemed institutes . This year we are very pleased that many students showed interest in geostatistics and we are especially proud to their contribution to the congress.

We truly hope that the significance of the geostatistics in modern science will be recognized through the work presented in this book and that events like this geomathematical congress will continue to grow every year.

Hope to see you next year!

The Editors

3D modelling of a Lower-Pannonian hydrocarbon reservoir sandstone group

Mihaly Apro
University of Szeged, Department of Geology and Palaeontology , Szeged Egyetem utca 2
apromisi@gmail.com

Abstract

Research aims to define the depositional systems and to do 3D facies analyses of a Lower-Pannonian sandstone group which consist of 3 separated sand bodies to locate the permable and impermeable zones between the reservoirs. The study area is located at Central Easter Hungary. The available datasets contained measured and interpreted well data, such as gamma ray (GR/TG), corrected spontaneous potential (SPC), shale volume (VSH), porosity (POR) and some cores as well.

The workflow started with the borehole correlation by SPC, GR/TG and POR logs and location of the tops and bottoms of the sandstone bodies. Mapping of the thickness was made in Surfer 10 software so the main transport directions could be defined. The stratigraphic models were created at the next step in RockWorks 15. After the core analysis the lithology types could be spread out to all of the wells were identified with cluster analysis. Porosity and shale volume were used as input data. Lithology, porosity and sand content models of the reservoirs were created afterwards. In the end Sequential Gaussian Simulation for porosity and sand content modelling was applied for the reservoir zones and from these ones E-type expected value models was made in SGeMS to validate the deterministic models.

The geometry of sand bodies and the distribution of petrophysical properties suggest turbidite facies for the bottom one which had NNW transport direction; also turbidite facies for middle ones which came from N; and channel facies for top reservoir which was progradating on the middle lobe. From this facies architecture and core analysis, sand/mud rich submarine fan was defined. The sand bodies represent distal part of this system but the progradation can be followed. Finally thickness of separator marl were mapped to recognise the possible fluid flow connection zones between the reservoirs.

Key words: *basin modelling, Lower-Pannonian, facies, depositional system, simulation*

1. INTRODUCTION

The aim of this work was to define the depositional system of a Lower-Pannonian (Upper Miocene) sandstone group in Central Eastern Hungary which was supported by classic and stochastic geostatistical analyses for the creation of the 3D facies architecture. The input dataset consist of measured (such as gamma ray (GR/TG), corrected spontaneous potential (SPC) etc.) and interpreted (porosity (POR), shale volume (VSH), etc.) well log data and cores for the micro scale analysis**.**

2. METHODS AND WORKFLOW

First of all, thickness maps were created by *simple kriging* which was based on the borehole correlation when the top and the bottom surfaces of the sandstone group were located. Three units were recognised from the electrofaceis analysis: (1) cylinder shape, (2) funnel shape, (3) bell shape which were distinguished from well logs. The stratigraphic models were created by *inverse distance* algorithm supplemented with *densify*, decluster*, smoothing* and *high fidelity* options from previous results and the base grids were applied for the warping option for the further steps. Four lithology types were defined after the core analysis. There were shale/marl, siltstone, silty sand and clean sand. With cluster analysis (input: POR, VSH) these lithologies were able to be spread out to all of the wells and then the lithology models by *lithoblending* algorithm supplemented by *randomized blending* option.

The most important process for the facies identification was the modelling of petrophisycal properties (porosity and sand content). In classic geostatistical way they were made by *inverse distance (anisotropy) algorithm* with *smoothing, warping, high fidelity and decluster** as well.

In the stochastic approach, variogram based Sequential Gaussian Simulation and in one case Sequential Gaussian Co-simulation were applied for simulating the petrophysical properties to validate the previous deterministic models.

2.1. Applied algorithms

The exactness of outcomes of modelling depends on the chosen algorithms. If the conceptual model was specified the selection of algorithm was easier. In this case, turbidite facies was stated from previous studies so the following ones were chosen during the modelling.

2.1.1. Inverse distance (anisotropic)

A common solid modelling method using a weighted average approach to compute node values was used. This algorithm assigns a voxel node value based on the weighted average of neighbouring data points, either all points or those directionally located, using fixed or variable weighting exponents (RockWorks, 2013).

It has 3 versions (isotropic, anisotropic, and weighted) but only the anisotropic subtype was applied which instead of using control points for inverse distance modelling, the program would look for the closest point in each 90-degree sector around node (RockWorks, 2013).

2.1.2. Lithoblending

Algorithm assigns the solid model voxel nodes by looking outward horizontally from each borehole in search circles of ever-increasing diameter. It first assigns the voxels immediately surrounding each borehole the closest lithology value. It then moves out by a voxel, and assigns the next "circle" of voxels to the closest lithology value. It continues in this manner until the program encounters a voxel that is already assigned (presumably from another borehole), in which case it skips the node assignment step. Once all nodes are assigned, the searching and assigning is terminated (RockWorks, 2013).

2.1.3. Sequential Gaussian Simulation (SGSM)

Pre-processing: Normal score transformation (it made the data to Gaussian variables) of the data was required for applying SGSM. Based on the normalized data the variogram had to be defined for the process.

For instance, if Z(u) is a multivariate Gaussian random function with 0 mean, unit variance, and a given covariance model. Realizations of Z, conditioned to data (n) can be generated by following process:

1. Define random path visiting each node of the grid once
2. At each node u, the local conditional cumulative distribution function is Gaussian, its mean is estimated by simple kriging and its variance is equal to the simple kriging variance. The conditioning data consist of both neighbouring original data (n) an previously simulated values
3. Draw a value from that Gaussian conditional cumulative distribution function and add the simulated value to the data set
4. Proceed to the next node in the path and repeat the two previous steps until all nodes have been visited

Post-processing: Back-transformation of the realizations based on normalized data is required and E-type expected value model have to be apply to average the equiprobable realizations (Remy, 2004; Pyrcz & Deutsch, 2014).

2.1.4. Sequential Gaussian Co-simulation (COSGSIM)

Simulation of one variable using data of multiple types or, more commonly, realizations from a previous variable for conditioning (Pyrcz & Deutsch, 2014).

If $Z_1(u)$ and $Z_2(u)$ are two correlated random variables. $Z_1(u)$ is called the primary variable, and $Z_2(u)$ the secondary variable. The implementation of the COSGSIM simulation of the primary variable Z1 conditioned to both primary and secondary data is described in the following process:

1. If necessary, transform Z_1 and Z_2 into Gaussian variables Y_1 and Y_2. Make sure that the transformed variables Y_1 and Y_2 are at least bigaussian.

2. Simulate variable Y1: (same as 2.1.3. 1-4.)
3. "Back-transform" the simulated values $y_{1;1};\ldots;\ y_{1;N}$ into $z_{1;1};\ldots;\ z_{1;N}$:

$$z_{1,i} = F_1^{-1}(G_1(y_{1,i})) \quad i = 1,\ldots\ldots,N$$

where F_1 is the target distribution function of Z_1 and G_1 is the standard normal cumulative distribution function.

The algorithm COSGSIM allows to choose between solving a full cokriging system, or using either Markov Model 1 (MM1) or Markov Model 2 (MM2) (Remy, 2004). MM1 was chosen so in this type correlation coefficient between the two correlated random variables have to be granted.

3. RESULTS

On the **Figure 1** the thickness map of the top reservoir created by simply kriging is presented with the location of the boreholes. The main transport direction could be recognised from the thicker zones. A bifurcated linear object is located on the studied area, come from North.

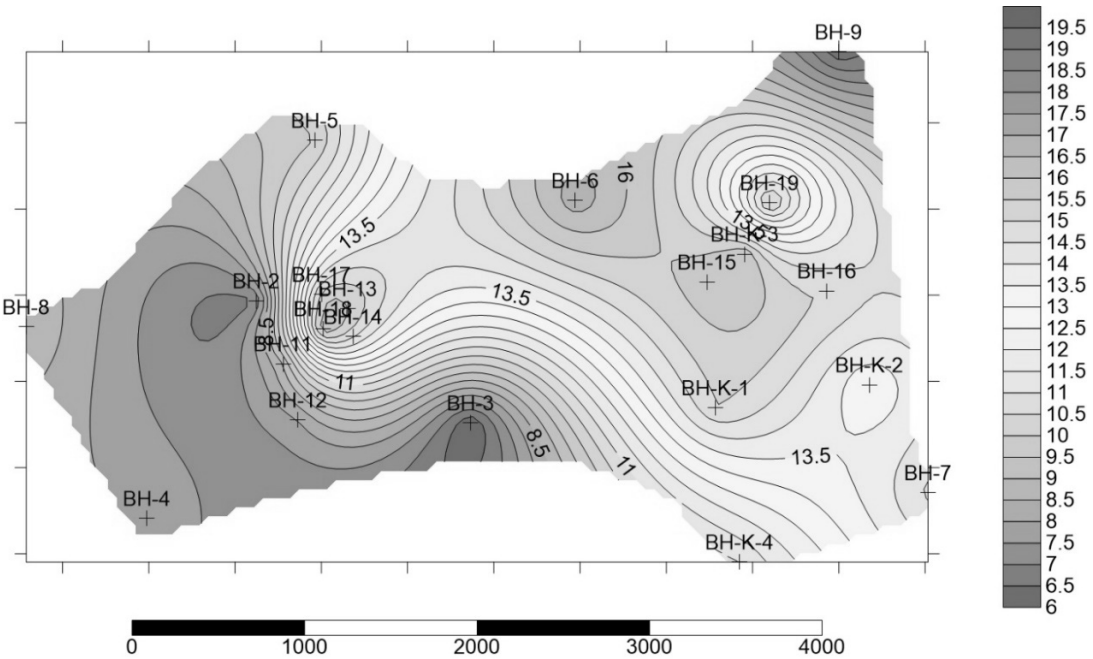

Figure 1: *The thickness map of the top reservoir of the sandstone group*

This consideration is supported by deterministic stratigraphic (**Figure 2**) and lithology models (**Figure 3a**).

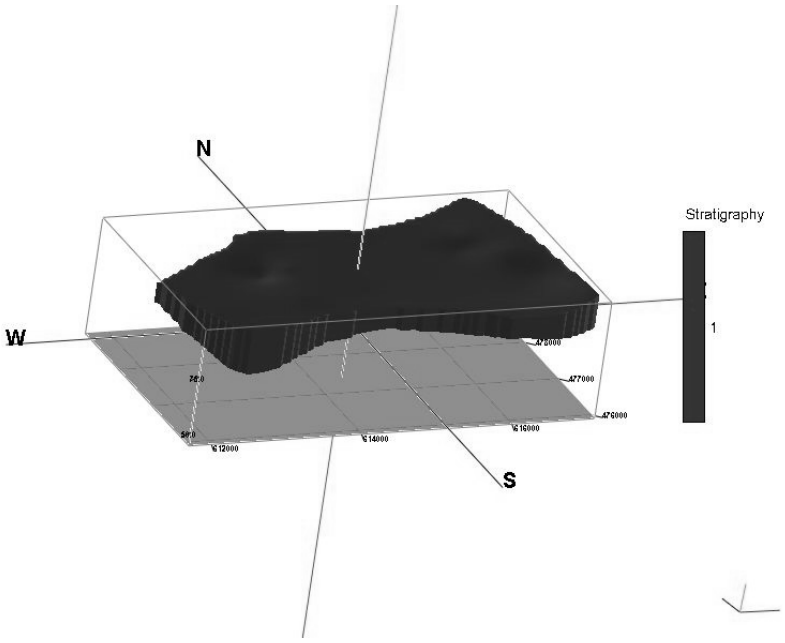

Figure 2: *Stratigraphic model of the top reservoir of the sandstone group*

At the west side of the area fining upward (FU) electro sequence is occurred with discrete upper limit but at the east side full FU sequence is followed.

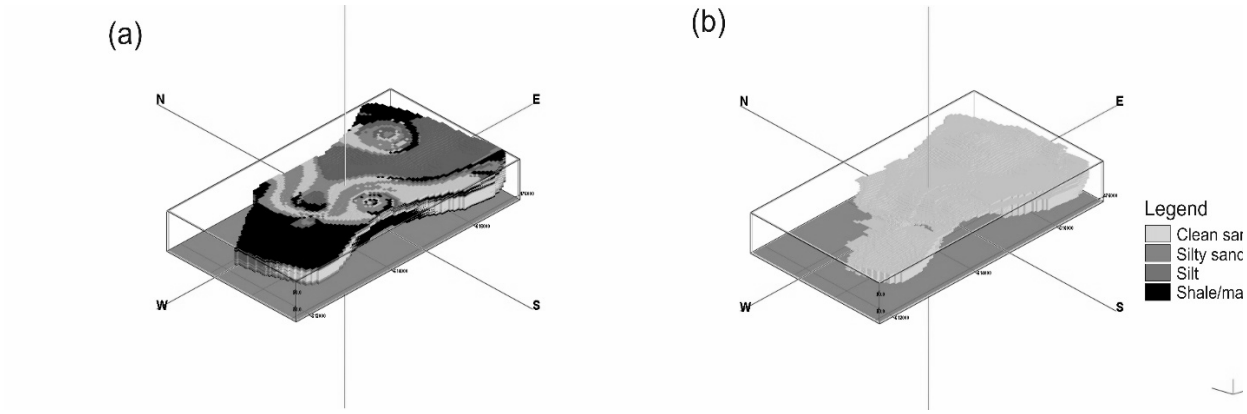

Figure 3: *Lithology model of the top reservoir of the sandstone group*

The higher values of the porosity and sand content models made by inverse distance algorithm also represent the mentioned linear object (**Figure 4a, b**).

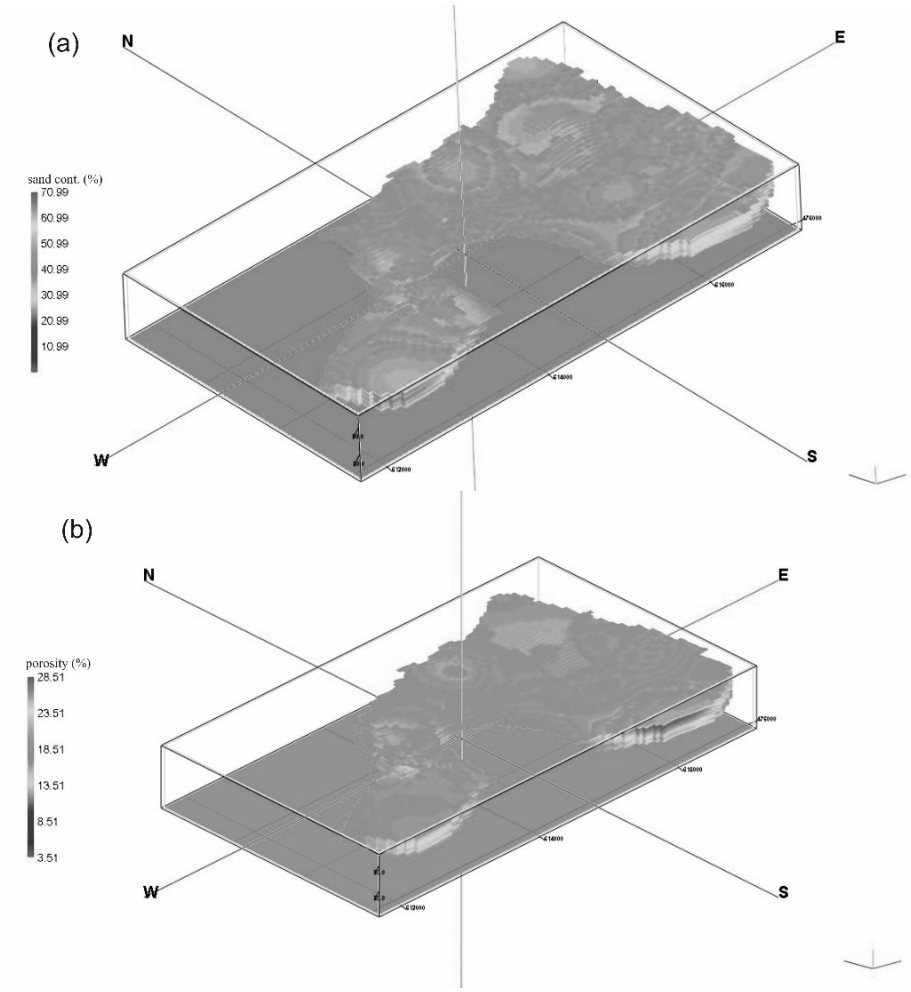

Figure 4: *Petrophysical models of the top reservoir (a: sand content; b: porosity)*

From BH-3 lenticular bioturbated graded bedding, from BH-K-2 massive sandstone with scour marks and from BH-K-3 lenticular, convolute bedding were identified after the core analysis related to the presented reservoir.

In the end, porosity (**Figure 5a**) and sand content (**Figure 5b**) simulations were created by stochastic algorithm to validate the deterministic models. This reservoir is represented a bifurcated channel system of proximal part of a submarine fan.

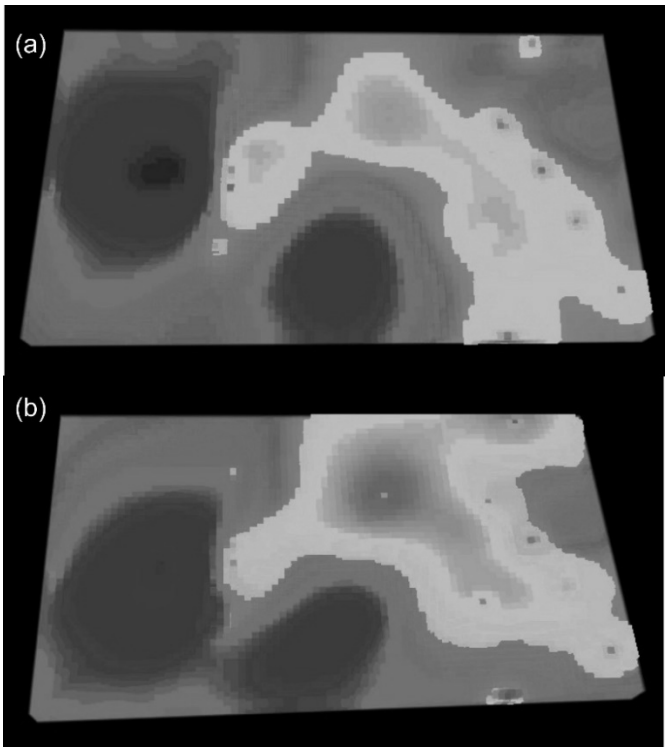

Figure 5: *Higher values of (a) stochastic porosity expected value model (20–28%) and (b) stochastic sand content expected value model (60–100%)*

4. CONCLUSION

Based on the Reading & Richards (1994) the Lower-Pannonian sandstone group was classified into mud/sand-rich submarine fan system because of its facies architecture (geometry), its lithology and petrophysical characterization and its sand content ratio (50-70%).

5. REFERENCES

READING G. H. & RICHARDS M. (1994): Turbidite Systems in Deep-Water Basin Margins Classified by Grain Size and Feeder System–AAPG Bulletin, V.78, No. 5 (May 1994) 792–822 p.

REMY N. (2004): Geostatistical Earth Modelling Software:User's Manual

PYRCZ J. M. & DEUTSCH C. V. (2014): Geostatistical reservoir modelling. Oxford University Press p.400

ROCKWORKS 15 (2013): User Manual. RockWare Earth Science & GIS Software

Geometrical parametrization of structural elements of deep-water clastic depositional systems: a case study from Pannonian-basin

Szabolcs Borka[1], Janina Horváth[1], János Geiger[1]

[1]University of Szeged, Department of Geology and Paleontology, Egyetem u. 2-6, 6722 Szeged, Hungary, borka.szabolcs@gmail.com

There are several simulation methods - like multiple-point or object-based simulation - which can handle and honour the geometries of depositional structural elements. The parametrized geometry adds an extra but quasi-subjective information to our 3D geological model. Two assumptions must be completed: (1) well-definable geometries corresponding to the architectural elements (2) it is assumed that exactly one sedimentary or lithological facies belongs to each structural element and the flow properties are determined by these structural elements.

The case study takes place in the southern part of the Great Hungarian Plain (Algyő field, Hungary). The formation is a sand/mud-rich submarine fan system.

Five clusters were revealed by Box-Cox transformation, principal component analysis and neural network technique. In addition, well-logs, core samples, 2D maps with discrete variables, sand and porosity contour maps were used to determine the architectural elements and their geometries. The measurement of the latter is well-documented in the literature. For example, in the case of a sinusoid object (channel) one should measure the amplitude, the wavelength, the width, the thickness etc. of the object. Finally, two sinusoid channels were recognizable and measureable related to cluster 4 and 5.

These parametrized geoobjects with their own facies can be used for constructing training images of multiple-point simulation or for direct description of the objects regarding the object-based method.

Key words: *geometry, architectural element, deep-water depositional system, geoobject, geobody*

1. INTRODUCTION

There are several clastic depositional environments which possess sub-environments with well-definable geometries. This parametrical information can be easily revealed in modern environments by orthophotos of fluvial or upper and lower deltaic plain systems, or subaqueous seismic profiles and 3D maps of deep-water submarine fan systems.

The situation is different in case of ancient systems beneath the surface. There are only pointwise data e.g. well-logs, core samples, core plugs as hard data, and seismic profiles and/or (attribute) maps as soft data. Furthermore, usually a theoretical geologic model with architectural elements is available. These theoretical models are derived from observations of modern environments, analogs and experiences of decades of oil and gas exploration.

Integration of the available information (hard data, soft data, theoretical model) gives the conceptual geological model (Pyrcz and Deutsch, 2014). The geostatistical method (i.e. deterministic estimation or stochastic simulation) of the integration determines the ability to honour these inputs.

Probably the most conventional method is the variogram and cell-based algorithm. It can handle continuous variables (sequential Gaussian simulation) and categorical variables (sequential indicator simulation) as well. There isn't any kind of geometrical data in the inputs because the algorithm can't manage it.

Contrary to this, multiple-point (cell-based), object-based and process mimicking (non cell-based) algorithms are able to handle the additional geological information e.g. geometry (**Figure 1**; Pyrcz and Deutsch, 2014). Including these additional parameters as inputs are based on the consideration that the flow properties in a clastic reservoir are mostly determined by the geometries and the lithofacies of ancient sub-environments. The latter means that these methods can use only categorical variables, and exactly one lithofacies belongs to an ancient sub-environment.

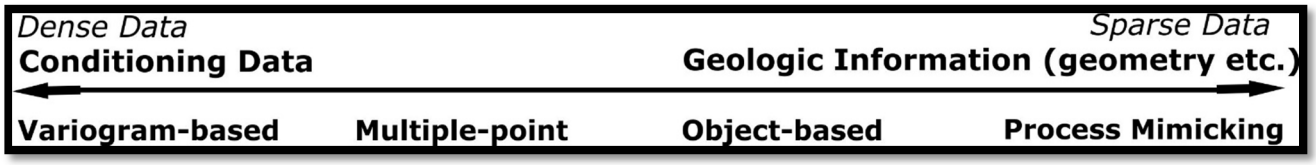

Figure 1: *Continuum of algorithms indicating the ability of reproduction of Conditioning Data (wells and trends) and/or Geologic information. Variogram-based methods usually fail to handle sparse data and vice versa (modified after Pyrcz and Deutsch, 2014)*

The parameter of geometry can be regarded as a quasi-subjective geological data. Although the method of measurement has widespread literature, the final result moderately depends on the practitioner. Moreover the defined geometry possesses a distribution (mean, minimum and maximum values etc.), but it isn't as verifiable as the parameters and results of variogram-based algorithms.

2. GEOLOGICAL SETTING OF THE AREA OF INTEREST

The case study is located in Algyő sub-basin of the Pannonian-basin in the Great Hungarian Plain.

The following main depositional environments characterized Lake Pannon: (1) fluvio-lacustrine and deltaic plain (2) delta front and delta slope (3) prodelta (4) deep-water systems (5) basin plain (Bérczi, 1988).

The formation of the case study belongs to Szolnoki Formation as a submarine fan system (Gajdos et al., 1983). In the Great Hungarian Plain its thickest sequences (approx. <1000 m) take place in deep sub-basins (Jászság Basin, Derecske Trough, Makó Trough, Békés Basin) (Juhász, 1994).

3. METHODS

To measure a geometry of an architectural element, a visually adequate map showing the geometries in question is needed. If there is enough dense data (wells, 3D seismic lattice or 2D seismic profile), a deterministic or stochastic contour map with continuous variables can be regarded as a good basis.

Another approach is clustering the continuous variables into discrete variables and using them as hard data. Generally the result of this method doesn't give

lithofacies related to architectural elements, but 'pure' lithology components. Getting around this, well logs (which reflect the fining - and coarsening vertical trends e.g. GR, SP, RES, shale-content, sand-content) and sedimentologically described core samples were also used to identify the sedimentary facies (i.e. lithofacies).

Currently several parametric shapes (i.e. geobodies, geoobjects) are available. These geobodies are generalized shapes mimicking the true architectural elements.

In case of deepwater submarine complexes, the following geobodies are corresponded to the sub-environments:

- sinusoid objects: braided channels with (very) low-sinousity on the upper part of channelized lobes (coarse-grained systems, CGS) (Normark, 1970); leveed, meandering channels with high-sinousity on the mid-/lower-fan (fine-grained systems, FGS)(Reading and Richards, 1994)
- lobe objects: channelized lobes on the mid-fan (CGS) (Normark, 1970; Mutti, 1985); unchannelized lobes or sand sheets at terminus of meandering channels on the lower-fan (FGS) (Reading and Richards, 1994)
- bar objects: mouth-bar at terminus of main depositional valley on the lower part of upper-fan (FGS) (Normark, 1970)
- ellipsoid objects: crevasse splays attached to channels (Pyrcz et al., 2008; Maharaja, 2008)

Figure 2 shows the measureable parameters of these geobodies.

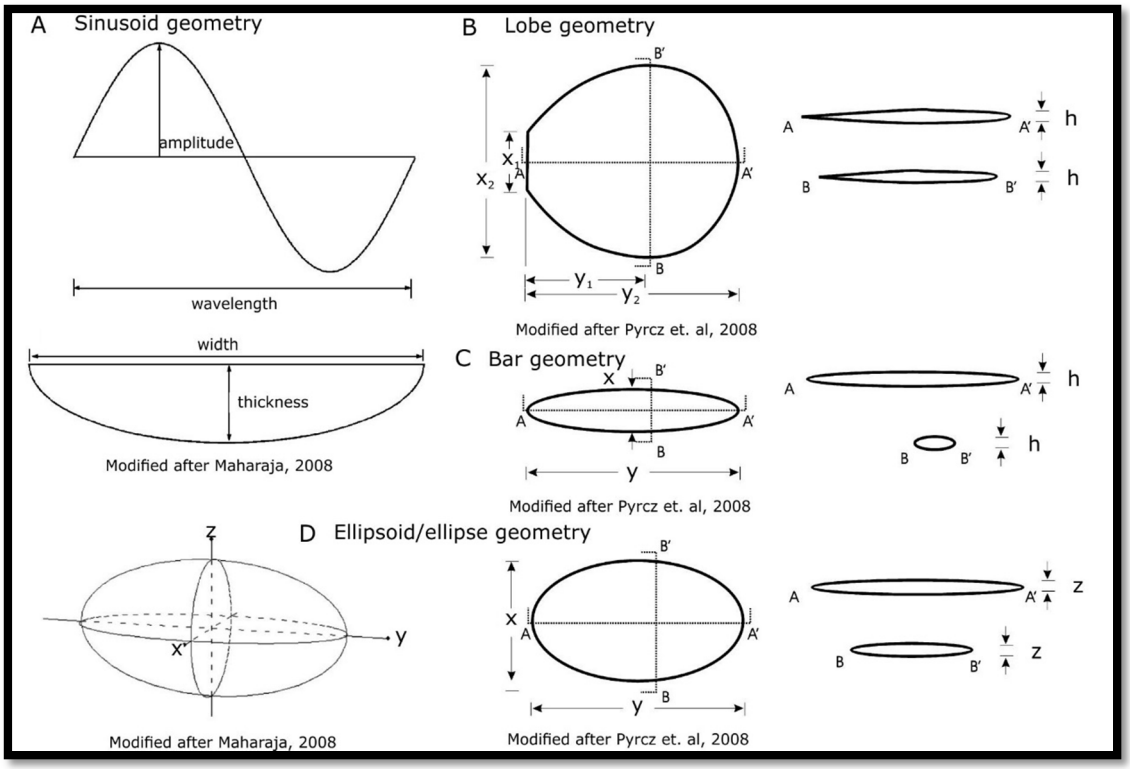

Figure 2 *Parameters of geoobjects (modified after Pyrcz et. al, 2008; Maharaja, 2008)*

(A) sinusoid geometry should be characterized by: amplitude, wavelength, width, thickness and sinuosity (ratio of true streamline length (on the interval of wavelength) and wavelength) of the geobody

(B) lobe geometry: mouth (x_1), width (x_2), length to largest width (y_1), total length (y_2), thickness (h) of the geobody

(C) bar geometry: width (x), length (y) and thickness of the geobody

(D) ellipsoid/ellipse geometry: semi-principal-axes (x, y, z) of a tri-axial ellipsoid.

4. RESULTS

In this study, results of an artifical neural-network clustering technique (data pre-processing: Box-Cox transformation and Principal Component Analysis, data: porosity, permeability, sand- and shale-content from well logs) were used to create 2D maps (slices) with discrete (five lithology clusters) variables. Two out of the five clusters were chosen with the highest porosity, sand-content and permeability (cluster 4-5, **Table 1**). Purpose of visualization (Golden Software's Voxler 3) was to examine what geometries are shown by cluster 4 and 5.

***Table 1**: General statistical character of cluster 4 and 5*

	FIAP		PERM		VSHA		VSND	
Clusters	4	5	4	5	4	5	4	5
N	503	328	503	328	503	328	503	328
Mean	18.39	20.25	32.24	87.16	15.30	8.79	65.93	71.23
Median	18.35	20.23	31.08	79.02	15.45	9.04	65.81	70.31
Std. deviation	0.77	1.00	15.16	41.79	2.76	2.58	3.07	3.84

A quasi-3D model (flatted to the impermeable argillaceous marlstone seal) was constructed by Voxler 3's FaceRender module. In this case cluster 4 and 5 show two sinusoid geobodies at 13 meters under the seal (**Figure 3**). Direct measurement isn't available in Voxler 3, so from the same depth, sand and porosity contour maps using kriging estimation were used to parametrize.

The two results show good similarity (**Figure 3**), although one is based on discrete, and the other one is based on continuous variables. Therefore measurement on the contour maps in Golden Software's Surfer 12 was valid. Measured parameters are shown in Figure 4.

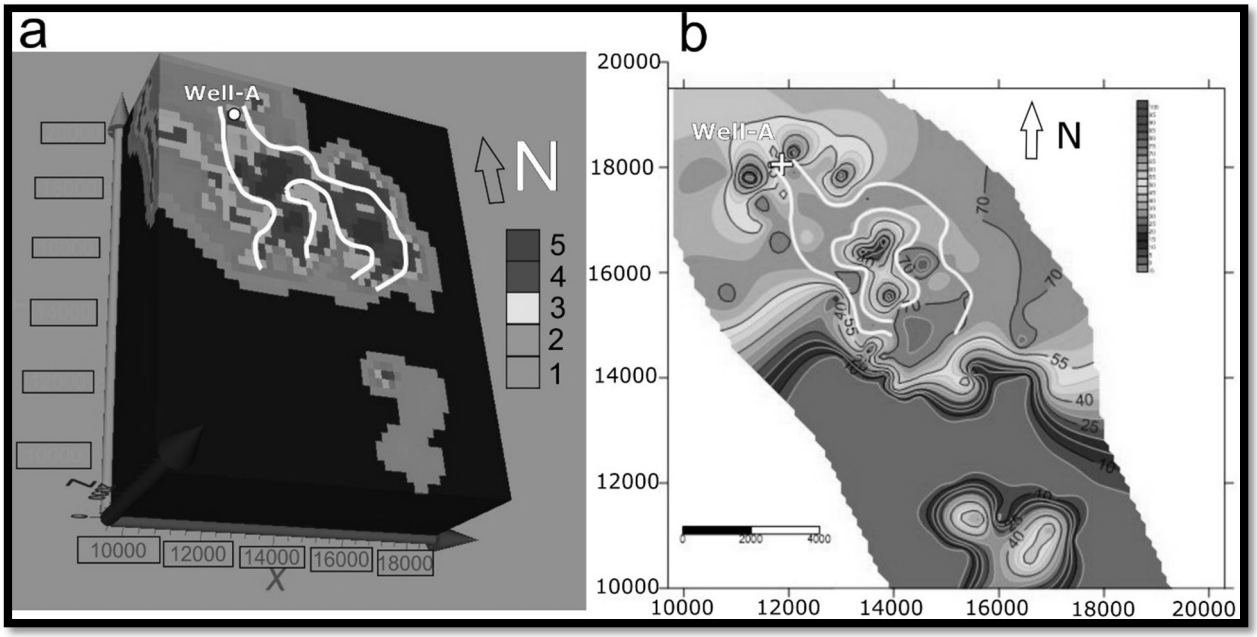

***Figure 3**: Picture 'a' shows two sinusoid geoobjects related to cluster 4 and 5; picture 'b' shows the same shapes in a sand-content contour map. The two slices are from the same depth, at 13 meters beneath the seal*

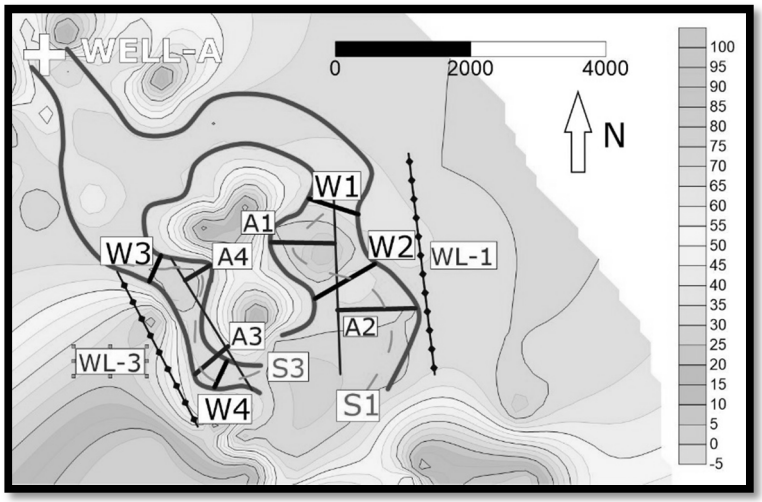

***Figure 4**: Notations with number 1 and 2 belong to the right sinusoid geoobject, with 3 and 4 belong to the left sinusoid geoobject; A – amplitude, W – width, WL – wavelength, S – length of streamline*

The geometrical values are summarized in **Table 2**. The sinusoid geoobjects could be well tracked through approximately 45 slices i.e. contour maps (0,4 meters/1 slice). This means that thicknesses of both of the bodies are 18 meters (0,4 m x 45).

***Table 2**: Measured values of the sinusoid geoobjects; A – amplitude, W – width, WL – wavelength, S – length of streamline, TH – thickness, SIN – sinuosity. Dimension: meter, except the SIN (ratio)*

Right geobody								Left geobody							
A1	A2	WL1	W1	W2	S1	SIN	TH1	A3	A4	WL3	W3	W4	S3	SIN	TH3
637	775	2156	496	685	2935	1.36	18	310	309	1658	277	286	2358	1.42	18

Core samples of Well-A were available from this depth. These can be characterized by massive, structureless fine sandstones with ripped intraclasts. They are deposits of sandy debris flows (Shanmugam, 2006) related to distributary channels or proximal part of lobes. The GR and SP logs show cylindrical shape which usually denotes channel (Reading and Richards, 1994).

5. CONCLUSIONS

On the basis of well logs, core samples and shapes (sinusoid geometry) of these geoobjects, they can be regarded as sinuous, meandering channels of a sand/mud (i.e. mixed) submarine fan system. Their sinuosities and thicknesses are approx. equals. However, the other parameters are higher in case of the

right meandering channel. These values can be used as direct parameters of an object-based algorithm, or to construct training image of a multiple-point simulation.

6. REFERENCES

BÉRCZI, I. (1988): Preliminary sedimentological investigation of a Neogene Depression in the Great Hungarian Plain. –In: ROYDEN, L. H., & HORVÁTH, F. (eds.): The Pannonian Basin: A study in basin evolution, AAPG Memoir 45, 107-116.

GAJDOS, I., PAPP, S., SOMFAI, A. & VÖLGYI, L. (1983): Az alföldi pannóniai (s.l.) litosztratigráfiai egységei, (Lithostratigraphic units of the Pannonian (s.l.) formations in the Hungarian Plain.). MÁFI, Budapest, 70 p.

JUHÁSZ, GY. (1994): Magyarországi neogén medencerészekpannóniai s.l. üledéksorának összehasonlító elemzése. Földtani Közlöny, 124/ 4, 341-365.

MUTTI, E., (1985): Turbidite systems and their relations to depositional sequences. -In: Zuffa, G.G. (Ed.), Provenance of Arenites. D. Reidel Publishing Company, 65–93.

NORMARK, W. R., (1970): Growth patterns of deep sea fans. AAPG Bulletin, 54., 2170–2195.

MAHARAJA, A. (2008): *TiGenerator*: Object-based training image generator, Computers and Geosciences. Elsevier, 34, 1753-1761.

PYRCZ, M.J. & DEUTSCH, C.V. (2014): Geostatistical reservoir modeling – 2nd edition. Oxford University Print, University of Oxford, 448 p.

PYRCZ, M.J., BOISVERT, J.B. & DEUTSCH, C.V. (2008): A library of training images for fluvial and deepwater reservoirs and associated code. Computers and Geosciences, Elsevier, 34, 542-560.

READING, H. G. & RICHARDS, M., (1994): Turbidite systems in deep-water basin margins classified by grain size and feeder system. AAPG Bulletin, 78, 792–822.

SHANMUGAM, G. (2006): Deep-Water Processes and Facies Models: Implications for Sandstone Petroleum Reservoirs. 1st ed., Elsevier, Amsterdam, The Netherlands, 498 p.

Application of Standard Deviation Trends on Well Log Data in Miocene, Pliocene and Pleistocene Sediments for Definition of Well Log Markers in Sava Depression, Pannonian Basin

Marko Cvetković
University of Zagreb, Faculty of Mining, Geology and Petroleum Engineering, Zagreb
marko.cvetkovic@rgn.hr

Well logs from selected well within the Sava Depression, Pannonian Basin were selected for testing the applicability of standard deviation curve trends as a general outliner for sedimentation trends, well log marker position and enhancing correlation possibility. These logs consisted of classic electric well log measurements which include self potential and shallow and deep resistivity. Standard deviation trends were made on several resolution scales for each well log curve, e.g. one meter, two and four meter span for selecting the best resolution for observing trend line breaks. Constructed curves show that general trends that can be defined can be correlated between wells, especially for the youngest Pliocene-Pleistocene ones. Breaks in trend curves in some cases coincide with traditionally positioned well log markers. In addition, these breaks in some cases can be observed in seismic cross sections furthermore determining their applicability. Analysis showed the usefulness of some basic mathematics principles as a tool for division of subsurface, especially in the sedimentary environments in which traditional well log markers are not to be expected (small, dynamic basins), e.g. in Pliocene and Pleistocene sediments in Sava Depression.

Key words: *standard deviation trends, well log markers, correlation, Sava Depression, Pannonian Basin*

1. INTRODUCTION

The Subsurface of the Croatian part of the Pannonian Basin (CPBS) has from late 1950' until now been divided upon E-log markers and borders established in Pletikapić (1969), Šimon (1973, 1980) and further discussed in a vast majority of works including Velić et al. (2002) and Saftić et al. (2003) (**Figure 1**). These markers and borders are determined on resistivity logs and some were treated as lithostratighaphic and chronostratigraphic borders which to a degree of accuracy is correct according to Vrbanac (2002). Some of them represent a characteristic feature on the resistivity curve which is a result of change in grain size marl. This feature can be observed regionally and is thus considered simultaneous in time through the Sava Depression according to Vrbanac (2002).

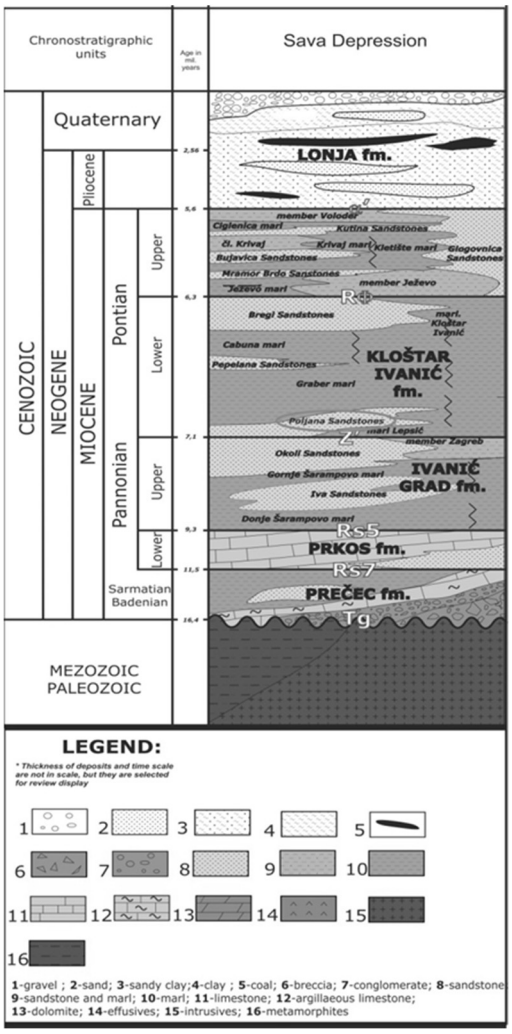

Figure 1: *Chronostratigraphic and lithostratigraphic units in Sava Depression (Šimon, 1980; Velić et al., 2002; Cvetković, 2013)*

The general problem with these kind of divisions based on regional characteristic features on well logs is:

- Subjectivity when interpreting their position,
- Dependency on relatively thick, fine grained sediments which were regionally deposited,
- Lack of applicability in more dynamic environments.

The latter was evident when a first division of the youngest sediments (Pliocene, Pleistocene and Holocene) was attempted first (Hernitz et al., 1980; Urumović et al., 1980) when no distinctive features were observed put the only attempted division was a great change of lithology which was interpreted as Upper to Middle Pleistocene border.

A simple mathematical approach was constructed to advance further determination of E-log markers and a basis for division of the youngest part of the sedimentary infill, e.g. Pliocene, Pleistocene and Holocene.

2. METHODS

The basic outline of the methodology was presented for determination of the position of well log marker α' by standard deviation data trends of the self potential (SP) curve values (Cvetković & Malvić, 2013). The approach considered standard deviation values of different data radius of SP curve and was focused on the applicability of determining only one E-log marker – α'.

Standard deviation is marked by a Greek alphabet letter σ and it represents a measurement of deviation of data from the mean value. **Equation 1** describes it:

$$\sigma = \sqrt{\frac{1}{n}\sum_{i=1}^{n}(x_i - \mu)^2} \qquad \text{(Eq. 1)}$$

whereas:

n – number of cases in the data set

μ – mean value of the data in the dataset

xi – i^{th} member of the dataset

In general, relative small values of the standard deviation represent a small variability of data, which in terms of our problematic represents a homogenous lithology or environment. On the other hand, relatively high standard deviation values correspond to high heterogeneity in the lithology composition. As digitalised well logs mostly have a resolution of 0.1 m this means that standard deviation was calculated based on 10, 20 and 40 data points or in other words a radius of 1, 2 and 4 meters around a data point on the well log curve.
Purpose of standard deviation value calculation is the construction of the cumulative standard deviation (CSTDEV) curves, which generally outline the dynamics of the sedimentation environment.

3. RESULTS

These CSTDEV curves were calculated for 38 wells from Sava Depression and plotted against known E-log marker/border positions. First task was to determine the possibility of usage of CSTDEV curves for trends that can be correlated among wells on a larger area in the youngest section (Pliocene and Pleistocene). These brakes were identified and noted as markers/borders Q, I, J and K (**Figure 2-4**) and can be correlated amongst wells successfully (**Figure 4**). Furthermore location of marker α' coincides well with the break in CSTDEV curve on both wells (**Figure 2, 3**) as well as some of the "older" markers (Rϕ, Z) coincide with breaks in CSTDEV curves although the morphology of break associated with the position of marker Z' on both wells is different (**Figure 2, 3**) but still observable.

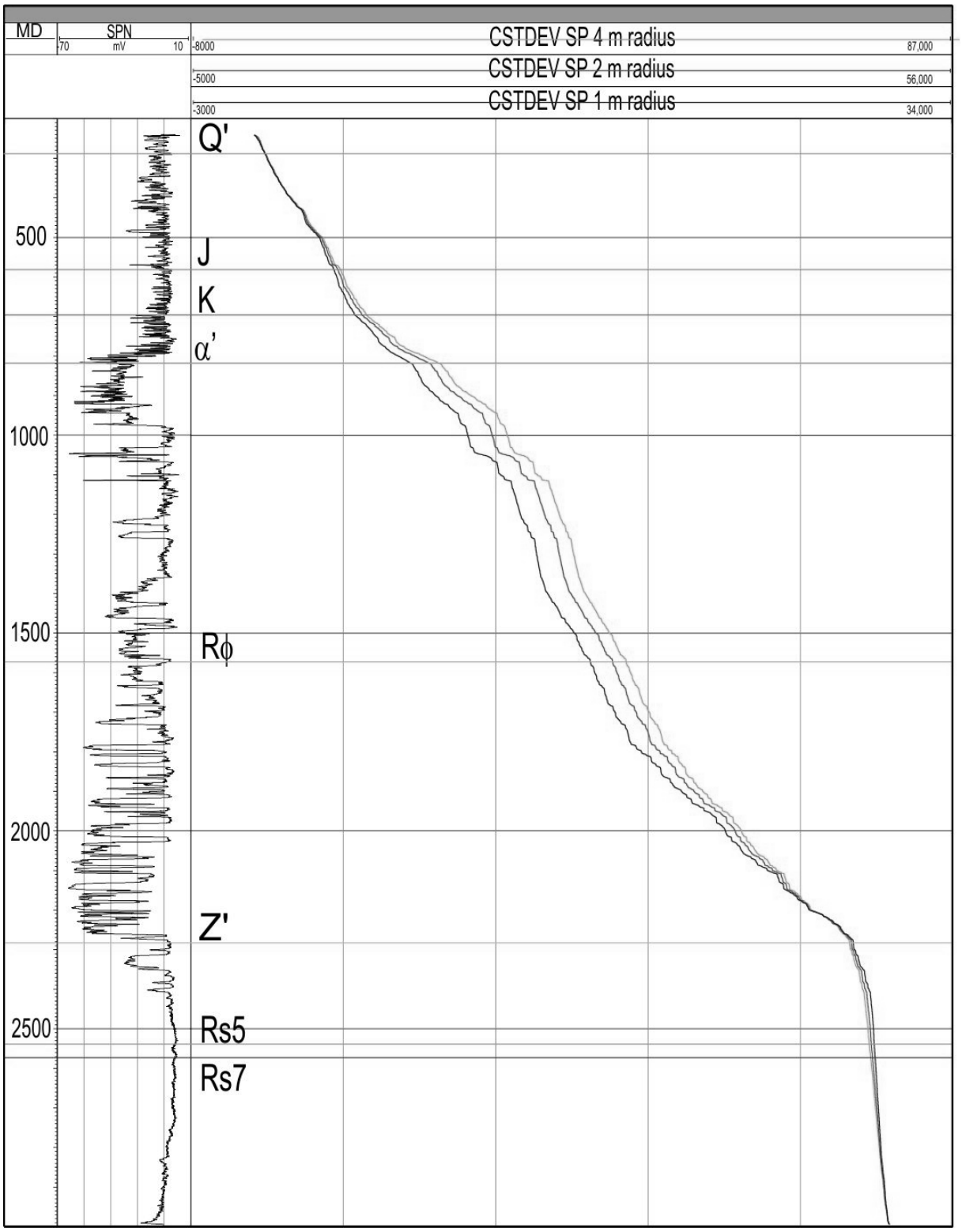

Figure 2: *Normalised SP (SPN) value and CSTDEV curves for Well A with pointed out interpreted well log markers (Q', J, K) based on CSTDEV curves and the ones from database (α', Rϕ, Z', Rs5 and Rs7)*

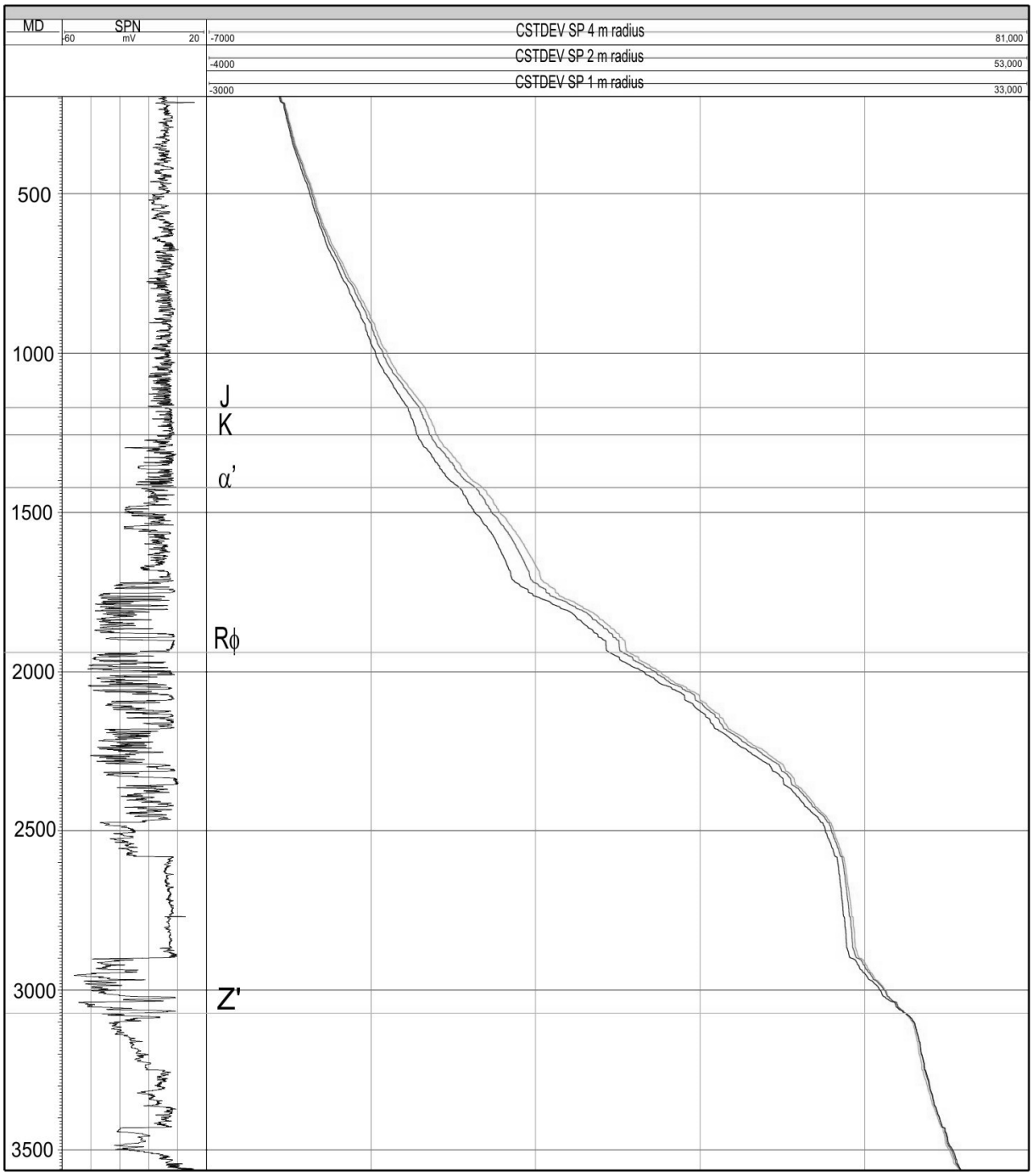

Figure 3: *Normalised SP (SPN) value and CSTDEV curves for Well B with pointed out interpreted well log markers (J, K) based on CSTDEV curves and the ones from database (α', Rϕ and Z')*

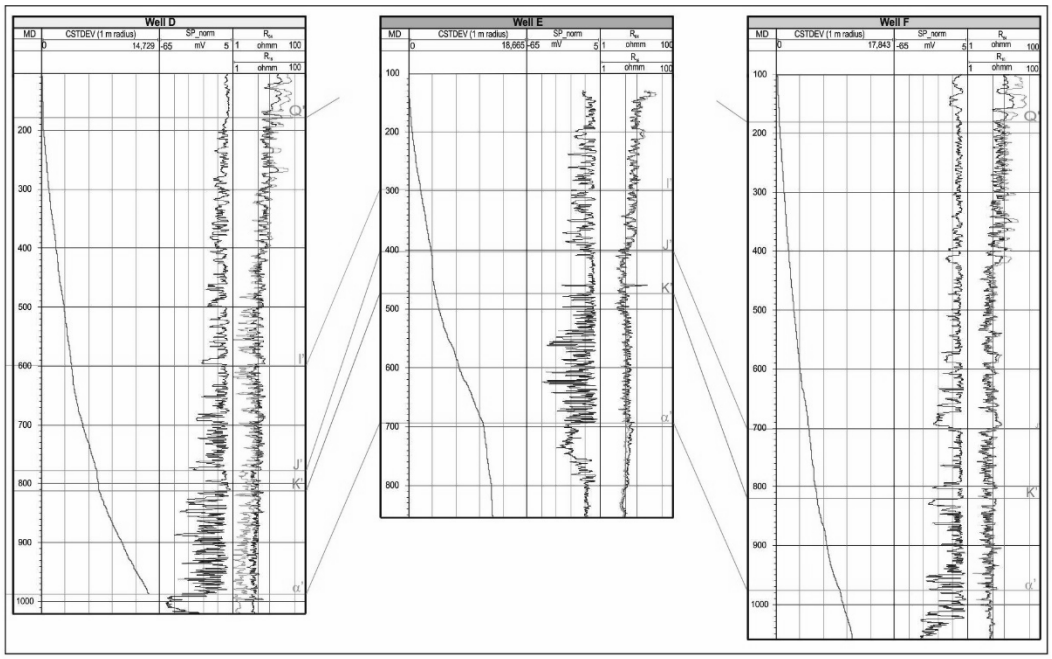

Figure 4: *Results of correlation of based on interpreted well log markers from Pliocene Pleistocene interval of Pannonian Basin infill (from Cvetković, 2013)*

4. CONCLUSIONS

Calculations of STDEV values and CSTDEV curves of E-logs, especially SP curve, can be used as an aid in placing well log markers in Miocene sedimentary infill where "traditional" types of Well log markers are placed. In the youngest part of the Pannonian Basin infill (Pliocene and Pleistocene) they can serve as a main tool in placing well log markers for regional correlation (Cvetković, 2013).

5. REFERENCES

CVETKOVIĆ, M. (2013): Naftnogeološki potencijal i litostratigrafska razradba trećega neogensko-kvartarnoga megaciklusa u Savskoj depresiji (Lithostratigraphic units of the third Neogene-Quarternary megacycle in the Sava Depression and their petroleum potential). PhD Thesis, University of Zagreb, Faculty of Mining, Geology and Petroleum Engineering, Zagreb, 175p. (in Croatian)

CVETKOVIĆ, M. & MALVIĆ, T. (2013): Defining electro-log markers in poorly consolidated, heterogeneous clastic sediments using standard deviation data trends – an example from the Sava Depression, Pannonian Basin System.- In:

16th Hungarian & 5th Croatian and Hungarian congress abstract and program book. Eds. Horváth, J ; Wágenhoffer, A; Geiger, J ; Cvetković, M ; Malvić, T., Hungarian Geology Society & INA Oil Industry Plc., Szeged, 1-4.

HERNITZ, Z., VELIĆ, J., KRANJEC, V. & NAJDENOVSKI, J. (1980): Prikaz diferencijalnih i maloamplitudnih struktura s primjerima iz Savske potoline (Panonski bazen). Nafta, 7-8, 399-409.

PLETIKAPIĆ, Z. (1969): Stratigrafija, paleogeografija i naftoplinonosnost Ivanić-Grad formacije na obodu Moslavačkog masiva. Disertacija, Rudarsko-geološko-naftni fakučtet, Sveučilište u Zagrebu, 71 p.

SAFTIĆ, B., VELIĆ, J., SZTANÓ, O., JUHÁSZ, G. & IVKOVIĆ, Ž. (2003): Tertiary subsurface facies, source rocks and hydrocarbon reservoirs in the SW part of the Pannonian Basin (northern Croatia and south–western Hungary). Geologia Croatica, 56, 1, 101–122.

ŠIMON, J. (1973): O nekim rezultatima regionalne korelacije litostratigrafskih jedinica u jugozapadnom području Panonskog bazena. Nafta, 24, 12, 623–630.

ŠIMON, J. (1980): Prilog stratigrafiji u taložnom sustavu pješčanih rezervoara Sava-grupe naslaga mlađeg tercijara u Panonskom bazenu sjeverne Hrvatske. Disertacija, Rudarsko–geološko–naftni fakultet, Sveučilište u Zagrebu, 66 p.

URUMOVIĆ, K., HERNITZ, Z., ŠIMON, J. & VELIĆ, J. (1976): O propusnom mediju kvartarnih te gornjo i srednjo pleistocenskih naslaga sjeverne Hrvatske. Zbornik radova IV. Jugosl. simp. o hidrogeol. i inž. geol., 1, 395-410.

VELIĆ, J., WEISSER, M., SAFTIĆ, B., VRBANAC, B. & IVKOVIĆ, Ž. (2002): Petroleum-geological characteristics and exploration level of the three Neogene depositional megacycles in the Croatian part of the Pannonian basin. Nafta 53, 6-7, 239-249.

VRBANAC, B. (2002): Facies and facies architecture of the Ivanic Grad Formation (Late Pannonian)—Sava Depression, NW Croatia. Geologia Croatica, 55, 1, 57–77.

The effect of climatic parameters on the nutrient cycle in the Kis-Balaton Water Protection System on a daily scale determined by wavelet coherence analysis

István Gábor Hatvani[1], Adrienne Clement[2], János Korponai[3], József Kovács[4]

[1]Institute for Geological and Geochemical Research, Research Center for Astronomy and Earth Sciences, Hungarian Academy of Sciences, H-1112 Budapest, Budaörsi út 45., *hatvaniig@gmail.com

[2]Budapest University of Technology and Economics, Department of Sanitary and Environmental Engineering, H-1111 Budapest, Műegyetem rakpart 3

[3]University of West Hungary, Department of Chemistry and Environmental Sciences, H-9700 Szombathely, Károly Gáspár tér 4., Hungary

[4]Eötvös Loránd University, Department of Physical and Applied Geology, H-1117 Budapest, Pázmány Péter stny. 1/C

Abstract – Lakes respond sensitively to environmental changes - such as climate change - and anthropogenic effects. Lake Balaton, the largest shallow lake in Central Europe, is no exception. To protect it against elevated nutrient loads, the Kis-Balaton Water Protection System was constructed with eutrophic and wetland habitats. This work aims to (i) demonstrate the lagged linear relationship between climatic parameters and primary nutrients in the different habitats of the Kis-Balaton Water Protection System and (ii) assess their common periodic behaviour. Cross correlation- and wavelet coherence analyses were conducted on water quality parameters (4 primary nutrients and suspended solids) and 4 meteorological parameters sampled daily (1995-2010) from four sampling sites. Results have highlighted (i) the different reaction times of the nutrients to changes in the weather conditions in the different habitats and (ii) the years with the highest and missing coherence in annual periodicity.

Key words: *climate, cross correlation, water quality, wavelet coherence analysis*

1. INTORDUCTION

Conserving the water quality of Lake Balaton, the largest shallow freshwater lake in Central Europe (watershed approx. 5181 km^2) is one of the primary goals in Hungarian water management. Being the largest tributary of the lake, the River Zala, supplies almost 50% of its water- and 35-40% of its nutrient input (Hatvani et al., 2014), therefore adversely affecting its water quality.

In the nineteenth century, after artificial modification of water level, and the regulation of the River Zala the former wetland areas of Kis-Balaton Wetland and the Lower Zala Valley, the filtering areas for the waters of the River Zala partially dried up and decreased in effectiveness. In the absence of the Kis-Balaton Wetland functioning as a filter, the waters of the River Zala entered Lake Balaton without having been naturally filtered resulting in the deterioration of Lake Balaton's water quality.

To handle these negative trends measures for nutrient control were taken (Hatvani et al., 2015) and the Kis-Balaton Water Protection System (KBWPS) was created in two constructional phases on the remains of the once Kis-Balaton Wetland. Phase I. (the Upper Reservoir, 18 km^2 **Figure 1**) was inundated and began operating in 1985 and it became algae dominated pond. It was able to remove about 20-30% of the P reaching the KBWPS. Phase II (the Lower Reservoir, **Figure 1**) was put into operation in 1992, but until 2014 only a part of it (16 km^2) was inundated, which is a reed-dominated area covered by macrophytes.

It is suspected that hydrochemical seasonality (e.g. Exner-Kittridge et al., 2016; Tanos et al., 2015) will be present/corrupted to a different degree in the River Zala and the different habitats of the KBWPS mirroring their local characteristics. Al ternate solution to the assessment of such phenomena could be found in the study of Molnár and Molnár (2012) and a similar study but on hydroclimatic records from east Central Europe in Kern and Sen (2016).

The main questions of the research therefore were: is the common annual period of the daily measured water quality- and the meteorological parameters (i) consistent in time, (ii) in phase and (iii) how did the changes in meteorology affect the different habitats and if so to what degree?

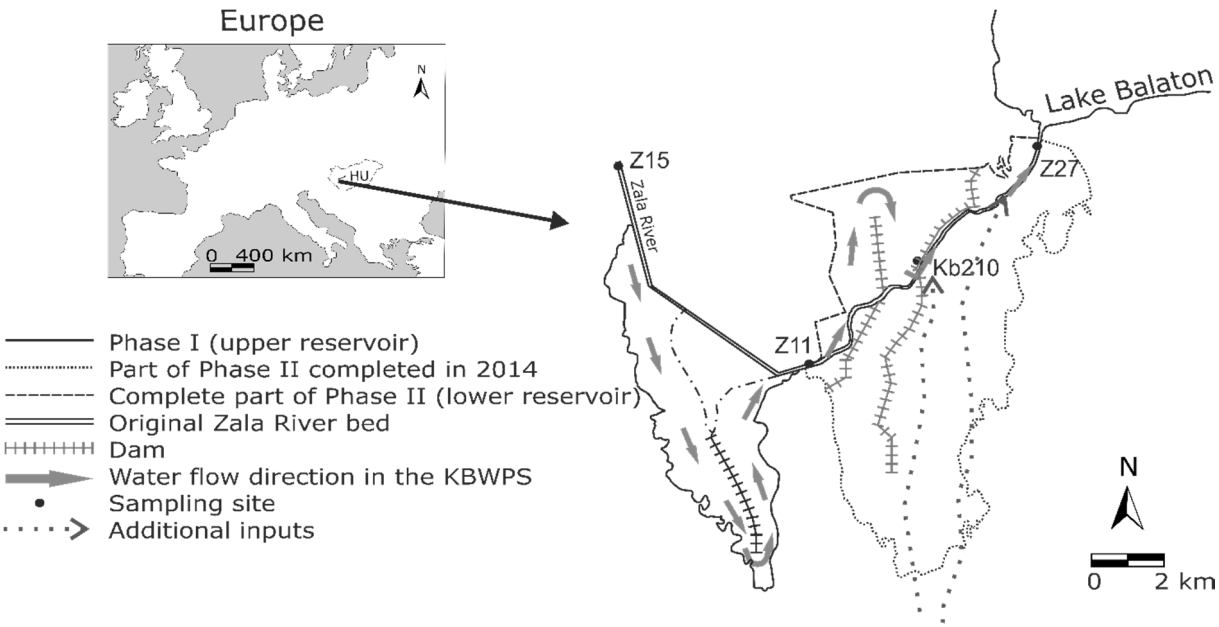

Figure 1: *Location of the study are and the analysed sampling sites.*

2. MATERIALS AND METHODS

2.1. Used materials

In the study the time series of 5 daily measured water quality parameters (WQPs) from the KBWPS (NO_3-N; total nitrogen (TN); total phosphorus (TP); soluble reactive phosphorous (SRP); and total suspended solids (TSS, mg l^{-1}) were involved along with global radiation (GR, J cm^{-2}), temperature (T, °C), precipitation (Prec, mm) and cloud cover (CC, tenths) (Spinoni et al., 2014) representing the background meteorological parameters (MP). All data were assessed using wavelet spectrum and wavelet coherence analyses (Torrence and Compo, 1998) for the time interval 1994-2010 from four sampling sites of the KBWPS. The sites were:

- "Z15", the input of the KBWPS, representing the River Zala,
- "Z11", the representing the outflow of Phase I typifying the water quality of the algae dominated eutrophic pond,
- "Kb210", the outflow of Phase II, typifying the macrophyte-dominated wetland habitat
- "Z27", the downstream outlet of KBWPS, including the outflow water of Phase II and additional external inputs from the watershed (**Figure 1**).

2.2. Methodology and software

As a first step cross correlation analysis (CCA) was used to see if significant lagged correlations exist in the data or not. Later, the periodic behaviour of the meteorological parameters was evaluated with wavelet spectrum analysis to find the periods lacking annual periodicity, and as a last step with wavelet transform coherence (WTC) the coherence of the periodic signal in the WQP and the MPs was explored. WTC resembles the traditional correlation coefficient but in a localized way in the frequency-time space (Grinstead et al., 2004). Four main characteristics of the WTC are used: (i) the presence of the coherent annual period in time, (ii) the maximum average cross−wavelet power and (iii) the phase differences between the pairs of WQPs and MPs.

For the calculations R was used: the CCA was done with a script of the authors, the WTCs were generated with the `WaveletComp` package.

3. RESULTS AND DISCUSSION

3.1. CCA results and behaviour of the meteorological parameters

On a 40 day scale the CCA did not give significant improvements in the linear relationship between the WQPs, amelioration in the second decimal place.

As expected (Kovács et al., 2010) the WSA of the MP indicated annual periodicity throughout the whole investigated period except for Prec. in the time series of which the major gap was present between ~2000 and ~2002. These were exceptionally arid years (Hatvani et al., 2014), therefore, it is expected that the WQP driven by Prec will be missing the annual periodicity.

3.2. Common presence of the annual period

The presence of the coherence in annual periodicity was transformed into percentages taking 100% as a significant presence for the whole period. WTC indicated that most of the parameter pairs (WQP & MP) have common annual periodicity in the whole time interval. The exceptions (**Figure 2**), however, hold key information about the KBWPS' functioning.

In the River Zala (site Z15) due to the sudden drop in precipitation causing a decrease in runoff (Hatvani et al., 2014) in the early 2000s a discontinuity appeared between the coherence of TSS and Prec.

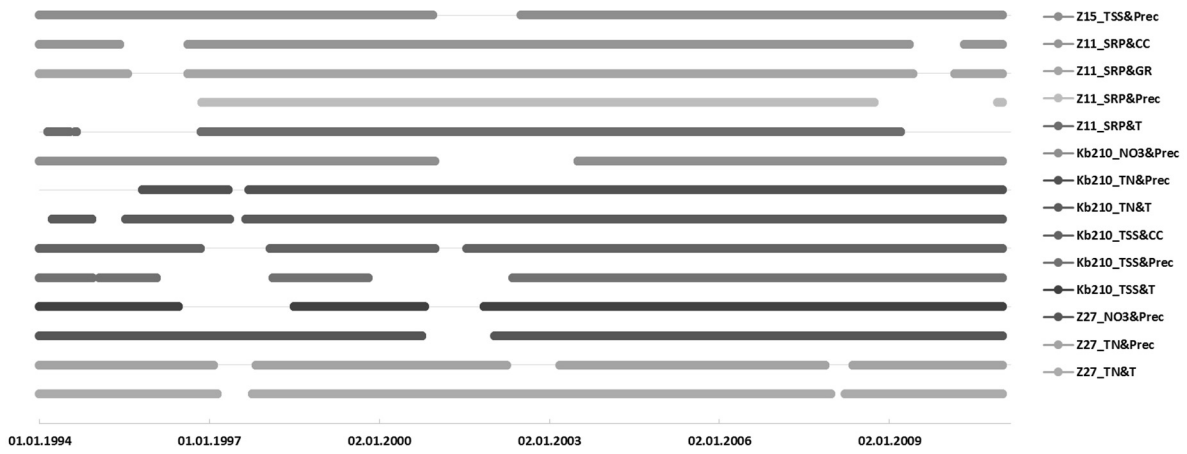

Figure 2: *Presence of annual coherence between those WQ and MP where the absence was higher than one year of the total time*

It could have been expected that e.g. P forms would show a similar behaviour at Z15, but do to their decreased contribution of diffuse origin this did not happen, since after 1990 the relative importance of point source P loads increased (Hatvani et al., 2015).

In the eutrophic pond (Phase I), however, the intermittent annual coherence between SRP and MPs diminished after 1996 and only returned after 2010 for yet unconfirmed reasons (**Figure 2**). Probably because 1997 and the ones around 2010 were exceptionally arid and cold, causing the biological processes to lose their importance.

In Phase II, the absence of coherency between the WQP and MP is mostly characteristic of the N forms and at Kb210 TSS. Besides a short period in the mid-1990s, the most characteristic gap can again be seen in the early 2000s (Figure 2). The first gap was presumably caused by a small the drop in runoff (Hatvani et al., 2014), not enough to cause disturbance in the annual periodic behaviour of Prec itself, but enough to change the processes in the vulnerable Phase II of the KBWPS (Kovács et al., 2010). In the time of the second gap

however, the drastic decrease in precipitation and runoff decreased the TSS loads (average annual sum TSS: 1995-'99: 1050t; 2000-'04:330t; 2005-'10: 375t) and caused a vast change in the processes of Phase II. As for the N forms, with the decreased runoff the decomposition processes - specifically denitrification -taking place in Phase II (Hatvani et al., 2011) was able to remove most of the N (Hatvani et al., 2014).

3.3. Phase differences and maximum average power

Besides TSS, the nutrient forms explored were all driven by the MP according to the phase differences. This indicates that the TSS content of the KBWPS in in the River Zala and Phase II after 2000 was leading the MP, which –being impossible - implies its independence with respect to annual periodicity. In Phase I it behaves similarly to TP being in phase and lead by T (by 1-2 months) & GR (lead by 2-3 months) indicating that TSS is composed mostly of algae. As for TP in Phase I its most likely in particulate form because of the algae, while in Phase II its WTC resembles that of SRP, since it is dissolves in the water.

Regarding TN its phase diagram is most coherent in Phase I, since N as a nutrient is mostly consumed by algae, thus its power is also the highest in the eutrophic pond (**Figure 3**).

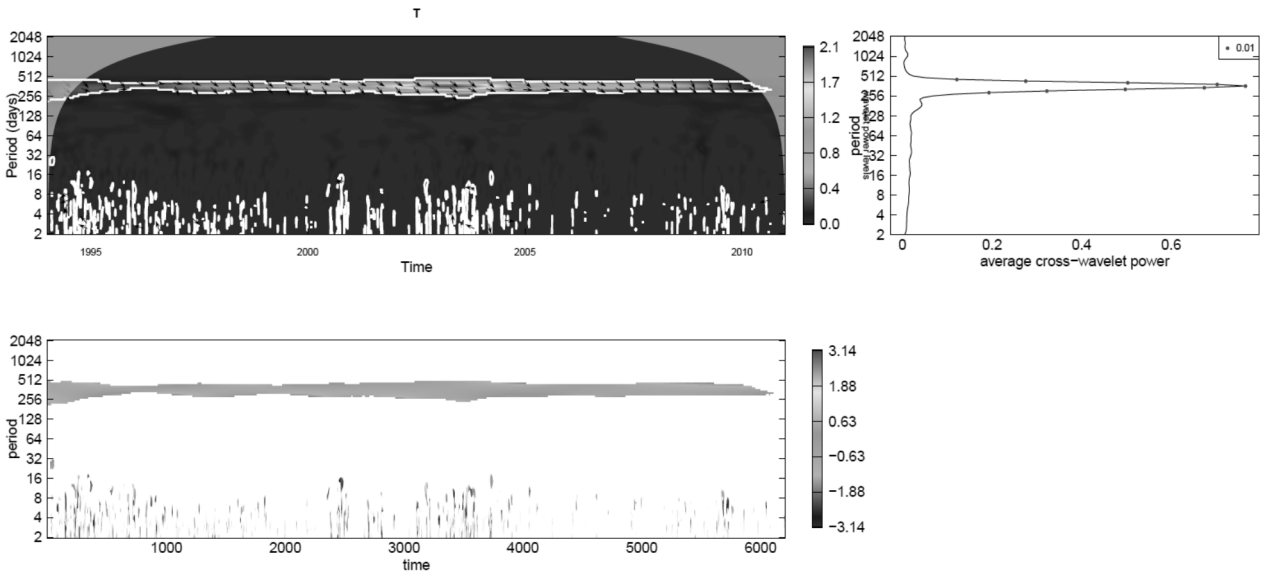

Figure 3: *Time–frequency coherency images (upper left panel) and time-averaged cross-wavelet power (upper right panel) of TN and T at site Z11. The white contours in the upper left panel and the red dots in the upper right one show the 95% confidence levels calculated based on 100 AR (1) surrogates. The black arrows indicate the phase-angle difference of the two parameters and the lower graph their continuous visualization. For further details see Rösch and Schmidbauer (2014).*

4. CONCLUSIONS AND OUTLOOK

Results draw attention to the fact that WTC is able to indicate the common trends of variables *localized* in the time frequency domain, even when CCA was incapable of such distinction.

Furthermore, the specific findings indicated that strong coherence is present on the annual scale between the water quality and the meteorological parameters in the Kis-Balaton Water Protection System and where coherence was lacking, it was most probably caused by the extreme weather conditions, e.g. droughts.

ACKNOWLEDGMENTS

Thanks for the support of the MTA "Lendület" program (LP2012-27/2012). This is contribution No. XX of 2ka Palæoclimatology Research Group.

5. REFERENCES

EXNER-KITTRIDGE, M., STRAUSS, P., BLÖSCHL, G., EDER, A., SARACEVIC, E., ZESSNER, M. (2016): The seasonal dynamics of the stream sources and input flow paths of water and nitrogen of an Austrian headwater agricultural catchment. Science of The Total Environment 542, Part A, 935-945.

GRINSTED, A., MOORE, J.C., JEVREJEVA, S. (2004): Application of the cross wavelet transform and wavelet coherence to geophysical time series. Nonlin. Processes Geophys. 11, 561-566.

HATVANI, I.G., CLEMENT, A., KOVÁCS, J., KOVÁCSNÉ, SZ.I. & KORPONAI, J. (2014): Assessing water-quality data: the relationship between the water quality

amelioration of Lake Balaton and the construction of its mitigation wetland. Journal of Great Lakes Research, 40 (1)

HATVANI, I.G., KOVÁCS, J., KOVÁCS, I.S., JAKUSCH, P., KORPONAI, J. (2011): Analysis of long-term water quality changes in the Kis-Balaton Water Protection System with time series-, cluster analysis and Wilks' lambda distribution. Ecological Engineering 37, 629-635.

HATVANI, I.G., KOVÁCS, J., MÁRKUS, L., CLEMENT, A., HOFFMANN, R., KORPONAI, J. (2015): Assessing the relationship of background factors governing the water quality of an agricultural watershed with changes in catchment property (W-Hungary). Journal of Hydrology 521, 460-469.

KERN, Z., SEN, A.K. (2016): Wavelet analysis of low-frequency variability in oak tree-ring chronologies from east Central Europe. Open Geosciences, 8(1) 290-296

KOVÁCS, J., HATVANI, I.G., KORPONAI, J., KOVÁCS, I.S. (2010): Morlet wavelet and autocorrelation analysis of long-term data series of the Kis-Balaton water protection system (KBWPS). Ecological Engineering 36, 1469-1477.

MOLNÁR, S., MOLNÁR, M. (2012): Comprehensive assessment of climate change policies and measures in Hungary: concerns and tasks in an underestimated challenge, IDŐJÁRÁS 116:(4). 297-321.

RÖSCH, A. AND SCHMIDTBAUER H. (2014): WaveletComp: A guided tour through the R-package. Downloaded on 01.05.2016 from http://www.hs-stat.com/projects/WaveletComp/WaveletComp_guided_tour.pdf

SPINONI J. AND THE CARPATCLIM PROJECT TEAM (39 AUTHORS; 2014): Climate of the Carpathian Region in 1961-2010: Climatologies and Trends of Ten Variables. Int. J. Climatol. 35, 1322-1341

TANOS, P., KOVÁCS, J., KOVÁCS, S., ANDA, A., HATVANI, I. (2015): Optimization of the monitoring network on the River Tisza (Central Europe, Hungary) using combined cluster and discriminant analysis, taking seasonality into account. Environ Monit Assess 187, 1-14.

TORRENCE, C., COMPO, G.P. (1998): A Practical Guide to Wavelet Analysis. Bulletin of the American Meteorological Society 79, 61-78.

Optimisation of cluster facies - why, how and how much cluster?

Janina Horváth[1], Szabolcs Borka[1], János Geiger[1]

[1]University of Szeged, Department of Geology and Paleontology, Egyetem u. 2-6, 6722 Szeged, Hungary, th.janina@geo.u-szeged.hu

Many studies classify or cluster clastic depositional datasets into lithofacies using graphical, multivariate statistical or neural network techniques. Each has able to handle large data set or great number of parameters therefore these multivariate statistical approaches are widely used in clastic sedimentology, and within that facies analysis. Furthermore, most of the techniques which try to separate more or less homogeneous subset can be subjective. This subjectivity raises several questions about the significance and confidence of clustering.

The goal of this study is to optimize clustering. This technique is able to describe sedimentary or lithological facies through common characteristics. Data transformation like Box-Cox transformation and principal component analysis (PCA) are able to improve clustering combined with artificial neural network (ANN). Using PCA helped us to reduce the redundancy of information coming from certain variables. This was corroborated by the correlation coefficients of the applied properties (porosity, permeability, sand content and shale content). Evaluation of the optimal number of clusters was also important. In this study, certain statistical tests were able to explain the variance of the dataset. F'test and "leave-one-out" classification were applied to determine stable clusters and optimal numbers of clusters. This approach was applied the clastic depositional data from a Miocene hydrocarbon reservoir (Algyő field, Hungary) to demonstrate the fidelity of the clustering method yielding five optimum cluster facies. These clusters are supported by both statistical tests and geological observations as well. These clusters represent lithological characteristics within a (delta fed) submarine fan system in the Pannonian-basin.

Key words: cluster analysis, data transformation, optimal number of cluster, submarine fan system

INTRODUCTION

The case study is located in a deep subbasin of the Pannonian-basin in the Great Hungarian Plain. According to Grund and Geiger (2011) and Borka (2016) the

study area was characterized as sequences of prodelta submarine fan. The analysis focused on the determination of lithology based on four variables coming from interpreted logs (porosity, permeability, sand content and shale content).

The analysis focused on the determination of lithology using separation of data space technique. There are many multivariate techniques (graphical, statistical, neural network methods) to separate data set and define subsets. These are based on genetically similar units that are very close in the multidimensional property space. In this case a neural network clustering was applied which method was presented in several papers (e.g. Horváth, 2015).

Core samples was also available from one well which included about continuous 35m. The core analysis was presented by Borka (2016). According to the core analysis a part of a typical mixed sand-mud submarine fan complex with quasi-inactive parts (zone of thin sand sheets and overbank), channelized lobes (persistent sandstones in them may denote distributary channels) and a main depositional channel was revealed. However, due to the low number of core samples it is difficult to extend the lithology information to the whole area which contains 141 wells. The core samples were kind of finger-posts in the interpretation of cluster results to define lithofacies. Nonetheless, it was complicated to determine the adequate number of clusters since the most essential parameters of clustering algorithms is to determine the number of clusters and the validity of clustering. Clustering is an unsupervised technique so the researcher has only little or no information about cluster number. At the same time, the number of cluster is a required parameter so this is a general problem and old as cluster analysis itself. Of course, geological knowledge about the field and information about the core samples can give a rough number of types as clusters. In addition, questions may arise: has the method ability to segregate all types in the property space or not, is the created subset adequately homogeneous or not? The most common problem if we separate too many – however homogeneous – groups, is it is not possible to label all of them geologically. As a contrary, if we have small number of clusters, it can be

relatively too heterogeneous and in this case it is hard to define them geologically, as well.

A number of authors have suggested various indexes to solve these problems but it means that usually the researcher is confronted with crucial decisions such as choosing the appropriate clustering method and selecting the number of clusters in the final solution. Numerous strategies have been proposed to find the right number of clusters and such measures (indexes) have a long history in the literature. The study focused on to determine the right number of clusters and to analyse some suggested sum of squares indexes (called WB indexes). The "leave-one out" (LOO) classification method was used in the discriminant function analysis (DFA) as cross validation (Asante and Kreamer, 2015).

METHODS

Neural network technique was used to determine the cluster facies based on the four mentioned variables. The applied dataset omitted the impermeable units and variables.

Usually clustering does not require normal transformation but most clustering algorithms are sensitive to the input parameters and to the structure of data sets. If good structure exists for a variable a transformed data which can approximate the symmetric distribution could be more efficient. It should be close to symmetry prior to entering cluster analysis (Templ et al. 2006). Significant skewness can be measured in the distribution of variables especially shale content and permeability (**Figure 1** base on **Eq.1.**). On the other hand principal component analysis (PCA) was applied as pre-process of clustering which also requires normal distribution.

$$y = x^{\alpha} = \begin{cases} \frac{(x+\alpha_2)^{\alpha_1}-1}{\alpha} & \alpha \neq 0 \\ \log(x+\alpha_2) & \alpha = 0 \end{cases} \qquad \textbf{Eq.1}$$

Box-Cox transformations (Box and Cox, 1964) of all single variables do not guarantee symmetry distribution, but more closeness to them (Asante and Kreamer, 2015; Templ et al., 2006). The applied transformation is modified the family of power transformation by Box and Cox (1964). This modified power

transformation defined those cases when variables are negative or equal to zero (**Eq.1**) (Sakia, 1992).

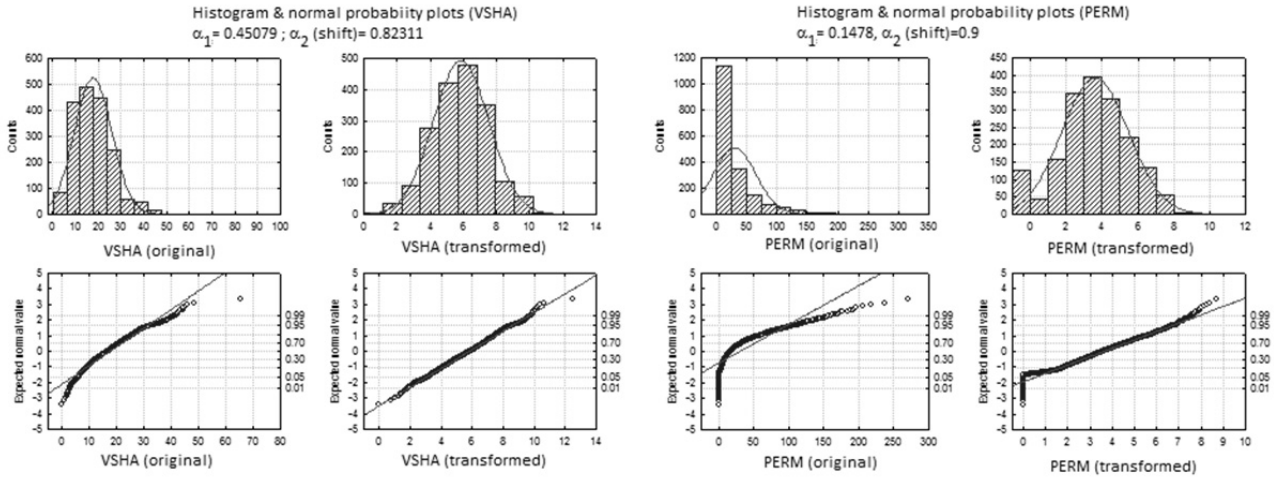

Figure 1: *Results of Box-Cox transformation*

Porosity and permeability variables were in significant correlation (coefficient was 0.72) hence PCA was used to reduce redundancy and create new components (one component is based on permeability and porosity and the second component is based on sand content and shale content). The goal of PCA method was to create new components which are able to preserve many as possible variances of the original variables' heterogeneity. On the other hand PCA required normal distributions as well.

NN clustering was run with PCA components. After the import of input data into the spreadsheet, the size of training set was fixed as 70% for all data points. For the validation and testing, 15-15% of the whole set was used, evenly divided. These three subsets were collected by the network in a random way to avoid bias. The learning rate of NN clustering converged monotonically in the [0,1] interval from the first to the last training cycle. The start value was specified as 0.05 and 0.002 for the end value.

The initial number of clusters was determined in low value which resulted a robust lithofacies and it was increased from value 3 to 8 one by one.

To determine the stable number of clusters DFA with LOO cross validation technique was used. A cluster structure was declared stable if DFA predicted at least 80% of the members in each cluster groupings. This threshold was set on

practical observations. Overall cross-validated results for each clustering results of stable clusters range from 88.0-91.9%.

To select the optimal number of clusters in the final solution, statistics test based on sum of squares was applied. Since a single statistics test method cannot be depended upon, more methods were used (Gordon, 1999 in Asante and Kreamer 2015). There are several suggested indexes depending on the sum of squares (**Eq.2-5**):

Hartigan (1975): $H_t = \log \frac{SS_b(K)}{SS_w(K)}$ **Eq.2**

Explained variance: $ETA_K^2 = \frac{SS_b(K)}{SS_t}$ **Eq.3**

Proportional reduction of error: $PRE_K^2 = \frac{SS_w(K)}{SS_w(K-1)}$ **Eq.4**

F-Max statistics: $F - Max = \frac{SS_b(K)/(K-1)}{SS_w(K)/(n-K)}$ **Eq.5**

Eq.5 is equal to the Calinsky and Harabasz index (1974) which is called the variance ratio criterion (VRC). Well-defined clusters have a large SSb and a small SSw. The larger the VRC ratio, the better the data partition is. So the optimal number of clusters is determined by maximum VRC. **Eq.2** is the Hartigan index, so-called crude rule of thumb which is able to estimate the optimal number of clusters with the minimum value of second differences.

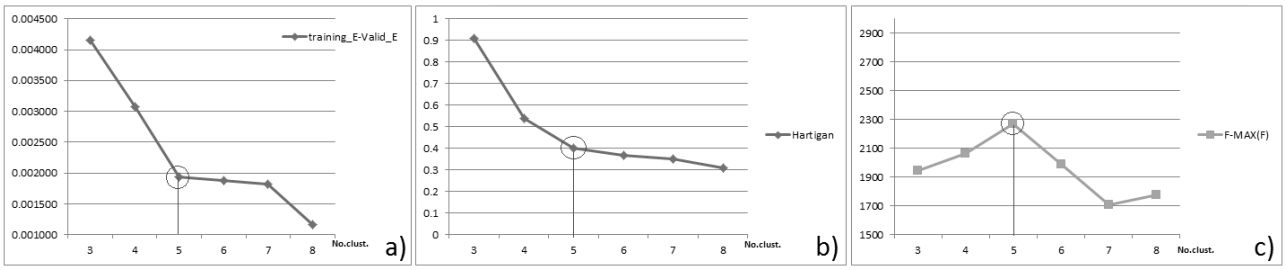

Figure 2: a) *Difference plot based on ANN;* ***b)*** *plot of Hartingan indexes,* ***c)*** *F-max(F) plot*

RESULTS

Optimal number of cluster

In the study, the cluster stability analysis by DFA have eventuated several stable cluster results (thresholds in excess of 80%); however according to cross validation the optimal number of cluster determined 5 number clusters solution.

Based on LOO 91.9% of cross-validated grouped cases are correctly classified. The analyses of differences reduction between training error (T_{error}) and validation error (V_{error}) showed the same optimum as well. The difference-plot (**Figure 2-a**) reached the elbow point at/in case of five cluster solutions. In the practice the error rate was acceptable if it was relatively low and the training-test-validation error rate approximated to each other. In addition, the plot of Hartigan values (**Figure 2-b**) or F-max(F) values (**Figure 2-c**) determined similar 'best fit' in case of five cluser solutions.

Table-1: *Test statistics results for estimating number of clusters*

No.clust.	3	4	5	6	7	8
ETA^2_K	0.681758	0.782905	0.848698	0.867727	0.878515	0.904526
PRE^2_K	not defined	0.317831	0.304513	0.123945	0.081557	0.214392

From the ETA^2_K values, three cluster solutions explained 68% of the variance in the dataset; four cluster solution expained ~78% and so (**Table-1**). The table-showe that the incement in the ETA^2_K significantly stopped from cluster five. Also the PRE^2_K values sharply decreased from cluster five.

Geological characterisation and labelling of clusters

According to the optimal number analysis that solution was described statistically which contained five clusters. The general statistical character of the five clusters is summarized in the **Table 2**.

Table 2: *Statistical characterisation of clusters based on the original data*

	FIAP						PERM					
	1	2	3	4	5	Total	1	2	3	4	5	Total
N	182	252	556	503	328	1821	182	252	556	503	328	1821
Mean	12.86	14.41	16.39	18.39	20.25	17.01	2.18	7.84	12.04	32.24	87.16	29.59
Median	12.84	14.49	16.45	18.35	20.23	17.24	1.22	5.56	11.54	31.08	79.02	16.63
Std. Deviation	1.43	1.73	0.83	0.77	1.00	2.52	2.37	8.72	5.44	15.16	41.79	35.09
	VSHA						**VSND**					
	1	2	3	4	5	Total	1	2	3	4	5	Total
N	182	252	556	503	328	1821	182	252	556	503	328	1821
Mean	33.07	11.29	22.83	15.30	8.79	17.65	52.60	66.67	59.54	65.93	71.23	63.70
Median	32.13	11.38	22.50	15.45	9.04	16.93	53.87	68.92	60.47	65.81	70.31	64.41
Std. Deviation	6.78	4.41	3.42	2.76	2.58	8.21	6.99	11.93	5.45	3.07	3.84	8.32

Based on the geological consideration five lithofacies could be identified within the prodelta submarine fan. In a sand-rich submarine fan system at least three types of sandy deposits could be defined which correlates with certain major units (1) zone of thin sand sheets and overbank, (2) channelized lobes (persistent sandstones, may including denote distributary channels) and (3) main depositional channel.

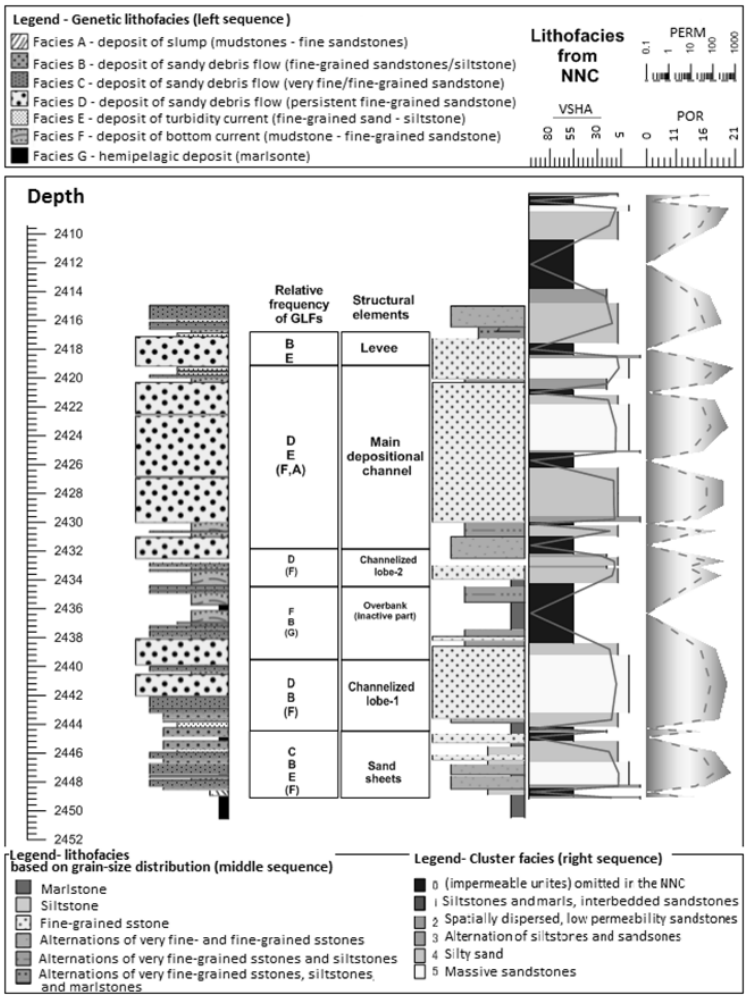

Figure 3: *Comparison of NNC lithofacies (right sequence) with genetic lithofacies (left sequence) and lithofacies based on grain-size distribution (middle sequence) (based on Borka, 2016)*

The results matched to the lithological description of core samples, too (**Figure 3**). Labelling of the cluster on the basis of cores and statistical characters are: (1) siltstones and marls, interbedded sandstones; (2) spatially dispersed, low permeability sandstones; (3) alternation of siltstones and sandstones; (4) silty sand; (5) massive sandstones.

SUMMARY

The transformed variables by Box-Cox and PCA process reduced impact of skewness and the redundancy in variables to avoid misclassification. The NN clustering with the final settings was validated using DFA LOO method. Members in each cluster groupings were validated by over 80% prediction. Evaluation of optimal cluster solution relied on more WB indexes. All of them determined the "best fit clustering" with "five number of clusters" solution. The separated clusters were suitable to identify the lithofacies within the study area which presents a sand-rich, delta fed submarine fan system. These facies are relating to the lithological units described by Borka (2016). These selected groups will be the basis of the 3D facies model and to analyse the spatial continuity of petrophysical properties within the single facies.

REFERENCES

ASANTE, J. KREAMER, D. (2015): A New Approach to Identify Recharge Areas in the Lower Virgin River Basin and Surrounding Basins by Multivariate Statistics. Mathematical Geosciences, 47/7, 819-842.

BORKA, SZ. (2016): Markov chains and entropy tests in genetic-based lithofacies analysis of deep-water clastic depositional systems. Open Geosci., 8, 45–51.

BOX, G.E.P. and COX, D.R. (1964): An analysis of transformations. Journal of the Royal Statistical Society, Series B, 26, 211-252.

CALINSKI, T., and HARABASZ, J. (1974): A dendrite method for cluster analysis. Communications in Statistics, 3/1, 1–27.

GRUND, SZ., and GEIGER, J. (2011): Sedimentologic modelling of the Ap-13 hydrocarbon reservoir. Central European Geology, 54/4, 327-344.

HARTIGAN, J. A. (1975): Clustering Algorithms. J. Wiley and Sons, New York, p 351.

HORVÁTH, J. (2015): Depositional facies analysis in clastic sedimentary environments based on neural network clustering and probabilistic extension (Phd dissertation), University of Szeged, 118 p.

TEMPL, M., FILZMOSER P., REIMANN C. (2006): Cluster analysis applied to regional geochemical Data: problems and possibilities, Research report, CS-2006-5.

SAKIA, R. M. (1992): The Box-Cox transformation technique: a review. The Statistician 41, 169-178.

Setting up a cost-effective agricultural drought monitoring system using spectral indices derived from MODIS satellite images in Hungary

András Gulácsi[1]

[1]University of Szeged, Institute of Environmental Sciences, P. O. Box 653, H-6701 Szeged, Hungary, gulandras90@gmail.com

Coupling reservoir permeability with granulometric heterogeneity using programming language R

Maja Hren[1], Marko Gaćina[1] and Domagoj Vulin[2]

[1]INA Plc., Av. V. Holjevca 10, 10000 Zagreb, Croatia, maja.hren@ina.hr

[2]University of Zagreb, Faculty of Mining, Geology and Petroleum Engineering, Pierottijeva 6, 10000 Zagreb, Croatia

The purpose of this study is to improve the permeability correlations, which mostly do not account for the effects of sorting. With an assumption that grain size distribution is connected with pore size distribution, statistical analysis of grain size, porosity and permeability was done. While there are published methods to estimate the grain size standard deviation and geometric mean from usually used uneven sieve mesh sizes, those parameters were obtained by statistical resampling method. Further distribution parameters (and types) were tested in statistical programming language R. Modified correlation for estimating permeability based on grain size is compared with published empirical correlations and gives the most satisfying results. Considering that the distribution type affects the correlation, further correlation modifications and improvements are proposed.

Key words: *Grain size distribution, permeability correlation, granulometric heterogeneity, programming language R*

1. INTRODUCTION

Reservoir heterogeneity and its characterization have been examined by numerous geostatistical models in the past decades. In order to predict spatial distribution of permeability at the every point of the hydrocarbon reservoir and interpolate and extrapolate the permeability where core or well data is not available, quantitative relationship of petrophysical parameters is about to be presented. Estimating permeability based on the grain size distribution should represent an applicable method whereas contains information on rock type,

textural properties, porosity and formation resistivity factor (tortuosity and cementation exponent). These factors are used to evaluate the reservoir heterogeneity. Statistical parameters calculated to predict variations of permeability can be derived from core samples, drill cuttings, well log data, or even microscopic sections. Further distribution analyses were tested in the statistical programming language *R,* and after obtaining distribution parameters, regression analysis was done. This case study shows how the variations of calculated reservoir properties affect sandstone permeability of Lipovljani (27 samples) and Pavljani (13 samples) oil-gas field in a mathematical expression.

2. RESERVOIR CHARACTERISTICS

2.1 Geological setting

Oil-gas field Lipovljani is a part of Panonian basin, Sava (Ilova) depression. Lipovljani reservoir is formed of clastic sediments, loosely lithified to lithified, fine-medium coarse sandstone made of quartz and mica. Oil field Pavljani is also a part of Panonian basin located in Drava (Bjelovar) depression. Both Lipovljani and Pavljani reservoir structure is anticline oriented NW-SE consisting mostly of sandstone accompanied with complex tectonics and numerous faults.

2.2 Laboratory petrophysics

Consolidated sediments from boreholes were analysed in laboratory. Cylindrical sandstone samples were drilled from the core. Prior to laboratory measurements, the original fluids and salts had to be removed from the samples (chloroform and methanol extraction). For grain size analysis, samples were taken at the corresponding depths as the plug samples.

Both porosity and permeability were tested on dried plugs. Porosity was determined by using gas porosimeter, with nitrogen as working fluid (for filling the porous space), and permeability has been determined by gas permeameter measuring pressure drop during the air flow through the sample.

Formation resistivity factor was determined on brine saturated plugs.
If the sample is 100% brine saturated, formation resistivity factor (F) equals (Eq. 1) (Archie, 1941):

$$F = R_o/R_w \qquad (1)$$

where F is formation resistivity factor, R_o is 100 % brine saturated plug resistivity, R_w is brine resistivity.

Archie (1941) gave formation factor versus porosity correlation (Eq. 2)

$$F = a/\Phi^m \qquad (2)$$

where a is tortuosity factor (depending on the lithology), Φ is porosity, m is Archie's cementation exponent.

2.3 Grain size analysis

Due to the depth of samples, they were lithified, so hydrochloric acid treatment was necessary in order to remove carbonate cement. Remaining grains were mechanically sieved through sets of 11-15 sieves and every fraction's pass corresponds with its weight. Detailed grain size distribution information for each sample was provided. Problem of uneven sieve mesh size was solved by statistical resampling method due to various sieve manufacturers. At each sieve, mass percent of grain has been recorded. Then, for each mass percent, the number of grains (at the same proportion) can be assumed. This assumption allowed more extensive statistical analysis of grain size distribution parameters.

3. INTERPRETATION

As mentioned above, numerous equations which estimate permeability using detailed information on grain size distribution have been developed in the past

decades. All the parameters calculated to predict variations of permeability used in this study are derived from the core samples. Results of tested models are compared and the applicable correlation was established with proposed modification.

The Kozeny-Carman equation (Eq. 3) (proposed by Kozeny, 1927 and modified by Carman, 1937) presents the empirical base of many theoretical models which use porosity and grain size parameters to relate with permeability.

$$k = \frac{\rho_w g}{\mu} \frac{\phi^3}{(1-\phi)^2} \frac{d_m^2}{180} \qquad (3)$$

where k is permeability, ρ_w *is* fluid density, μ *is* fluid viscosity, Φ *is* porosity and d_m *is* representative grain size.

It describes single phase fluid permeability in porous media comparing Darcy's with Hagen-Poiseuille law for laminar flow of an incompressible fluid through cylindrical capillary. The main disadvantage of this equation is the choice of the representative grain size which can surely lead to permeability uncertainty.

Consequently, formulas that contain unique input data and give the best correlation of measured and predicted permeabilities are Beyer's and van Baaren's.

Beyer's equation (Eq. 4) (1964) is the only equation which uses uniformity coefficient instead of porosity term unlike some other equations.

$$k = C\, d_{10}^2 \qquad (4)$$

where k is permeability, C is empirical term equals $4.5x10^{-3}log(500/U)$, d_{10} is effective diameter, U is uniformity coefficient, d_{60}/d_{10}.

Van Baaren's model (1979) links various petrophysical parameters such as grain size, porosity and cementation exponent. These two equations (5 and 6) are easy and very practical to use because they contain practical parameters, directly measurable.

$$k = 20,2\,\phi^{5,1}\,d^2 \qquad (5)$$

$$k = 18,8\;\phi^{3,64+m}\;d^2 \qquad (6)$$

where *k* is permeability, *Φ* is porosity, *m is* Archie cementation exponent, *d* is mean grain diameter.

Cementation exponent *m* was calculated from the porosity and formation factor relation (Figure 1 a-b).

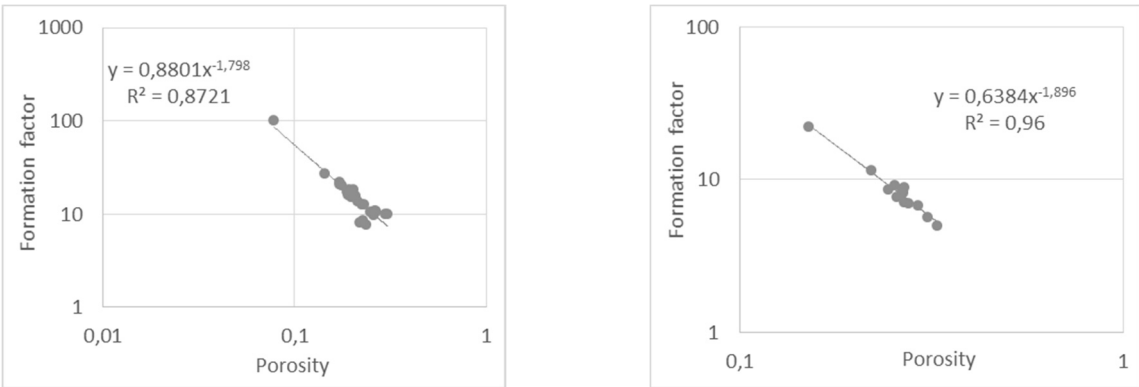

a) Lipovljani field b) Pavljani field

Figure 1: *Porosity and formation factor: calculating m*

In the following figures (Fig. 2 a-b and 3 a-b), correlations between measured and predicted permeability by the Beyer's and van Baaren's models are presented. Figure 2 a-b shows week correlations for both fields using Beyer's equation (Eq. 4). Figure 3 a-b and Figure 4 a-b show very good correlation using measured porosity and *m* calculated from formation resistivity factor test performed on each sample plug in the laboratory.

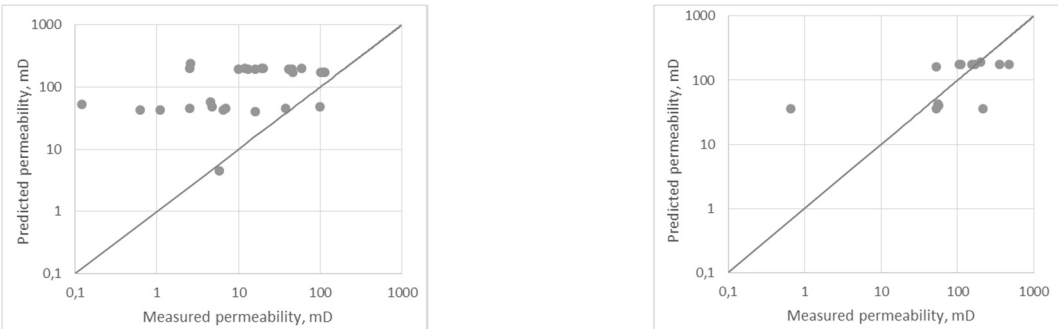

a) Lipovljani field b) Pavljani field

Figure 2: *Results obtained with Beyer's correlation*

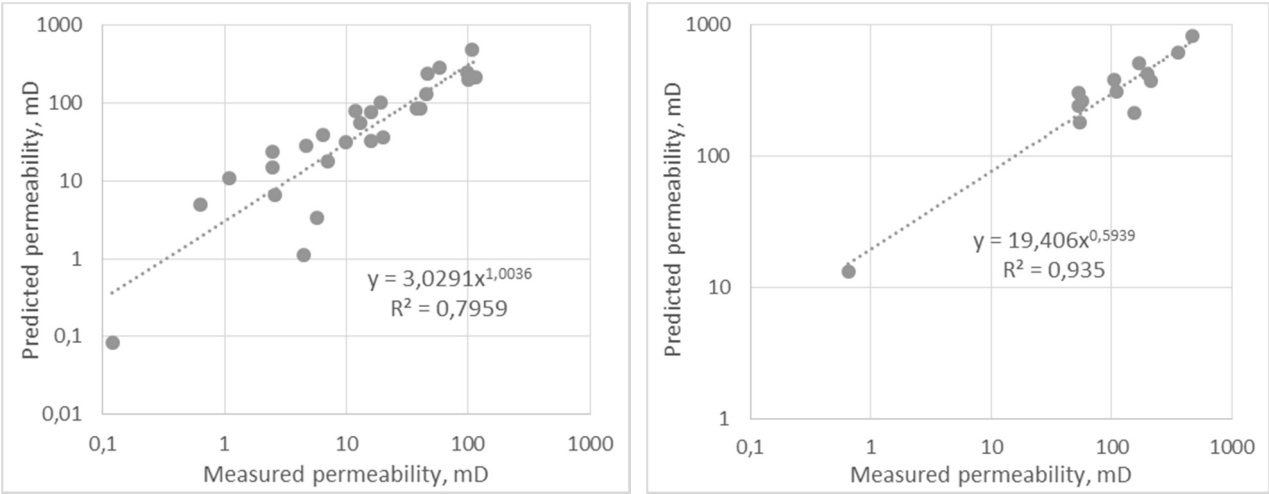

a) Lipovljani field b) Pavljani field

Figure 3: *Results obtained with van Baaren's correlation*

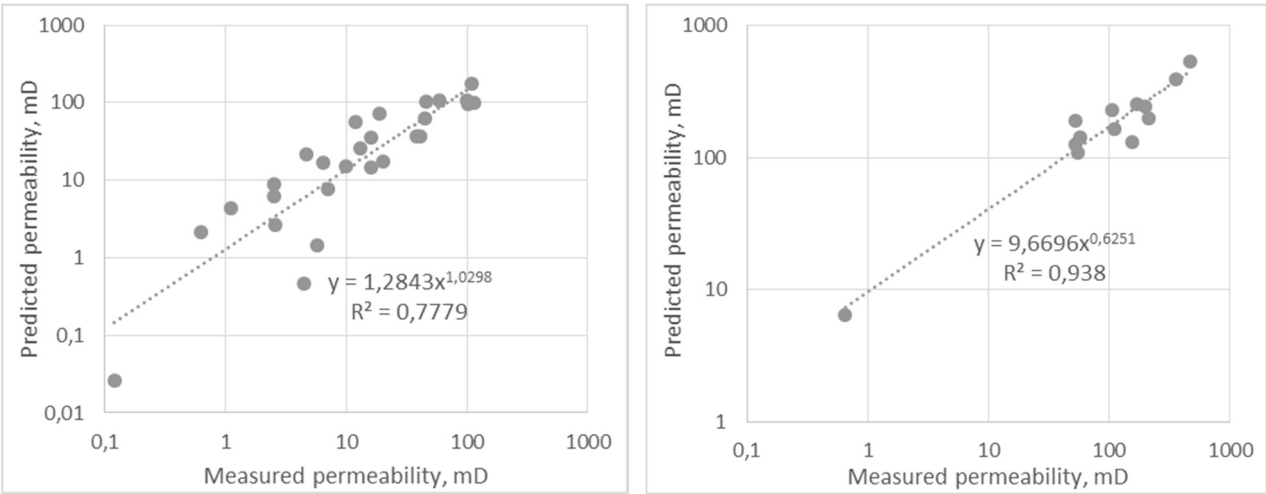

Lipovljani field Pavljani field

Figure 4: *Results obtained with van Baaren's equation, and by using porosity and m*

Despite these good results for both fields, modification of van Baaren's model (Eq. 6) was proposed in order to predict permeability where measured Archie's cementation exponent *m* is not available. Using regression analysis, the following equation (Eq. 7) was derived giving the best correlation using porosity and Archie's cementation exponent for each field (Figure 5 a-b) which was calculated from the porosity-formation factor relation (Figure 1 a-b):

$$k = 138,3\ \phi^{5,5+m}\ d^2 \qquad (7)$$

where *k* is permeability, *Φ* is porosity, *m is* Archie's cementation exponent, *d is* mean grain diameter.

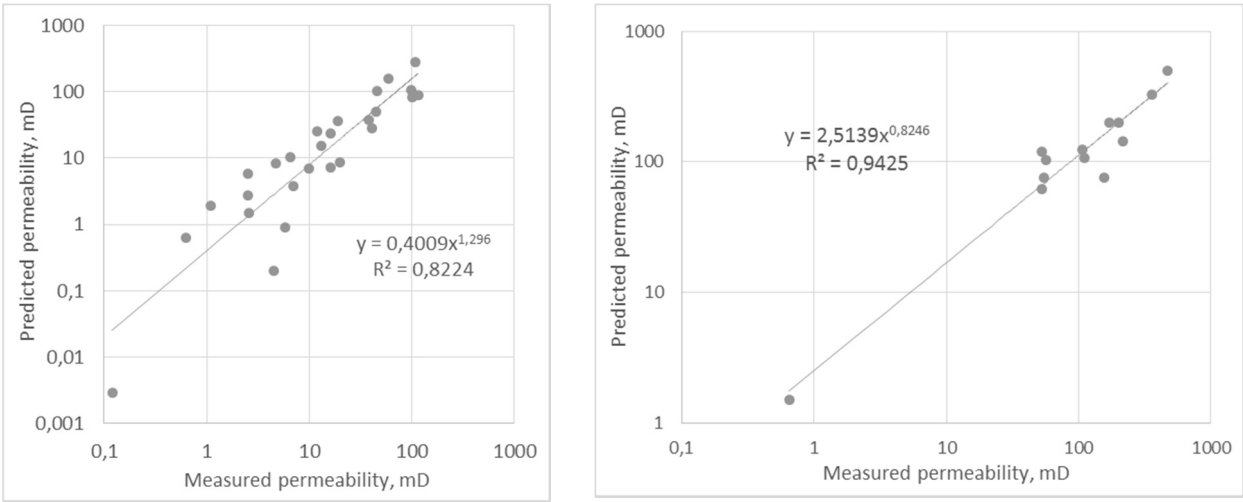

a) Lipovljani field b) Pavljani field

Figure 5. *Results with modified van Baaren's equation*

4. SUMMARY AND CONCLUSIONS

In this study, Beyer's and variants of van Baaren's equations for permeability estimation on Lipovljani and Pavljani oil fields were applied using experimental laboratory petrophysical data. The results show that Beyer's model is not suitable for tested consolidated sandstones samples. Though, van Baaren's models give reliable permeability estimation. Whereas there is no detailed data on physical properties of investigated fields, proposed modified van Baaren's equation for permeability estimation can be applied with high certainty.

5. REFERENCES

ARCHIE, G.E. (1941): The Electrical Resistivity Log as an Aid in Determining Some Reservoir Characteristics, Jour of Petrol Tech 5, Tech Pa. No 1422

BEYER, W. (1964): Zur Bestimmung der Wasserdurchlassigkeit von Kieson und Saunden aus der Kornverteilung. Wasserwirtschaft Wassertechnik 14, 165-169

CARMAN, P.C. (1937): Fluid Flow through Granular Beds. Transactions 15, 150, London: Institution of Chemical Engineers

KOZENY, J. (1927): Uber Kapillare Leitung des Wassers in Boden, Sitzungsber Akad. Wiss. Wien Mathematica Naturwiss 136, 271-306

van BAAREN, J. (1979): Quick-Look Permeability Estimates Using Sidewall Samples and Porosity Logs, Trans. 6th Annual European Logging Symposium, SPWLA, 1-10

Connectivity metrics and density-based clustering for uncertainty assessment

Noémi Jakab[1]

[1]University of Szeged, Department of Geology and Paleontology, Egyetem utca 2-6., 6722 Szeged, Hungary, j.noemi@geo.u-szeged.hu

The approach applied in this paper presents a way to characterize the uncertainty related to the outputs of a sequential Gaussian simulation. To assess the spatial uncertainty static connectivity attributes were used. These global metrics of connectivity also called geo-body or geo-object connectivity are derivative properties related to the overall structure of the simulated field. Based on these attributes stochastic images, which show the same characteristics from a statistical point of view, become distinguishable. The realizations of the sequential Gaussian simulation were then processed with the OPTICS (Ordering Points to Identify the Clustering Structure) algorithm, which is a density-based clustering method. The main advantages of this algorithm are the following: it does not require an a priori number of clusters to initialize, it is able to find arbitrarily shaped clusters, it is robust to outliers, has a notion of noise and it can handle data sets with large differences in densities.

Key words: *uncertainty assessment, sequential Gaussian simulation, connectivity, density-based clustering*

1. INTRODUCTION

Stochastic spatial simulations are widely used techniques to generate multiple, equally probable, alternative realizations of a spatial process and to assess the uncertainties related to it. Uncertainty is the result of the imperfectness of our knowledge when trying to characterize any spatial phenomenon. Therefore, it is an inherent feature of geological models. The importance of analysing, visualizing and communicating the uncertainty is unquestionable. However, a generally accepted unified approach has not been defined yet to perform this task.

The aim of this work is to present a novel method to characterize the model uncertainty by outlining subsets within the space of output realizations of a stochastic simulation. The presented approach utilizes static connectivity measures as the basis for differentiation between the individual stochastic images. To perform the subsetting, a density-based clustering method was applied on the stochastic images based on their connectivity attributes.

2. DATA AND METHODS

The input data originated from a slice of a CT image showing a core-size sedimentary structure. While the studied image itself holds low importance, such CT images can be viewed as analogues of the results of larger scale processes due to the fractal nature of the environment. Therefore, conclusions drawn from any study based on them can hold true invariant of the scale. The image and the corresponding dataset (**Figure 1**) consist of 16000 measured Hounsfield Unit (HU) values arranged on a regular 125 x 128 grid. From the exhaustive dataset, we retained a random set of 100 data locations and the corresponding values as hard conditioning data (**Figure 1**).

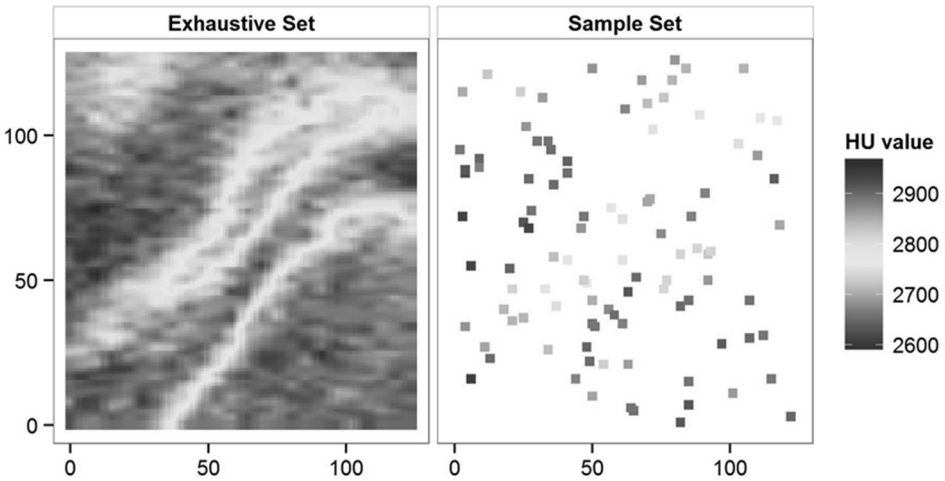

***Figure 6**: The exhaustive and the sample data set*

After transforming the data into the standard normal Gaussian distribution, the first step in the workflow (**Figure 2**) was the modelling of the variogram. The

aim of this step is to analyse and characterize the spatial continuity as well as to provide the required input values to the simulation system.

Using the variogram model and the normal score transform of the sample data set we performed a sequential Gaussian simulation as the next step. This type of simulation relies on the Gaussian model, which requires a parametric distribution. This entails the implicit assumption that the spatial variability of the studied attribute values can be fully characterized by a single covariance function (Isaaks, 1990, Gómez-Hernández and Srivastava, 1990).

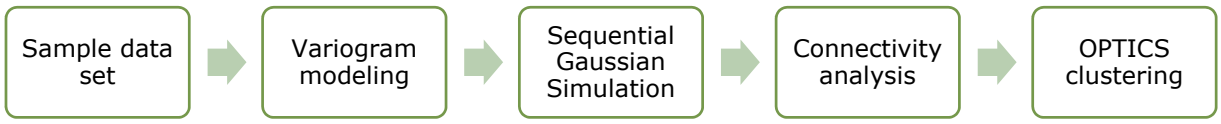

***Figure 7**: The applied workflow*

After the back-transform of the simulated normal score values, the following step in the workflow was to find attributes, which allowed discrimination between the realizations. To differentiate between the individual realizations different attributes had to be considered than the ones included in the simulation inputs. This can be explained by the fact that the simulation algorithm itself is constructed to produce outputs that replicate the modelled spatial continuity and the probability distribution of the conditioning data (Goovaerts, 1997).

To circumvent this difficulty, we can turn to the global metrics of connectivity, which are sometimes called geo-body or geo-object connectivity. These are derivative properties of the realizations not determined by the conditioning data**.** Geo-objects are groups of connected cells on a stratigraphic grid that have one or more rock property values that fall within given property ranges (Hovaldik and Larue, 2007). Based on these geo-objects, fields which otherwise show the same characteristics from a statistical point of view, become distinguishable (Renard and Allard, 2013).

There are several implementations from different authors available, such as the CONNEC3D by Pardo-Igúzquiza and Dowd (2003) or the code written by Deutsch (1998) to perform the static connectivity analysis. In this paper, we used the

landscape fragmentation statistics provided by the SDMTools R package, which is an implementation of FRAGSTATS by McGarigal et al. (2012). The approach identifies the connected geo-objects appearing in stochastic images in order to examine the geometric aspects of connected features. The connectivity analysis (**Figure 3**) consists of the following steps:

1. Define an attribute cut-off (binary indicator) of net cells
2. Scan through the field aggregating corner-, or edge-wise connected blocks of net cells
3. Collect all the identified geo-objects and their sizes for each realization in a data file

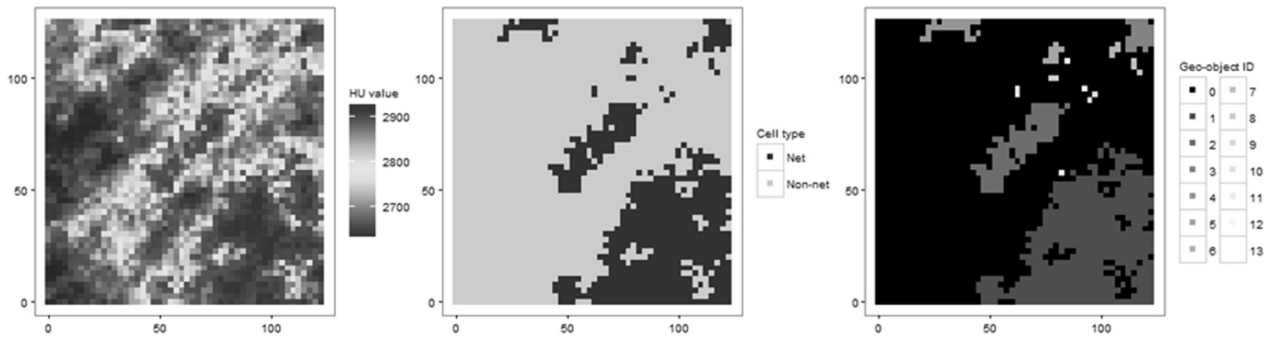

***Figure 8**: Steps of the connectivity analysis: a stochastic image (left), its indicator transform (middle) and the identified geo-objects (right)*

In the case of this data set, the indicator threshold defining net cells was set to 2700 Hounsfield Units, because values below this correspond to the highest valued porosities on the CT images. The result of the connectivity analysis was a data file containing the number of geo-objects occurring in each realization along with several different parameters of these geo-objects, such as the number of cells and core cells for each, perimeter, etc. For our further analyses, only the parameters of the largest geo-object on each stochastic image were used and redundant connectivity attributes (e.g. attributes which showed a correlation coefficient greater than 0.9 with other attributes) were removed. Based on the remaining attributes the dissimilarities of the data points representing the stochastic images were calculated.

The last step in the workflow was the density-based clustering of the stochastic images based on these dissimilarities. When applying density based approaches, clusters are regarded as regions in the data space in which objects are dense, and which are separated by regions of low object density (noise). From the available density-based clustering methods we utilized the OPTICS algorithm (Ankerst et al., 1999), which has the following advantages over the traditional clustering methods: (1) it does not require the user to specify the number or clusters *a priori*, (2) it can find arbitrarily shaped clusters, (3) it has a notion of noise while it is robust to outliers, (4) it requires only two parameters, which are easy to determine, if the data is well understood, and (5) it can handle data sets with large differences in densities.

The two required parameters for the initialization of the algorithm are ε and *MinPts*. Parameter ε is an upper limit of the search radius when looking for objects to build a cluster, and *MinPts* is the required number of objects within the search radius for forming the cluster. The algorithm does not produce a clustering of a data set explicitly; instead, it creates a graph of the database objects (the stochastic images in this case) representing their density-based clustering structure. The x-axis of this graph shows such an ordering of the database in which data points which are spatially close in the feature space remain close the ordering. At the same time, the corresponding values on the y-axis give the so-called reachability distance. This value essentially represents the smallest ε for which a neighbourhood with at least *MinPts* other data points exists for given point on the x-axis. This representation of the clustering structure is the reachability-plot: since points belonging to a cluster are close to each other and have low reachability distances, the clusters show up as valleys in the reachability plot.

3. RESULTS

The results coming from the method provide several insights about the model uncertainty and the clustering structure of the stochastic images. Firstly, the findings suggest that the level of uncertainty, which is expressed by the number of extractable clusters changes with the number of realizations. When running

the OPTICS analysis with the *MinPts* parameter set to 10, in the case of 20 realizations, only one cluster of 13 members is extractable. With the increase of the number of realizations, this structure slowly starts to change, and at 50 realizations a second cluster emerges. This clustering structure remains stable with minor changes (additional realizations merging into the existing clusters, and the forming of a smaller valley indicating a possible new cluster, but still with a lower number of members than the given *MinPts* parameter) until reaching 100 realizations. At this point, the third cluster appears, and moving further at 160 realizations another fourth cluster shows up.

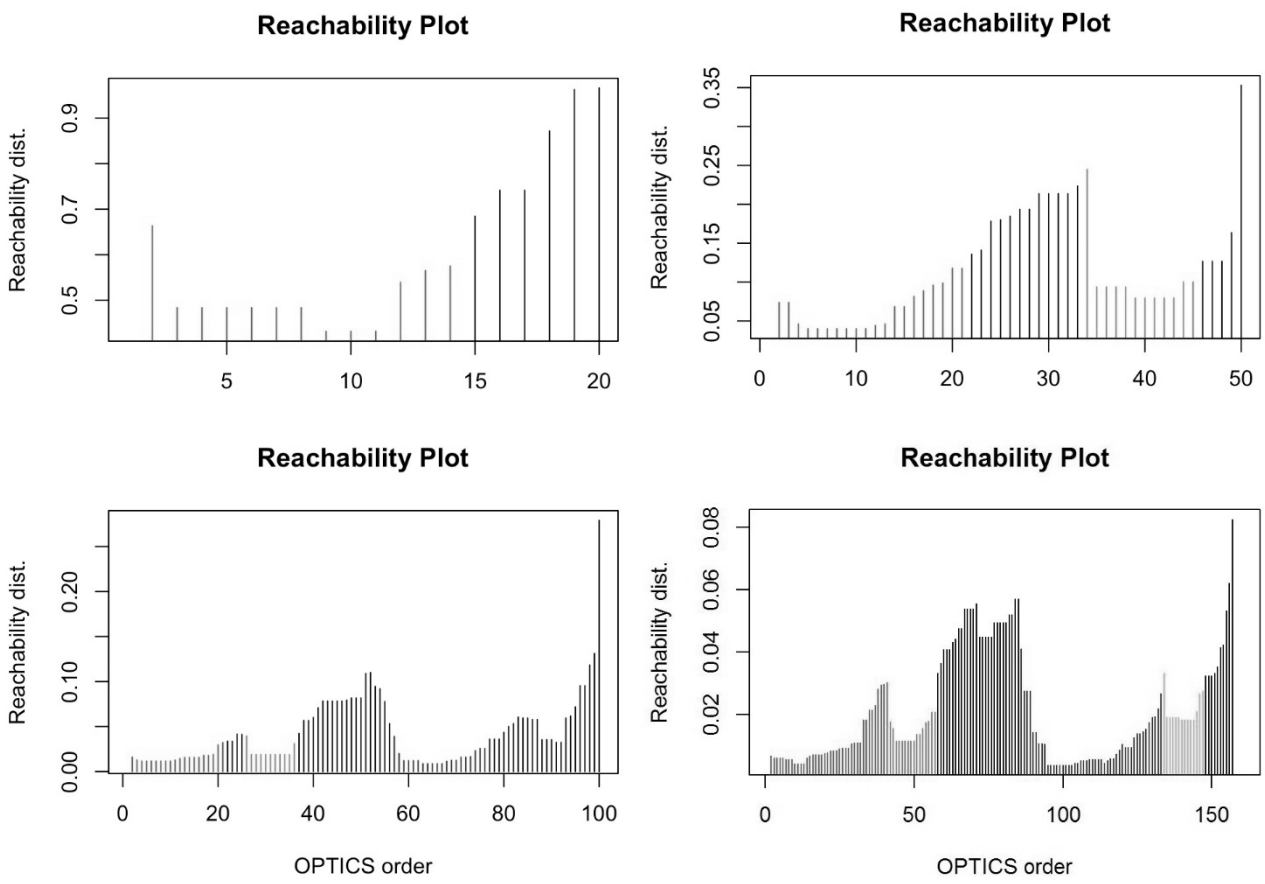

***Figure 9**: Reachability plots for 20, 50, 100 and 160 realizations*

Another useful feature of the reachability plot is that it also highlights the hierarchical structure of the clusters. On **Figure 4** we can examine the hierarchy of the four clusters identified from the 160 realizations. In fact, these are two

sub-clusters of the two larger clusters separated by the noise at the middle part of the reachability plot.

Looking at the maps of the probability values of net cells for each cluster, it is also evident that the groups extracted this way represent characteristically different scenarios, and have a meaning from the practical point of view. For example, the three scenarios extracted from 100 realizations provide a low, a medium and a high estimate about the global spread of net cells (**Figure 5**).

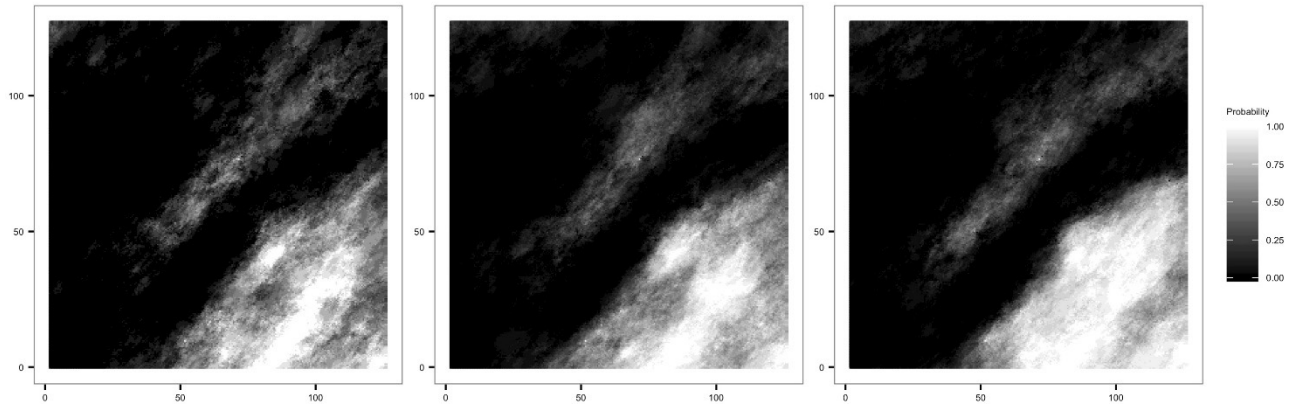

***Figure 10**: The extracted scenarios from 100 realizations*

4. DISCUSSION AND CONCLUSIONS

The presented method enables the practitioner to extract characteristically different scenarios from the outputs of a stochastic simulation. The scenarios generated this way are meaningful subsets: they present greatly differing pictures about the connectivity features, thus, they also represent significant differences in flow properties.

Since the applied density-based clustering method does not require an *a priori* given number of clusters, it facilitates the extraction of groups which are naturally present in the feature space. This prevents forcing any assumption about the number of clusters onto the results, thereby the method is able to highlight the relationship between the number of realizations, the number of extractable clusters and the uncertainty without any bias.

Another advantage of the method is that it is able to reflect the hierarchy of the clustering structure while providing a more straightforward overview about the data than the traditional hierarchical clustering methods. This is especially true when the number of observations is high.

5. REFERENCES

ANKERST, M., BREUNIG, M.M., KRIEGEL, H.-P. & SANDER, J. (1999): OPTICS, ACM SIGMOD Record, 28(2), pp. 49–60.

DEUTSCH, C.V. (1998) Fortran programs for calculating connectivity of three-dimensional numerical models and for ranking multiple realizations, Computers & Geosciences, 24(1), pp. 69–76.

GOOVAERTS, P. (1997) Geostatistics for natural resources evaluation. 1st edn. United States: Oxford University Press Inc.

HOVADIK, J.M. & LARUE, D.K. (2007) Static characterizations of reservoirs: refining the concepts of connectivity and continuity, Petroleum Geoscience, 13(3), pp. 195–211.

ISAAKS, E.H. (1990) The Application of Monte Carlo Methods to the Analysis of Spatially Correlated Data. PhD Thesis. Stanford University.

JAIME GÓMEZ-HERNÁNDEZ, J. & MOHAN SRIVASTAVA, R. (1990) ISIM3D: An ANSI-C three-dimensional multiple indicator conditional simulation program, Computers & Geosciences, 16(4), pp. 395–440.

MCGARIGAL, K., S.A. CUSHMAN, & E ENE. (2012) FRAGSTATS v4: Spatial Pattern Analysis Program for Categorical and Continuous Maps. Computer software program produced by the authors at the University of Massachusetts, Amherst. Available at the following website: http://www.umass.edu/landeco/research/fragstats/fragstats.html

PARDO-IGÚZQUIZA, E. & DOWD, P.A. (2003) CONNEC3D: a computer program for connectivity analysis of 3D random set models, Computers & Geosciences, 29(6), pp. 775–785.

RENARD, P. & ALLARD, D. (2013) Connectivity metrics for subsurface flow and transport, Advances in Water Resources, 51, pp. 168–196.

Spatial structure analysis of a geological map for digital soil mapping purposes

Piroska Kassai[1], István Sisák[1]

[1]University of Pannonia, Georgikon Faculty, Department of Plant Production and Soil Science

H-8360 Keszthely, Deák Ferenc u. 16, Hungary, piroska.kassai@gmail.com

The aim of this study was to develop a quantitative method to extract information from geological maps which can be used as input in digital soil mapping (DSM). Detailed soil information is strongly needed in various areas of applications. It would be particularly important to create detailed soil maps for the watershed of Lake Balaton to assess diffuse loads. DSM means computer-assisted prediction of soil type and soil property maps with help of a variety of statistical models that combine soil observations with ancillary data on soil forming factors. The study contributes to this current methodological development by bringing in geological information. Geological formations and soil types did not correlate directly, but spatially continuous, lithologically homogeneous groups of categories make geological data useful. This study demonstrates a quantitative method how to combine geological information into categories for DSM.

The geological map of the watershed of Lake Balaton was analysed. This assessed map was derived from 1:100 000 scale surface geology map using polygon clipping. Boundary line segments of neighbouring polygons have been evaluated and Chi-squared method was used to produce a neighbourhood grade matrix. The geological formations were classified based on spatial pattern and lithological features using two step clustering method. This newly developed geological map will be the basis of a detailed predictive soil map in the future.

Key words: *boundary segment based Chi-square calculation, digital soil mapping, geology quantification, two step clustering, watershed of Lake Balaton*

1. INTRODUCTION

The watershed area of Lake Balaton was already examined in detail from different aspects. For environmental reasons it would be particularly important to create fine scale soil information. With the help of which, diffuse phosphorus loads due to erosion and runoff processes could be more accurately identified. Traditionally soil survey is considered to be very expensive, DSM is used increasingly in mapping soil types and soil properties. With help of DSM, soil maps can be created at lower costs in less time and with steadily increasing accuracy as the methodology improves. DSM uses the available soil mapping data and other ancillary data to represent soil formation. As geology is one of the most important factors it is crucial to take it into account.

Geological maps can provide a vast amount of information but only a part of this can be used in soil prediction. On the watershed of Lake Balaton, 143 different geological formations were described, but significantly less soil types (16 soil types and 30 subtypes) are distinguished. Geological units are traditionally classified on the basis of their age and genesis, lithologically very similar rocks may have been formed in different ways. In the light of soil formation these genetic differences are irrelevant thus it is obvious, that geology formations have to be fused into broad categories. Nevertheless, it should be mentioned that the same scale soil maps (AGROTOPO, MÉM-NAK) are clearly less detailed than the 1:100 000 scale geology map and based on the number of the polygons and their average size the right scale is much smaller than the one at which maps were drawn (BENŐ, 2014). However, this cannot be the sole reason of the fact that much more geology units are defined on the area than soil forming rocks and because of this it is an important step to simplify the geology map and make geological data usable for DSM. The goal of this study was to develop a quantitative method on how to combine geological information into categories which can be used as an input in digital soil mapping to produce detailed soil maps in the future.

2. MATERIAL AND METHODS

The geological map of the watershed of Lake Balaton was analysed. This assessed map was derived from 1:100 000 scale surface geology map published by the Geological Institute of Hungary (PELIKÁN&PEREGI 2005). ArcGIS 10.0 was used for map data handling and interpretation and SPSS 13.0 for data analysis.

The most detailed soil type maps for this area which are available in digital format are the AGROTOPO database (1:100 000) and the MÉM-NAK genetic soil map (1:200 000). These soil maps were compiled in the 1970s-80s. The 1:100 000 scale geology map was not available during the compilation of these maps as it was published in 2005. Geology is usually taken into account while drawing soil polygon boundaries. The 1:100 000 scale geology map provides more recent and spatially more accurate information so it should be used in creating more detailed soil maps.

In the first step a neighbourhood matrix was created using the method of a previous analysis (SISÁK et al. 2015) The length of each line segment between the geology unit polygons was determined. The outer boundary line of the watershed and the border lines with lakes were not considered since only one of the neighbouring polygons had geology data. Then the sum of lengths for each geology unit combinations was calculated and thus, a square matrix with dimensions of 143 by 143 was created. Then the following theoretical length for each matrix element was calculated:

$$L_{ij\text{-}est} = \Sigma L_i \times \Sigma L_j / L_{tot},$$

where $L_{ij\text{-}est}$ = the estimated length for an individual category combination, L_i = the total length of the $i^{\text{-th}}$ category in the rows of the matrix, L_j = the total length of the $j^{\text{-th}}$ category in the columns of the matrix, L_{tot} = the total length of all categories (grand total of the matrix). Then the following P similarity (neighbourhood) matrix was calculated:

$$P_{ij} = \log [(L_{ij} / L_{ij\text{-}est})) \times 100],$$

where L_{ij} = the actual length for an individual category combination. This is the logarithm of the percent ratio between actual and theoretical lengths. Zero values in the main diagonal and missing combinations have no logarithm thus, in this similarity matrix complete similarity (main diagonal) and complete dissimilarity (non-existent combinations) cannot be distinguished. To alleviate this problem the similarity (neighbourhood) matrix was converted into $P`_{ij}$ dissimilarity (distance) matrix. All length ratios were less than ten billion thus, 10 (= $\log 10^{10}$) was selected as the maximum dissimilarity.

With help of this dissimilarity matrix it can be identify which of the 143 geological units are found next to each other and how much is the probability of the neighbourhood pairs compared to the theoretical probability calculated from the distribution of the category border lengths.

As an addition to the statistical approach, a combined approach was also applied. 31 geological categories out of the 143 geological formations were created based on their lithological importance as soil parent materials (**Table 1**). During this categorisation, the age and the genesis of rocks were not considered. As the dissimilarity matrix contains continuous variables and geological categories are categorical variables, a method was needed which can handle both. Thus, a two-step cluster analysis (SPSS 13.0) was conducted for the classification of the 143 units.

Table 1: *the 31 categories of the 143 formations based on lithological features*

	lithology		**lithology**
1	clay	17	basalt
2	silt	18	kaolinite
3	sand	19	geyserite
4	gravel	20	acid metavolcanoclastic rock
5	varied clastic sediments (clay, silt, sand, gravel)	21	bauxite
6	fine clastic sediments (clay and silt)	22	shale
7	coarse clastic sediments (gravel and sand)	23	quartzite
8	loess	24	alginite
9	sandstone	25	limestone with flint and tuff
10	limestone	26	thermal spring sediment
11	limestone with flint	27	fine clastic sediment with peat
12	dolomite	28	lime mud
13	mixed carbonate rocks (dolomite and limestone)	29	lime mud and silt
14	varied clastic rocks (with carbonate content)	30	red clay
15	marl (and other carbonate rocks with fine clasts)	31	anthropogenic formations
16	carbonatic rocks with coarse clasts		

3. RESULTS AND DISCUSSION

First, the clustering of the 143 units was carried using the two kinds of variables (categorical and continuous) at the same time. However, the result of this clustering has not been satisfactory because the final units were too diverse. This was solved with carrying out a clustering solely for the continuous variables (distance matrix). The cluster number was set based on the cluster quality graph (**Figure 1**). The aim was to achieve acceptable number of clusters, thus it was set to 60. Then, the variable with 60 clusters and the variable representing 31 geological categories were used in another two step cluster analysis to achieve a set of combined categories representing both aspects.

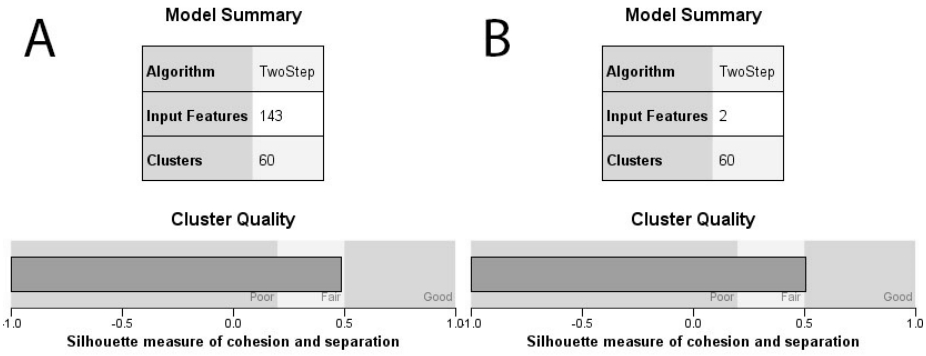

Figure 1: *A: the cluster quality of the clustering the continuous variables (distance matrix), B: the cluster quality of the clustering the two categorical variables (lithology categories and clusters derived from the distance matrix)*

With this clustering, 45 of the final groups contain lithologically homogeneous units. The remaining 15 included mainly those units which were already categorised as independent geological categories at the beginning of the analysis. These units cannot be combined with any other units based on their lytholgical features (for example, Gánt Bauxite Formation, Pula Alginite Formation…etc.) This shortcoming of the clustering was solved by separating the independent geological categories from these clusters. Then, the clustering result was added to the map and after that further lythologically same clusters could be combined based on their spatial proximity with weak or non-existent neighbourhood.

With the result of this analysis, the 143 geological units were reduced to 43 lythologically homogeneous cluster (**Figure 2**). However the number of polygons was only slightly reduced because of the fractured geology of the hills north of the lake.

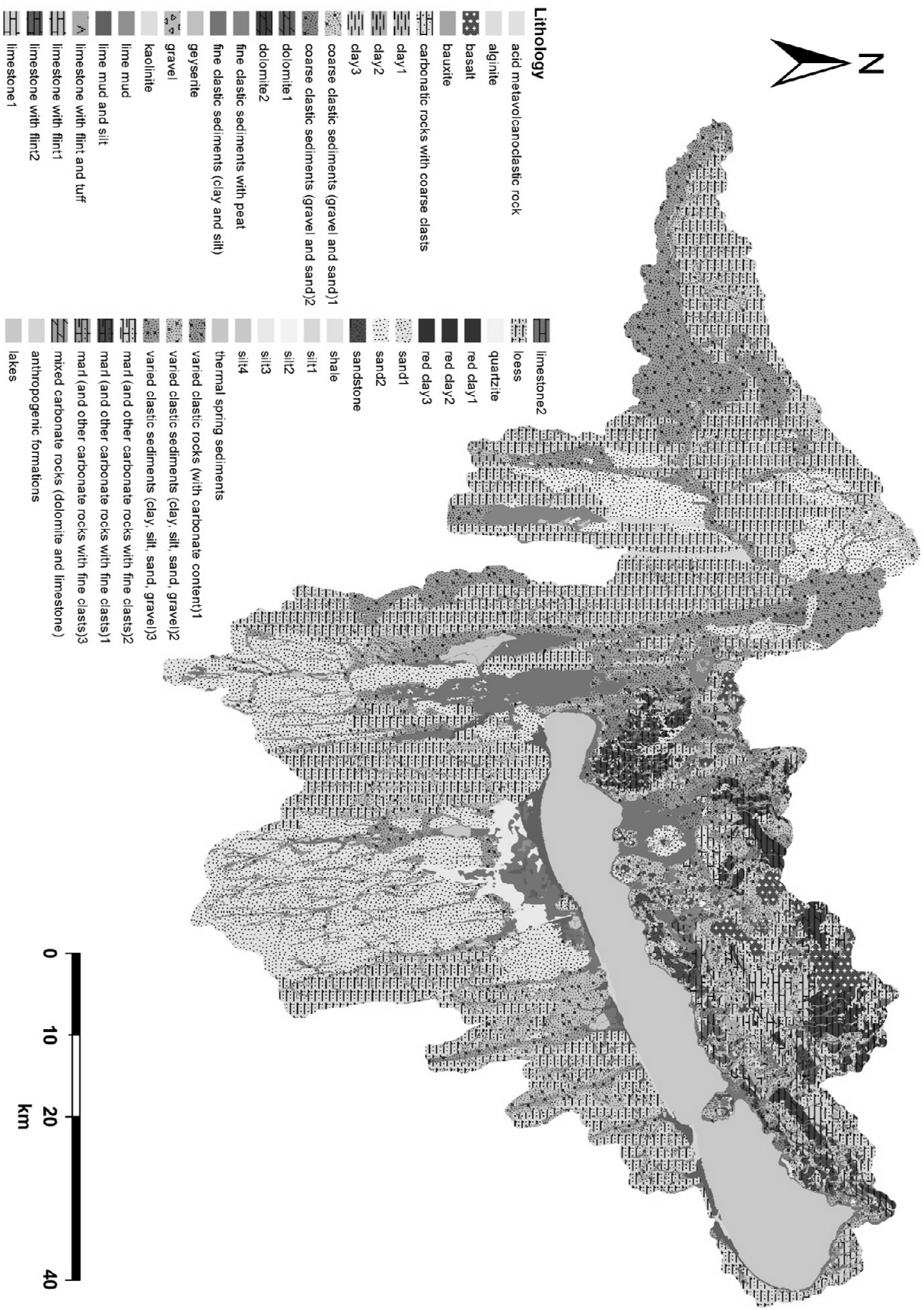

Figure 2: *the simplified geology map of the watershed of Lake Balaton*

REFERENCES

BENŐ, A. (2014): Egy országos talajtérkép digitalizálása, publikálása a Georgikon Térképszerveren, és felhasználása integrált talajtérkép létrehozására. *(Digital publication of a nationwide soil map and creating a conceptual soil map– in Hungarien)*.–Unpub. BSC Thesis, Georgikon Faculty, Department of Plant Production and Soil Science, University of Pannonia, Keszthely, 51 p.

MÉM (1983–1988): Magyarország agrotopográfiai térképe 1:100 000 *(Agrotopographic map of Hungary).* Budapest, MÉM Országos Földügyi és Térképészeti Hivatal, 84 térképlap (mapsheet), 51x 66 cm.

MÉM-NAK (1983): Magyarország genetikai talajtérképe 1:200 000 *(Genetic soil map of Hungary)* Budapest, Mezőgazdasági és Élelmezésügyi Minisztérium.

PELIKÁN, P., PEREGI, Zs. (2005): Magyarország földtani térképe *(Surface geology map of Hungary)* 1:100 000, Magyar Állami Földtani Intézet http://mafiloczy.mafi.hu/Fdt100/

SISÁK, S., KOCSIS, M., BENŐ, A., VÁRSZEGI, G. (2015): Method development to extract spatial association structure from soil polygon maps. Hungarian Geographical Bulletin 64, 1, 65–78.

Experimental investigation of stress-dependent petrophysical behaviour of reservoir rocks

Péter János Koroncz[1], Ferenc Fedor[2]

[1]GEOCHEM Ltd, LotNo: 0222/35, Kővágószőlős, Hungary, koroncz.peter@geochem-ltd.eu

Effective stress can have a great effect on petrophysical and geomechanical behaviour of reservoir rocks. The aim of this study was to investigate the stress sensitive behaviour of different kinds of reservoir rocks from the Carpathian Basin.

For this purpose, detailed laboratory analysis was performed to investigate porosity, permeability and ultrasonic velocity as a function of confining pressure in the range of 5-50 MPa.

Our results indicated a significant decrease of porosity and permeability and the increase of acoustic wave velocity with the increase of hydrostatic stress. Comparing loading and unloading cycles hysteresis was observed in the case of compressional and shear wave velocities respectively.

Key words: *Petrophysics, rock mechanics, porosity, permeability, ultrasonic velocity*

1. SAMPLES AND TEST METHODS

Six sandstone samples were selected from Hungarian hydrocarbon reservoirs for studying the effect of pressure on porosity, permeability and acoustic properties in laboratory. Measurements were performed on cylindrical plugs in a high pressure hydrostatic cell, applying confining pressure in the range of 5-50 MPa using 5 MPa pressure steps. Since pore pressure was kept 0 MPa during the measurement, confining pressure is equal with effective pressure. Before the measurements, samples were dried at 80°C for 72 hours and stored in desiccator.

Porosity and Klinkenberg permeability were measured with Vinci Technologies Coreval 700 instrument following API 40 recommendations (API, 1998).

For the determination of ultrasonic wave velocities and dynamic elastic parameters a new equipment was developed based on pulse-transmission

method. The central frequency of the transducers was 1 MHz in the case of compressional and shear waves respectively. For an accurate and exact determination of flying times (Figure 1), a new algorithm was developed based on Akaike Information Criteria (Akaike, 1973). The accuracy of the system was tested on reference aluminium plugs.

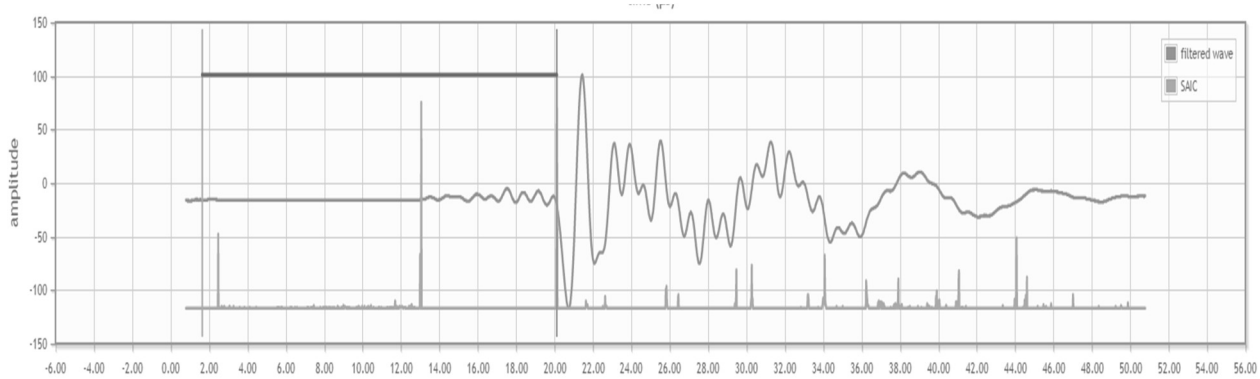

Figure 1: *Automatic first break "pick up" of S-wave for determination of flying time.*

In the case of isotropic and linear elastic media dynamic elastic moduli can be calculated as follows (ASTM, 1997a):

$$E_{dyn} = \frac{\rho \cdot V_S^2 (3V_P^2 - 4V_S^2)}{(V_P^2 - V_S^2)}$$

for Young's modulus (E) and

$$\nu_{dyn} = \frac{V_P^2 - 2V_S^2}{2(V_P^2 - V_S^2)}$$

for Poisson's ratio (ν), where V_P and V_S are the compressional and shear wave velocities and ρ is the bulk density of the sample.

2. RESULTS

Table 1: *Test results at 5 MPa and 50 MPa*

Sample	P [MPa]	φ(%)	K∞(mD)	Vp [m/sec]	Vs [m/sec]	Poisson [-]	Young [GPa]
S-01	5	11,52	0,27	2904	1979	0,07	18,6
	50	10,57	0,16	3995	2618	0,09	22,8
S-02	5	19,5	20,48	2755	1769	0,15	14,5
	50	18,68	17,21	3516	2251	0,15	16,7
S-03	5	11,85	1,9	2931	1926	0,12	18,4
	50	11,23	1,54	4004	2604	0,10	21,1
S-04	5	10,11	0,05	3511	2331	0,11	27,9
	50	9,27	0,02	4334	2813	0,10	30,0
S-05	5	17,91	9,66	3130	1939	0,19	17,9
	50	17,14	8,27	3787	2366	0,19	20,0
S-06	5	30,57	457,83	2174	1343	0,19	7,4
	50	28,01	387,4	2732	1741	0,21	7,4

Table 1 summarizes porosity, permeability, acoustic wave velocity and calculated elastic parameter data measured at 5 MPa and 50 MPa confining pressure. During permeability, measurement of the S-06 sample (marked with green dots) a damage phenomena could be observed. For the comparison of stress sensitive behaviour of the studied samples, each petrophysical parameter was normalized with the initial value (Figure 2). In this case initial pressure was 5 MPa. The results indicated that in case of individual samples the parameters show different responses to effective stress. Furthermore, the change of parameters have non-linear characteristic.

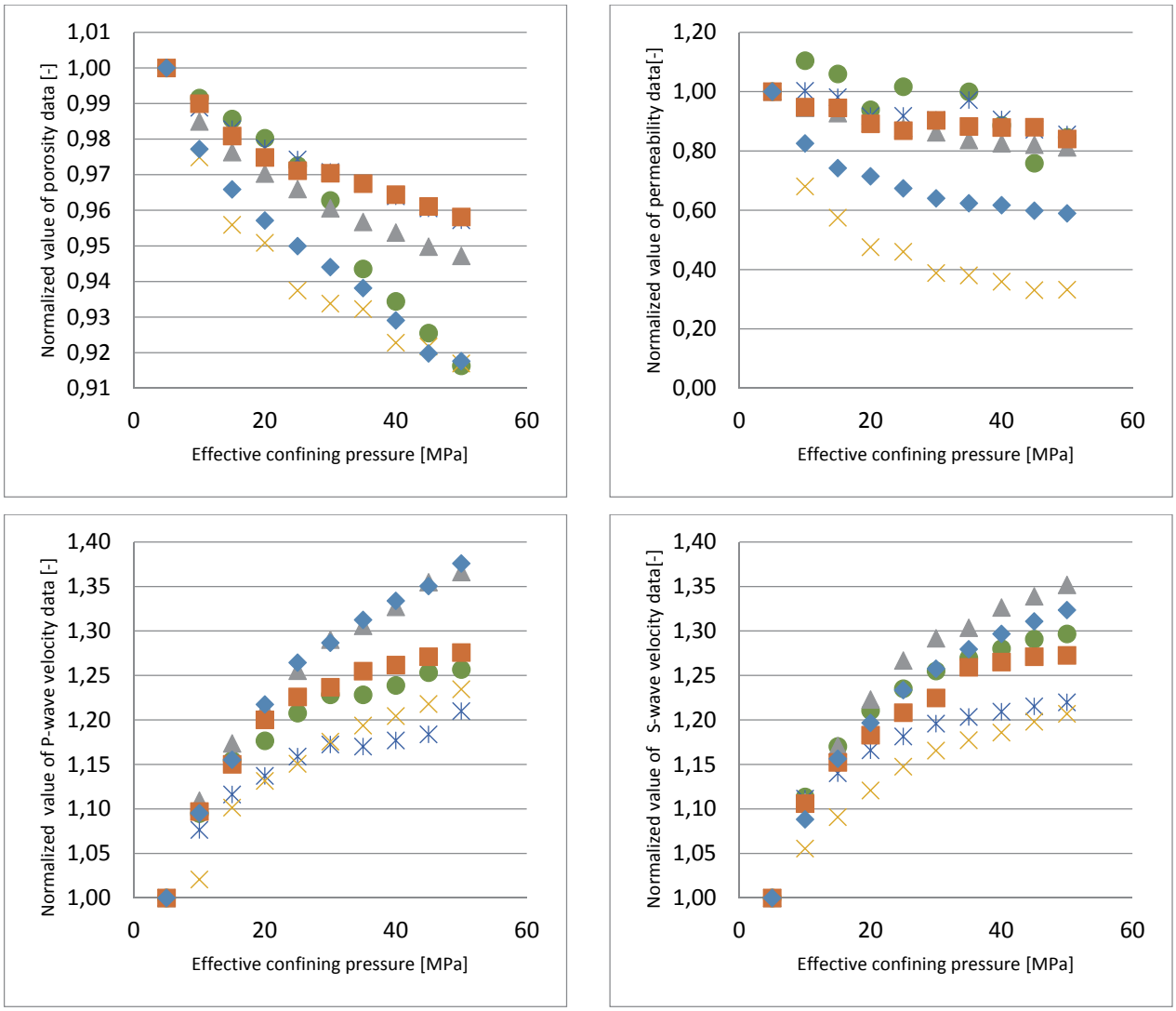

Figure 2: *Plots of normalized porosity, permeability, compressional and shear wave velocities as a function of confining pressure*

For the comparison of stress sensitive behaviour of different petrophysical parameters, the correlation was analyzed between normalized variables for each sample (Table 2).

Table 2: *Correlation between normalized variables*

	p-φ	p-k∞	p-Vp	p-Vs	φ-k∞	φ-VP	φ-VS	k∞-VP	k∞-VS	k∞-E
S-01	-0,978	-0,892	0,959	0,948	0,961	-0,989	-0,986	-0,977	-0,986	-0,972
S-02	-0,956	-0,871	0,905	0,920	0,946	-0,985	-0,984	-0,944	-0,927	-0,944
S-03	-0,966	-0,968	0,954	0,937	0,996	-0,999	-0,993	-0,993	-0,989	-0,995
S-04	-0,937	-0,868	0,958	0,954	0,977	-0,982	-0,994	-0,941	-0,970	-0,945
S-05	-0,978	-0,851	0,903	0,865	0,850	-0,971	-0,950	-0,817	-0,757	-0,797
S-06	-0,990	-0,808	0,900	0,906	0,807	-0,844	-0,854	-0,619	-0,621	-0,641

Although very limited data is available, it is important to note that very high correlation could be observed in the rate of change between different independent variables.

3. SUMMARY

The pressure sensitivity of petrophysical parameters was investigated on six sandstone samples from various Hungarian reservoirs with different depth intervals.

Stress sensitivity of petrophysical parameters exhibit strong correlation in the case of individual samples.

Due to acoustic instrument development the accuracy of ultrasonic velocity measurements could be improved to a great extent.

In the further research it is important to study these relationships in the field scale.

References:

AKAIKE, H. (1973): Information theory and an extension of the maximum likelihood principle. –In B. N. Petrov and F. Csaki (Eds.),Second international symposium on information theory. Academiai Kiado, Budapest, 267-281

API RP 40, Recommended Practices for Core Analysis, second edition. 1998. Washington, DC: API.

ASTM 1997a. Laboratory determination of pulse velocities and ultrasonic elastic constants of rock (D2845-95). In 1997 Annual Book of ASTM Standards, Vol. 4.08. American Society for Testing and Materials (ASTM), Philadelphia, Pa. pp. 254–259.

Influence of dissolved oxygen on nitrates concentration in Zagreb aquifer

Zoran Kovač[1], Krešimir Pavlić[1] and Zoran Nakić[1]

[1]University of Zagreb, Faculty of Mining, Geology and Petroleum Engineering, Pierottijeva 6, 10000 Zagreb, Croatia, zoran.kovac@rgn.hr

Nitrates present one of the most common and widespread groundwater pollutants in the world. Although there are numerous potential sources of nitrates, lot of studies showed high correlation between agriculture and the concentration of nitrates in groundwater. Nitrates are defined as one of the five main groups of contaminants in the study area. Zagreb aquifer is designated as part of the country`s strategic water reserves, protected by the Croatian State. It is the main source of potable water for the inhabitants of the City of Zagreb and Zagreb County. Nitrates concentration depend on the aerobic and anaerobic conditions in the aquifer. Even though there are several indicators of the aerobic and anaerobic conditions in the groundwater, concentrations of dissolved oxygen present the most important one. Most research has shown that the boundary among aerobic and anaerobic conditions is between 1 and 2 mg l^{-1} O_2. The goal of this work was to estimate the influence of dissolved oxygen on nitrates concentration using parametric (Pearson) and nonparametric (Spearman) correlation coefficients. T-test was used for the calculation of correlation coefficients statistical significance (α=0.05). Chemical substance analysed mostly from national monitoring programme of the Croatian Waters, for 166 observation wells were analysed. Analyses mostly date from 1991 to 2015. Both correlation coefficients showed that there is good to very good positive, statistically significant correlation between two variables what indicates that natural conditions in the Zagreb aquifer have influence on the stability of nitrates concentration in groundwater.

Key words: *Dissolved oxygen, nitrates, Zagreb aquifer, correlation*

1. INTRODUCTION

Nitrates present one of the most common groundwater contaminants in the world (Pena-Haro et al., 2009). They don`t have the ability to bond on soil by adsorption and are subject to leaching due to infiltration of precipitation, which results in their infiltration to deeper soil layers and groundwater (Mkandawire, 2008). Even though numerous studies showed strong relationship between agricultural activity and the concentration of nitrates in groundwater (Pena-haro et al., 2009; Li et al., 2010; Hosono et al., 2013), there are also some natural factors that have influence on their transformation, stability and mobility through the unsaturated- and saturated zone. Aller et al. (1987) reported seven main parameters that control groundwater pollution potential: depth to aquifer, recharge, aquifer media, soil media, topography, impact of vadose zone media and hydraulic conductivity, while Lake et al. (2003) determined four different parameters that have influence on groundwater vulnerability to nitrate pollution: surface leaching, soil characteristics, drift cover and aquifer type. Nitrates leaching from unsaturated zone is the consequence of complex interaction between many factors, e.g. land use practice, on-ground nitrogen loading, recharge, soil characteristics and nitrogen dynamics and depth to water table (Almasri, 2003; 2007). When nitrates reach groundwater, they depend on transport processes such as advection, dispersion or diffusion. Also, geochemical processes, such as denitrification, and aerobic or anaerobic conditions play major role in stability of different nitrogen compounds in groundwater. Dimkić et al. (2008) stated that nitrates are found in predominantly aerobic media, where they have high mobility. Even though there are different indicators of aerobic and anaerobic conditions, concentrations of dissolved oxygen present the most important one. Dimkić et al. (2008) suggested that predominantly aerobic conditions prevail in groundwater where concentrations of dissolved oxygen are greater than 1 mg l^{-1}.

The goal of this work was to estimate the influence of dissolved oxygen on nitrates concentration using correlation coefficients. Pearson *r* and Spearman *ρ* correlation coefficients were calculated for average, maximum and minimum

concentrations of dissolved oxygen and nitrates which were recorded in the research area, while statistical significance was calculated using *t-test* (α=0.05).

2. RESEARCH AREA

Zagreb aquifer is located in the northwest part of the Republic of Croatia. Groundwater from the Zagreb aquifer is the only source of potable water for inhabitants of the City of Zagreb and part of Zagreb County. It is designated as part of the country`s strategic water reserves. Nitrates present one of five main groups of contaminants in the groundwater of the research area (Nakić et al., 2013). It consist of two Quaternary aquifers, deposited during the Middle and Upper Pleistocene and Holocene (Velić and Durn, 1993; Velić et al., 1999). Aquifers present single hydrogeological unit, but indicate geochemical stratification along the depth (Marković et al., 2013). In hydrogeological terms, Quaternary deposits consist of three units. The overburden is made of silt and clay, a shallow aquifer is made of gravel with sand, while deeper aquifer is characterised with lateral and vertical alterations of sand, gravel and clay (Nakić et al., 2013). Zagreb aquifer is an unconfined aquifer with main groundwater flow from W/NW to E/SE. It is in direct contact with Sava River, which presents the main source of recharge. Miletić and Bačani (1999) showed using water balance analysis that Sava River contributed to groundwater recharge of Zagreb aquifer in 1998 for about 73%. Groundwater levels are declining on average for 1-2 meters every 10 years, while decrease in permanent groundwater reserves is about 7% (Bačani et al., 2010). Generally, during high water levels Sava River gives water to aquifer, while during medium- and low water levels the river is tapping the aquifer (Posavec, 2006). The thickness of the unsaturated zone varies from 2 to 8 m. The upper part of the unsaturated zone mainly consists of silty and sandy material, while in the lower part gravels dominate (Ružičić et al., 2012). Hydraulic conductivity of the unsaturated zone varies from 1.26 to 1015 m day^{-1}, while in the aquifer the values go up to 3000 m day^{-1} (Nakić et al., 2013). Elevated nitrates concentrations are registered in the some parts of the aquifer, especially in the inflow areas of wellfields Mala Mlaka, Velika Gorica, Sašnjak and Žitnjak. Average nitrates concentrations reach values greater than

40 mg/l NO_3^-. The highest values are recorded at the central part of the City of Zagreb (**Figure 1**).

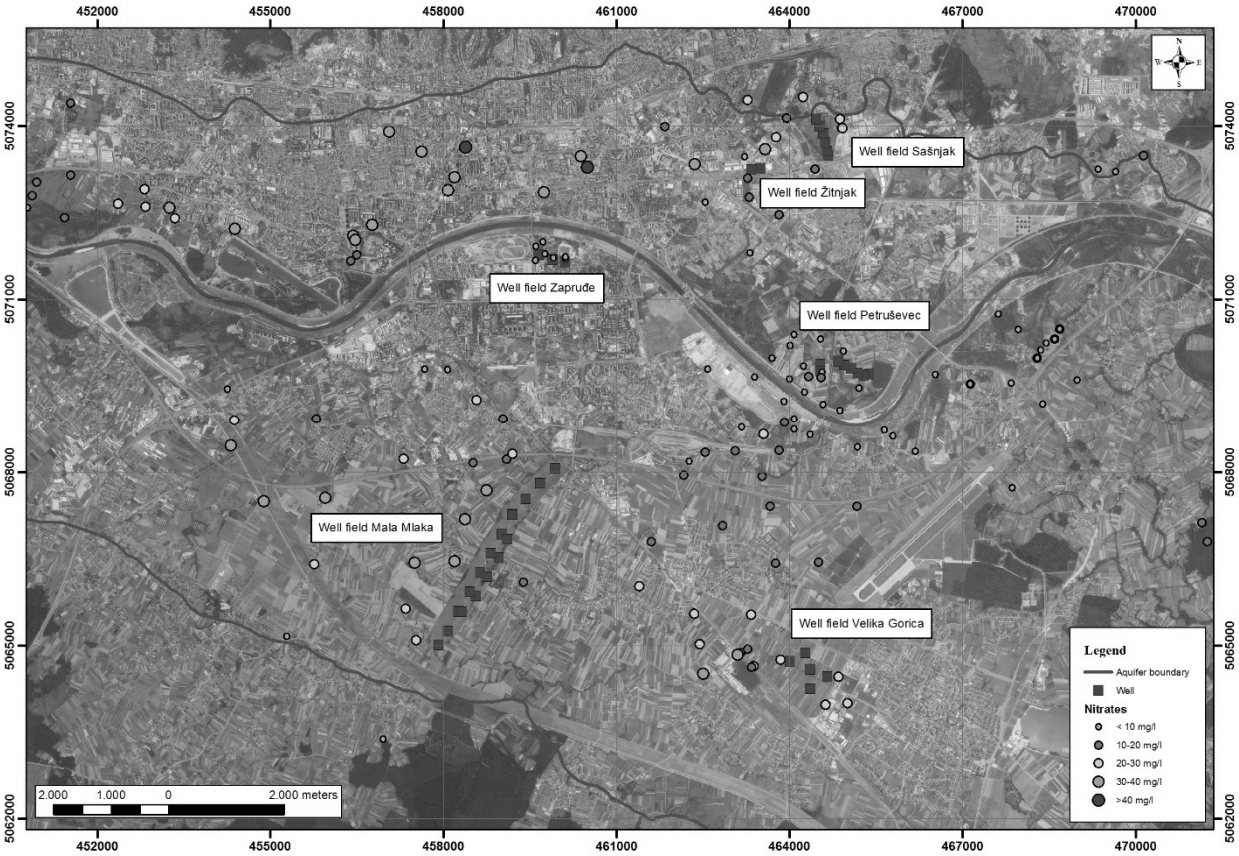

***Figure 11**: Average nitrates concentrations at Zagreb aquifer.*

Most of the well fields are located in the central part of the aquifer. Wells generally engage water from the shallower aquifer, whose thickness extends from 5 to 40 m. The thickness of the deeper aquifer is from 0 to 60 m and it generally occurs in the eastern part of the investigated area (Nakić et al., 2011). Concentrations of dissolved oxygen are mostly higher than 1 mg l^{-1} of dissolved oxygen in the western and central part, and lower in the eastern part (**Figure 2**). Anaerobic conditions occur in parts of aquifer with the biggest depth. Also, data from most observation wells suggest that in the study area prevail dominantly aerobic conditions what is very important for the stability of the nitrates concentrations in groundwater. Agriculture, leakage from septic tanks and sewage network present main potential sources of nitrate pollution. Agricultural activity is more common on the right bank of the Sava River.

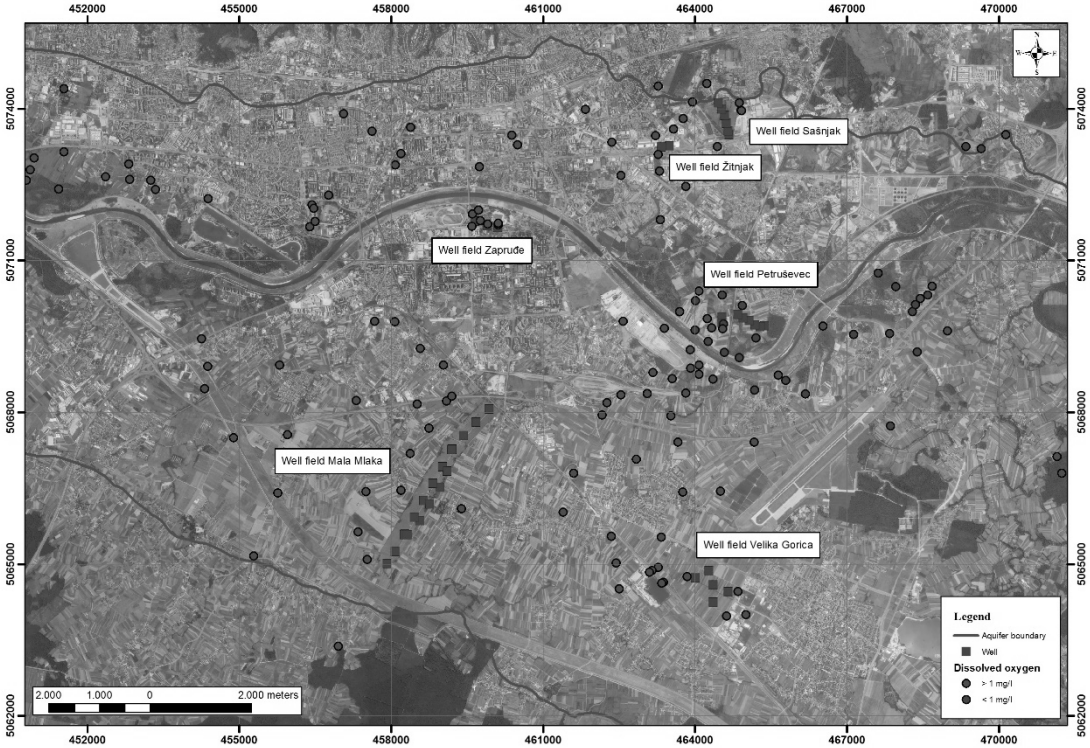

***Figure 12**: Average dissolved oxygen concentrations at Zagreb aquifer.*

3. DATA AND METHODS

Pearson (parametric) and Spearman (non-parametric) correlation coefficients were used for testing the dependance between average-, maximum- and minimum concentrations of nitrates and dissolved oxygen in groundwater from Zagreb aquifer. There are different classifications concerning the interpretation of correlation coefficients. For example, Udovičić et al. (2007) stated that correlations coefficients values from 0 to ±0.25 indicate absence of correlation, values from ±0.25 to ±0.50 poor correlation, values from ±0.50 to ±0.75 moderate to good correlation and values from ±0.75 to ±1 very good to excellent correlation. Data are mainly from national groundwater quality monitoring programme of Croatian Waters. All correlations were made in Microsoft© Excel using *correl, rank.avg* functions and regression data analysis. Data were used from 166 observation wells in period from year 1991 to 2015. In the observed period, some observations wells were excluded from the monitoring programme, while other were included. This fact and different sampling intervals generated various numbers of available chemical analysis

data for correlation studies. For testing statistical significance of calculated correlation coefficients t-test was used (α=0.05).

4. RESULTS AND DISCUSSION

Results suggest that the highest correlation is between average nitrate and dissolved oxygen concentrations, while the smallest is for maximum concentrations (**Table 1)**. It is clear that all correlation coefficients are statistically significant at the observed level of significance and that all *ρ* values are generally higher than *r*. Correlations mostly present statistically significant positive moderate to good correlation, while *r* between maximum NO_3^- and O_2 concentrations showed poor correlation and *ρ* for average NO_3^- and O_2 concentrations showed very good correlation. Results indicate that nitrates to certain extent depend about the dissolved oxygen concentrations.

Table 1*: Correlation results.*

NO_3^- (mg/l) vs. O_2 (mg/l)	Pearson (r)	p-value	Spearman (ρ)	p-value
Average	0.74	4.88E-30	0.78	8.06E-35
Maximum	0.41	3.42E-8	0.51	1.64E-12
Minimum	0.52	4.03E-13	0.61	3.61E-18

5. CONCLUSION

Elevated nitrates concentrations are present in some parts of the Zagreb aquifer. Even though they are mostly the result of the anthropogenic influence, one of the natural factors that in some extent control their stability are concentrations of dissolved oxygen and the existence of dominantly aerobic conditions in majority of the aquifer. Results have shown good to very good, statistically significant and positive correlations between nitrates and dissolved oxygen where ρ gave slightly higher values. Results indicate that natural conditions, more or less altered by human impact, have influence on the stability and mobility of nitrates concentration in the Zagreb aquifer, but also on the processes that control decrease or increase in nitrates concentrations. This thesis can be also tested with more sophisticated statistical tools like multiple

regression or multivariate analysis or in a later state dynamic factor analysis (Kovács et al., 2015; Hatvani et al., 2015). For example, multiple regression could show the joint influence of average, maximum and minimum O_2 concentrations on NO_3^- concentrations, while cluster analysis could group wells with same O_2 and NO_3^- behaviour.

6. REFERENCES

ALLER, L., BENNETT, T. & LEHR, J.H. (1987): DRASTIC: a standardized system for evaluating groundwater pollution potential using hydrogeologic settings. US EPA/600/2–87/035.

ALMASRI, M.N. (2003): Optimal management of nitrate contamination of ground water. PhD Dissertation. Utah State University, Logan, Utah, 229 p.

ALMASRI, M.N. (2007): Nitrate contamination of groundwater: A conceptual management framework. Environmental Impact Assessment Review 27, 220-242, doi:10.1016/j.eiar.2006.11.002.

BAČANI, A., POSAVEC, K., PARLOV, J., ŽUBČIĆ, M., KOVAČ, Z., PLETIKOSIĆ, N., BEDENICKI, N., KLANFAR, M. & DVORABIĆ, A. (2010): Prva faza izrade programa mjera za zaštitu i sanaciju u zonama zaštite izvorišta (*engl. The first phase of development of the programme of measures for protection and remediation in water resource protection zones – in Croatian*). –Unpub. Faculty of Mining, Geology and Petroleum Engineering, University of Zagreb, Zagreb.

DIMKIĆ, M.A., BRAUCH, H.J. & KAVANAUGH, M. (2008): Groundwater management in large river basins. IWA Publishing, Alliance House, Biddles Ltd, Norfolk, UK.

HATVANI, I.G., KOVÁCS, J., MÁRKUS, L., CLEMENT, A., HOFFMANN, R. & KORPONAI, J. (2015): Assessing the relationship of background factors governing the water quality of an agricultural watershed with changes in catchment property (W-Hungary). Journal of Hydrology 521, 460-469, doi: 10.1016/j.jhydrol.2014.11.078.

HOSONO, T., TOKUNAGA, T., KAGABU, M., NAKATA, H., ORISHIKIDA, T., LIN, I. & SHIMADA, J. (2013): The use of $\delta^{15}N$ and $\delta^{18}O$ tracers with an understanding of groundwater flow dynamics for evaluating the origins and attenuation mechanisms of nitrate pollution. Water Research 47, 2661-2675, doi:10.1016/j.watres.2013.02.020.

KOVÁCS, J., MÁRKUS, L., SZALAI, J. & SZÉKELY KOVÁCS, I. (2015): Detection and evaluation of changes induced by the diversion of River Danube in the territorial appearance of latent effects governing shallow-groundwater fluctuations. Journal of Hydrology 520, 314-325, doi: 10.1016/j.jhydrol.2014.11.052.

LAKE, I.R., LOVETT, A.A., HISCOCK, K.M., BETSON, M., FOLEY, A., SUNNENBERG, G., EVERS, S. & FLETCHER, S. (2003): Evaluating factors influencing groundwater vulnerability to nitrate pollution: developing the potential of GIS. Journal of Environmental Management 68: 315–328.

LI, S.L, LIU, C.Q., LANG, Y.C., ZHAO, Z.Q. & ZHOU, Z.H. (2010): Tracing the sources of nitrate in karstic groundwater in Zunyi, Southwest China: a combined nitrogen isotope and water chemistry approach. Environmental Earth Sciences 60, 1415-1423, doi: 10.1007/s12665-009-0277-0.

MARKOVIĆ, T., BRKIĆ, Ž. & LARVA, O. (2013): Using hydrochemical data and modelling to enhance the knowledge of groundwater flow and quality in an alluvial aquifer of Zagreb, Croatia. Science of the Total Environment 458–460, 508–516, doi: 10.1016/j.scitotenv.2013.04.013.

MILETIĆ, P. & BAČANI, A. (1999): EGPV: Izrada bilansa (*engl. Development of water balance – in Croatian*). Knjiga 4, četvrti dio. Faculty of Mining, Geology and Petroleum Engineering, University of Zagreb, Zagreb.

MKANDAWIRE, T. (2008): Quality of groundwater from shallow wells of selected villages in Blantyre District, Malawi. Physics and Chemistry of the Earth 33, (8–13), 807–811, doi:10.1016/j.pce.2008.06.023.

NAKIĆ, Z., RUŽIČIĆ, S., POSAVEC, K., MILEUSNIĆ, M., PARLOV, J., BAČANI, A. & DURN, G. (2013): Conceptual model for groundwater status and risk assessment - case study of the Zagreb aquifer system. Geologia Croatica, Vol. 66, No 1, doi: 10.4154/GC.2013.05.

NAKIĆ, Z., POSAVEC, K., PARLOV, J. & BAČANI, A. (2011): Development of the Conceptual Model of the Zagreb Aquifer System. The Geology in Digital Age: Proceedings of the 17th Meeting of the Association of European Geological Societies, MAEGS 17 / Banjac, Nenad (ur.). - Belgrade: Serbian Geological Society, 2011. 169-174 (ISBN: 978-86-86053-10-7).

PENA-HARO, S., PULIDO-VELAZQUEZ, M. & SAHUQUILLO, A. (2009): A hydro-economic modelling framework for optimal management of groundwater nitrate pollution from agriculture. Journal of Hydrology 373, 193-203, doi:10.1016/j.jhydrol.2009.04.024.

POSAVEC, K. (2006): Identifikacija i prognoza minimalnih razina podzemne vode zagrebačkoga aluvijalnog vodonosnika modelima recesijskih krivulja (*engl. Identification and prediction of minimum ground water levels of Zagreb alluvial aquifer using recession curve models – in Croatian*). –Unpub. PhD Thesis, Faculty of Mining, Geology and Petroleum Engineering, University of Zagreb, Zagreb, 89. p.

RUŽIČIĆ, S., MILEUSNIĆ, M. & POSAVEC K. (2012): Building Conceptual and Mathematical Model for Water Flow and Solute Transport in the Unsaturated zone at Kosnica Site. Rudarsko-geološko-naftni zbornik (0353-4529) 25; 21-31.

UDOVIČIĆ, M., BAŽDARIĆ, K., BILIĆ-ZULE, L. & PETROVEČKI, M. (2007): Što treba znati kada izračunavamo koeficijent korelacije? (engl. What we need to know when calculating the coefficient of correlation?). Biochemia Medica 17(1):1–138.

VELIĆ, J. & DURN, G. (1993): Alternating Lacustrine-Marsh Sedimentation and Subaerial Exposure Phases during Quaternary: Prečko, Zagreb, Croatia. Geologia Croatica, vol. 46, no. 1, p. 71–90.

VELIĆ, J., SAFTIĆ, B. & MALVIĆ, T. (1999): Lithologic Composition and Stratigraphy of Quaternary Sediments in the Area of the "Jakuševec" Waste Depository (Zagreb, Northern Croatia). Geologia Croatica, vol. 52, no. 2, p. 119–130.

Applications of different mapping methods for sandstone distribution in south-eastern part of Sava Depression

Ana Majstorović Bušić[1], Mohamad Alzenab[1] and Kristina Novak Zelenika[1]

[1] INA d.d., Šubićeva 29, 10000 Zagreb, ana.majstorovic@ina.hr

Sava Depression represents the south-western margin of the Croatian part of the Pannonian Basin System. Evolution of the Sava Depression began in Miocene. Its development continued during the whole Miocene, Pliocene and finally Quaternary. Most of the hydrocarbon prone sandstones were sedimented during Late Pannonian and Early Pontian. During that time sedimentation was represented with considerable environmental changes where turbiditic currents mechanisms dominated. The studied area belongs to the southeastern part of the Sava Depression and includes several oil and gas fields. Effective thickness of the sandstones members within Kloštar Ivanić Formation (approximate Early Pontian age) are derived from the 97 exploration wells. Data represent effective thickness of Poljana sandstones (analysed interval between petrophysical markers Rni- Z) and Bregi sandstones (analysed interval between petrophysical markers Rfi –Delta). The applied mapping methods are Convergent Interpolations, Moving Average and Ordinary Kriging made by Petrel software.

On maps interpolated with Moving Average and Ordinary Kriging almost concentric areas can be observed - so-called Bull's eye effect. Convergent Interpolation method gave a better estimate than other two methods and more realistic sandstone distribution maps. It is selected as the most appropriate method for mapping these set of data point.

Key words*: Convergent interpolation, Moving Average, Ordinary Kriging, sandstones, Sava Depression, Croatia*

1. INTRODUCTION

The studied area belongs to the south-eastern part of the Sava Depression and includes several oil and gas fields. Evolution of the Sava Depression began in Miocene and its development continued during the whole Miocene, Pliocene and finally Quaternary. Sava Depression represents the south-western margin of the Croatian part of the Pannonian Basin System (CPBS) (e.g. Pavelić, 2002; Malvić, 2012). Most of the hydrocarbon prone sandstones were deposited during Late Pannonian and Early Pontian. During that time sedimentation was represented with considerable environmental changes where turbiditic currents mechanisms dominated. The main sources of medium to fine-grained sandstones were Eastern Alps (Malvić and Velić, 2011). These clastics had been several times re-deposited and moved to tectonically instable slope or ramp and, after tectonic displacement, transported by turbidites in different parts of depressions (e.g. Velićet al., 2002; Vrbanac et al., 2010; Malvić and Velić, 2011). This mechanism was active periodically, interrupted typical hemipelagic sedimentation in lacustrine environment in CPBS. That resulted in monotonous alteration of sandstone and marlstone lithofacies through most of Pannonian and Pontian stages. Homogenous alteration of sandstones and marls in deeper parts is characterized by regional e-log markers which are regularly used in regional correlation of lithostratigraphic units in CPBS (Malvić and Velić, 2011).

2. INPUT DATA AND METHODS

Effective thickness of the sandstones members within Kloštar Ivanić Formation (approximate Early Pontian age) are derived from the 97 exploration wells. Data represent effective thickness of Poljana sandstones (analysed interval between petrophysical e-log markers Rni - Z) and Bregi sandstones (analysed interval between petrophysical e-log markers Rfi –Delta). Effective sandstone's thickness was calculated by using spontaneous potential log (SP). The applied mapping methods are Convergent Interpolations, Moving Average and Ordinary Kriging made by Petrel software. General purpose of Convergent Interpolation methods is to build structural surfaces. Typical surface forms they are applied to are roughly horizontal. Its algorithm in Petrel uses a series of refinements to locally tune the surface to the neighbouring data and reduces wild extrapolation.

Moving Average algorithm creates poor geological forms averaging the data between the points i.e. this method calculates the values of grid nodes from averaged data measured in a particular ellipsoid or circle that surrounds each grid node. Kriging is a geostatistical method, based on calculations of spatial dependence using variogram analyses (oriented ellipse of influence) to define the directional bias for linear interpolation of node values from neighbouring points. Basics about geostatistical methods can be find in de Wijs (1951), Deutsch and Journel (1997), Dubruble (1998), Malvić (2008).

3. RESULTS AND CONCLUSION

The results of Poljana sandstones mapping with different methods are presented on **Figures 1, 2** and **3**. Different Maps of Bregi sandstones are presented on **Figures 3, 4** and **5**.

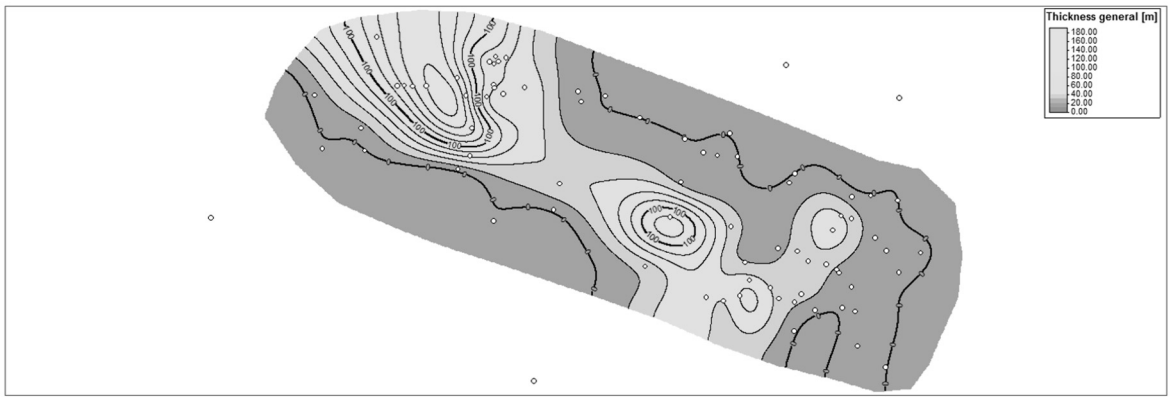

Figure 1: *Effective thickness map of the Poljana sandstone obtained by Convergent Interpolation method*

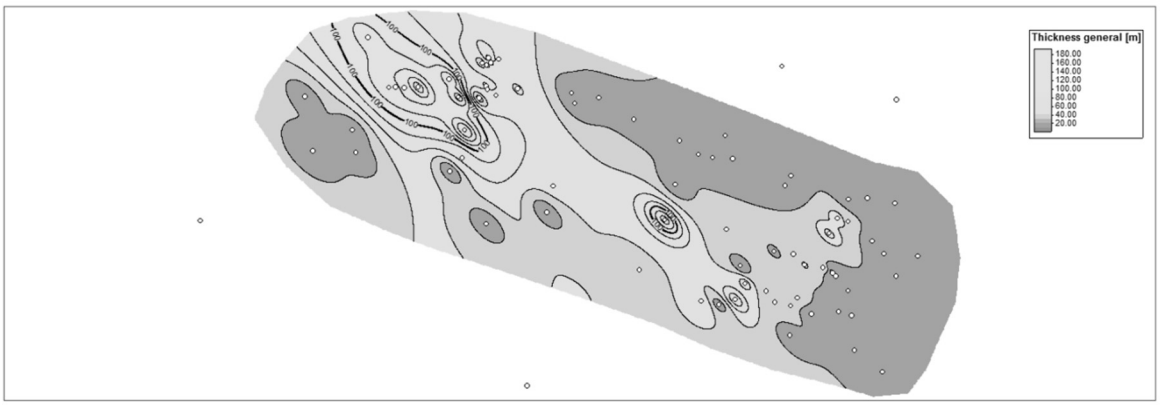

Figure 2: *Effective thickness map of the Poljana sandstone obtained by Moving Average method*

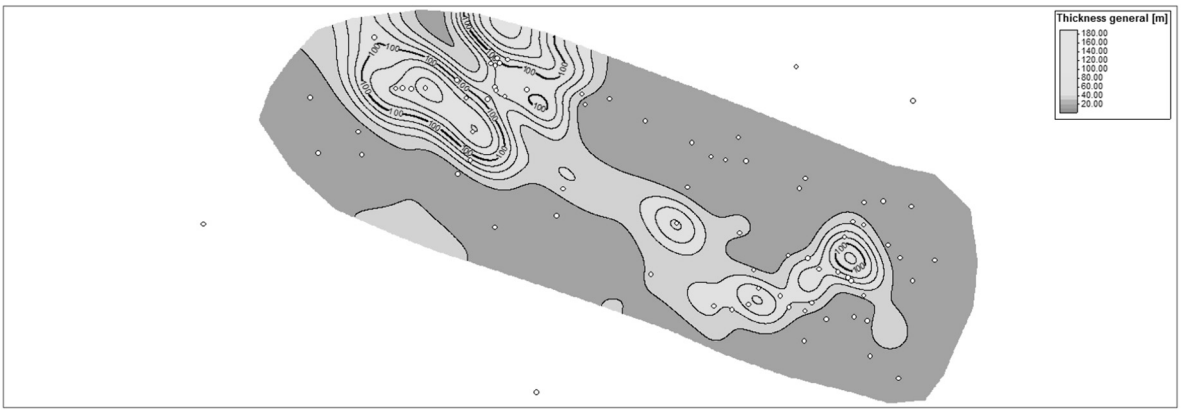

Figure 3: *Effective thickness map of the Poljana sandstone obtained by Ordinary Kriging method*

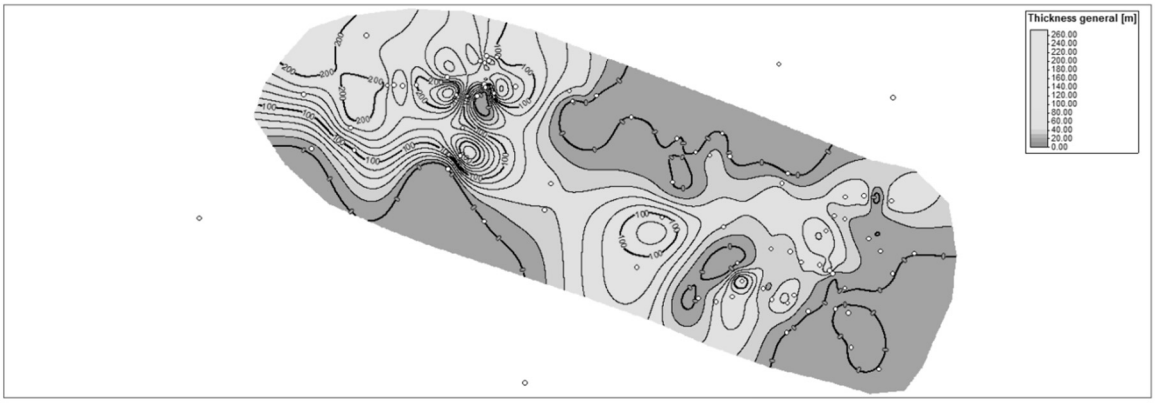

Figure 4: *Effective thickness map of the Bregi sandstone obtained by Convergent Interpolation method*

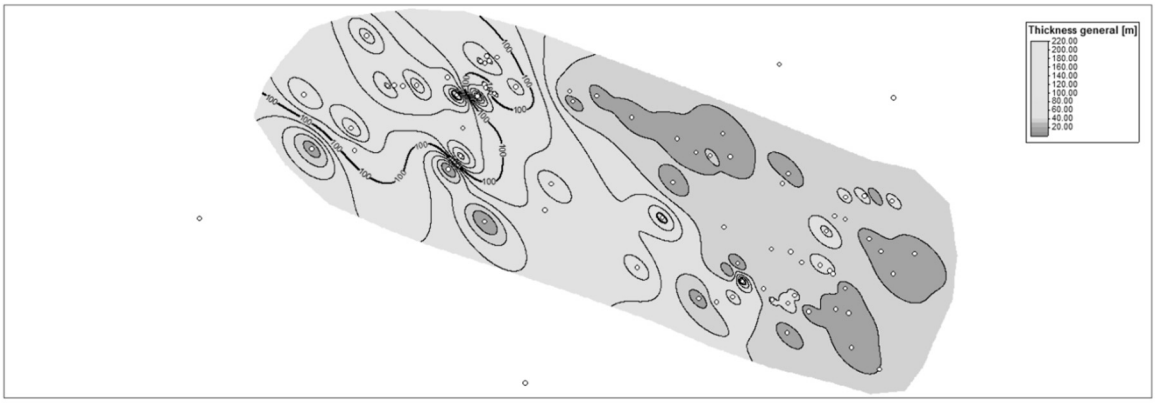

Figure 5: *Effective thickness map of the Bregi sandstone obtained by Moving Average method*

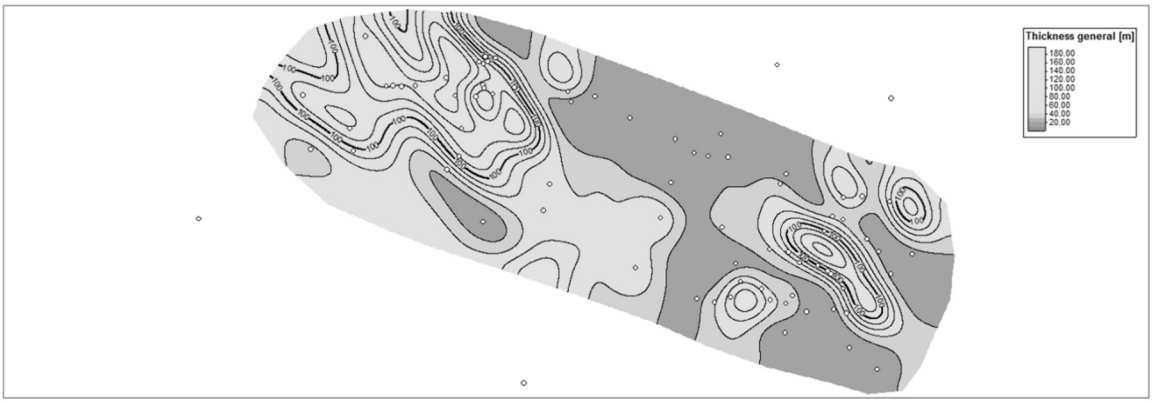

Figure 6: *Effective thickness map of the Bregi sandstone obtained by Ordinary Kriging method*

According to Malvić and Velić (2011) Early Pontian sandstones were deposited through turbiditic currents in the deepest part of sedimentation area and the main source of material were Eastern Alps. All of the maps (**Figures 1-6**) clearly prove such theory and show main material transport direction (NW-SE). But, beside this direction there is another one (S-N) direction observed, especially on **Figures 1, 4** and **6**. It could point to another, local material source. Local material source can be assumed during Early Pontian because of continuous lake shallowing and continuous uplifting of the mountains with Palaeozoic and Mesozoic basement.

On maps interpolated by Moving Average and Ordinary Kriging methods (**Figures 2, 3, 5** and **6**) almost concentric areas can be observed, so-called Bull's eye effect. Convergent Interpolation method (**Figures 1** and **4**) gave a better estimate than other two methods and more realistic sandstone distribution maps. It is selected as the most appropriate method for mapping these set of data point.

4. REFERENCES

de WIJS, H.J. (1951): Statistics of ore distribution. Part I: frequency distribution of assay values. Journal of the Royal Netherlands Geological and Mining Society, 13, 365-375.

DEUTSCH, C.V. & JOURNEL, A.G. (1997): GSLIB: Geostatistical Software Library and User's Guide, 2nd edn. Oxford University Press, New York, 369 p.

DUBRUBLE, O. (1998): Geostatistics in Petroleum Geology. AAPG Education Course Note, Series #38, AAPG and Geological Society Publishing House, Tulsa, 210 p.

MALVIĆ, T. (2008): Primjena geostatistike u analizi geoloških podataka. INA-Industrija nafte, Zagreb, 103 p.

MALVIĆ, T. (2012): Review of Miocene shallow marine and lacustrine depositional environments in Northern Croatia. - Geological quarterly. 56, 3; 493-504.

MALVIĆ, T. & VELIĆ, J. (2011): Neogene Tectonics in Croatian Part of the Pannonian Basin and Reflectance in Hydrocarbon Accumulations. –In: SCHATTNER, U. (ed.): New Frontiers in Tectonic Research: At the Midst of Plate Convergence, InTech, Rijeka, 352 p.

PAVELIĆ, D. (2002): The south-western boundary of Central Paratethys. Geologia Croatica, 55, 1, 83-92.

VELIĆ, J., WEISSER, M., SAFTIĆ, B., VRBANAC, B. & IVKOVIĆ, Ž. (2002): Petreloleum-geological characteristics and exploration level of the three Neogene depositional megacyclus in the Croatian part of the Pannonian basin. Nafta, 53, 6-7, 239-249.

VRBANAC, B., VELIĆ J. & MALVIĆ T. (2010): Sedimentation of deep-water turbidites in main andmarginal basins in the SW part of the Pannonian Basin. *Geologica Carpathica,* Vol. 61, No. 1, pp. 55-69, ISSN 1335-0552.

Petrophysical modelling of the Upper Pannonian reservoirs in Sava Depression

Kristina Novak Zelenika[1], Renata Vidaček[1], Tomislav Ilijaš[1] and Petar Pavić[1]

[1]INA- Oil Industry Plc. Exploration and Production of Oil and Gas, Sector for Geology and Reservoir Management, Šubićeva 29, 10000 Zagreb, kristina.novakzelenika@ina.hr;

Abstract:

Deterministic methods are still widely used for reservoir characterization and modelling although it is clear that our knowledge about underground cannot be completely known, i.e. without any uncertainty. This is why sometimes stochastic methods can give better solution, since they include uncertainty in their calculations. This paper shows testing of the deterministic (Ordinary Kriging) and stochastic (Sequential Gaussian Simulations) methods for porosity distribution in Lower Pontian hydrocarbon reservoirs in the Sava Depression. Ten realizations were obtained by Sequential Gaussian Simulation. Although 10 realizations is enough only for the rough insight into geological underground uncertainty, the obtained results were satisfied. Areas with the highest uncertainties were well observed in the maps. Many problems in numerical simulation appeared due to high differences in values between neighbour cells. For that reason Ordinary Kriging as a deterministic method was used for the modelling of the same reservoirs. Smooth transitions between neighbour cells eliminated all the numerical modelling problems and Ordinary Kriging maps showed channel sandstone with transitional lithofacies in some reservoirs.

Key words: *Geostatistics, Ordinary Kriging, Sequential Gaussian Simulations, hydrocarbon reservoirs, Sava Depression.*

1. INTRODUCTION

Geostatistics, as a part of geomathematics began its development in the second half of the last century. Geostatistical methods can be divided into deterministical and stochastical methods. In deterministical methods, all the conditions which can influence to estimation, have to be completely known. It is clear that geological underground is only one, but since the description of the underground is based on well data (point data) it is not possible to be absolutely sure that the solution obtained with geostatistical methods is absolutely correct. This is why all geostatistical methods contain some uncertainty, they estimate underground conditions and they can provide only the most probable solution or the solution which is the closest to the truth. Most of the geostatistical methods are used in petrophysical modelling. In reservoir characterization, petrophysical modelling, especially porosity modelling is important for getting insight into different properties distribution and in this way knowledge about sedimentary environments and depositional mechanisms could be increased. Within this paper, porosity modeling has been performed. Two different distribution methods were tested and analysed in order to choose more acceptable one. Applied methods were Ordinary Kriging technique (OK), very well described by de Wijs (1951), Krige (1951), Matheorn (1965), Hohn (1988), Isaaks & Srivastava (1989), Doubruble (1998), Malvić et al. (2008), and Sequential Gaussian Simulations (SGS), described in Isaaks (1990), Gomez - Hernandez & Srivastava (1990), Goovaerts (1997), Deutsch & Journel (1998), Geiger (2006) and Malvić (2008).

2. GEOLOGICAL DESCRIPTION OF THE STUDY AREA

Study area is located in the north-western part of the Sava depression. Structurally it is an asymmetrical brachianticline, with somewhat longer axis of northwest-southeast strike, with slightly pronounced peak in the southern part of the structure. A series of faults of NW-SE strike extend along the western part of the field.

Lithologically hydrocarbon-bearing rocks of the study field consist of medium and fine-grained sandstones (lithoarenites) in continuous alternation with marls.

The whole series was divided into 11 sandstone intervals. All of the reservoirs in the series (S1-S11) were classified as Upper Pannonian. Some of the reservoirs are elongated along NW-SE direction and they could represent channel sediments. Other reservoirs have greater areal extent and minor thickness variability representing rather sand lobes or similar type of deposits.

3. INPUT DATA AND MODELING PROCESS

Input data set used for geological model construction comprised of well log data (from 86 wells), quantitative log analysis, core data (from 28 wells) and already constructed 3D structural model. All those data have been integrated and analysed. Geological model was built with cell dimensions 50x50 m.

Basics for petrophysical modelling is to perform reliable structural model. Tops and bottoms of the 11 sandstone reservoirs (22 horizons) together with interlayered marls determined 21 zones. Two types of reservoirs were recognised: reservoirs with relatively uniform gross reservoir thickness on the field area and those with great lateral thickness variability. The latter have been identified as channel bodies. According to that observation, type of layering within the individual zone in the model was adopted. It was concluded that better layering method in the case of reservoirs recognized as channel bodies with great lateral variability of thickness, is layering with constant layer thickness (2 m) and following the top of reservoir while in the other case proportional layering was chosen. Difference between "Follow top" and "Proportional" type of layering is given in **Figure 1**.

Analysis of petrophysical parameters was performed using (1) the epilog analyses of porosity and (2) cored intervals-porosity measurements. Cored wells and intervals, as well as wells with Epilog analysis are distributed all over the field and are representative of lithological and petrophysical parameters of the analysed Lower Pontian sandstone series.

After correction for overburden pressure, depth correlation of log analyses and coring data was performed. In most cases smaller corrections were necessary (up to 5 m) during correlation of depth intervals (**Figure 2**).

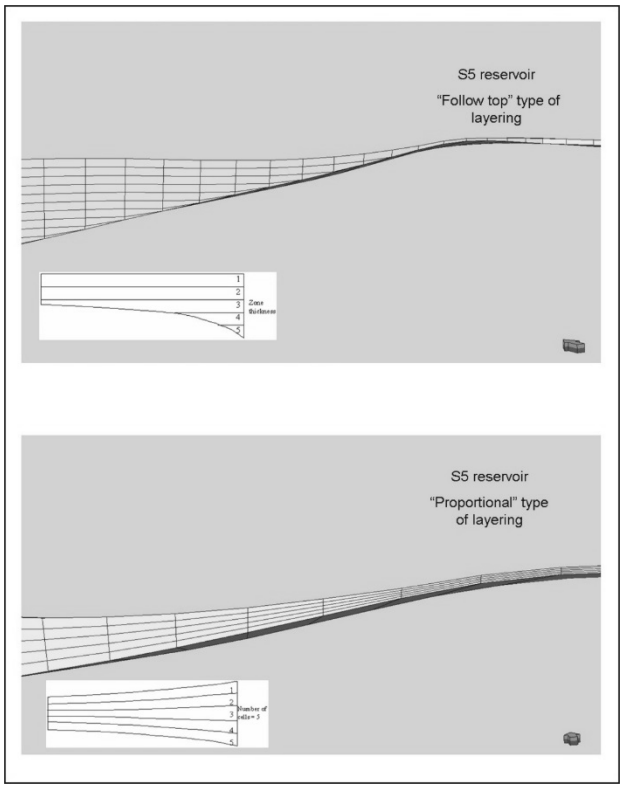

***Figure 1**: Two types of layering*

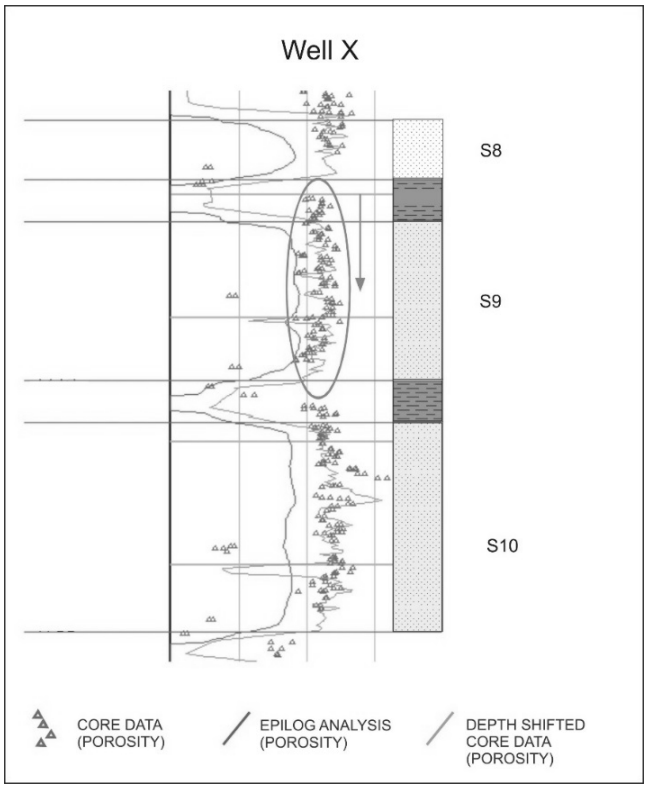

***Figure 2**: Depth shifting*

Input data for porosity modelling included porosity measured on core samples as well as porosity resulted from quantitative log analysis (Epilog). Generally, log porosity was significantly underestimated (especially for interval from 0 to 15%) comparing to porosity measured on core samples under reservoir conditions. Therefore, two mathematical relation equations; one for the lower and another one for the higher porosity values have been applied on Epilog derived porosity in order to obtain more reliable porosity data (**Figure 3**). The results are corrected porosity logs for all wells having porosity logs from quantitative log analysis.

Corrected porosity logs were then upscaled in the model representing input for porosity modelling. Upscaling is a process of averaging input data in the model cells containing well data. In this way just one value is assigned to cell.

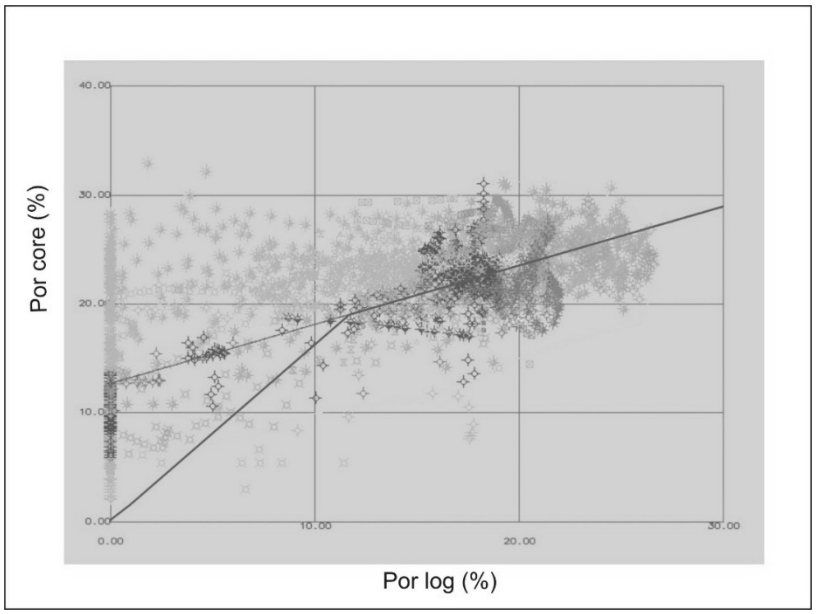

***Figure 3**: Cross plot diagram porosity (core) vs. porosity (epilog analysis)*

Before porosity distribution, data analysis was performed and variograms for each reservoir were calculated. Different stochastical and deterministical methods of porosity distribution were examined.

In the first phase, 10 realizations of Sequential Gaussian Simulations (SGS) of porosity distribution was performed. Although, for the sake of uncertainties, E-type of estimation would be best choice to use, it was decided to show two realizations, because, from statistical point of view, all of realizations are equally probable. **Figure 4** shows two different realizations for the S6 and S5 reservoirs. Maps clearly show some areas with huge differences between estimated cell values in different realizations, for example northern and north-eastern parts of the S6 reservoir and eastern part of the S5 reservoir. Those parts are areas with the highest uncertainty, caused by lack of well data.

Due to the simulated values which were significantly different in neighbouring cells, many problems occurred in numerical simulation as proved by sensitivity performed on required simulation time (**Figure 6**).

Finally, to avoid problems in numerical modelling, porosity has been distributed using Ordinary Kriging method (**Figure 5**). Synthetic lithofacies log had been created based on porosity (if the porosity was higher than 11% lithofacies log represents sandstones, otherwise it represents marls) and it had been used as

bias for porosity upscaling. In that way input porosity data are weighted according to prevailing lithofacies. Cut-off for porosity was chosen based on experience. Porosity logs had been upscaled using arithmetic average methods for each reservoir. Channel sandstone body (S5 reservoir) is very well observed in Ordinary Kriging map (**Figure 5** right). It is clearly seen that the higher porosities are in the channel centre, while toward its border porosity decreases. It could point to existence of the transitional lithofacies like sandy marls and marly sandstones. Smooth transition between neighbour cells makes Ordinary Kriging solution more acceptable in numerical modelling (**Figure 6**).

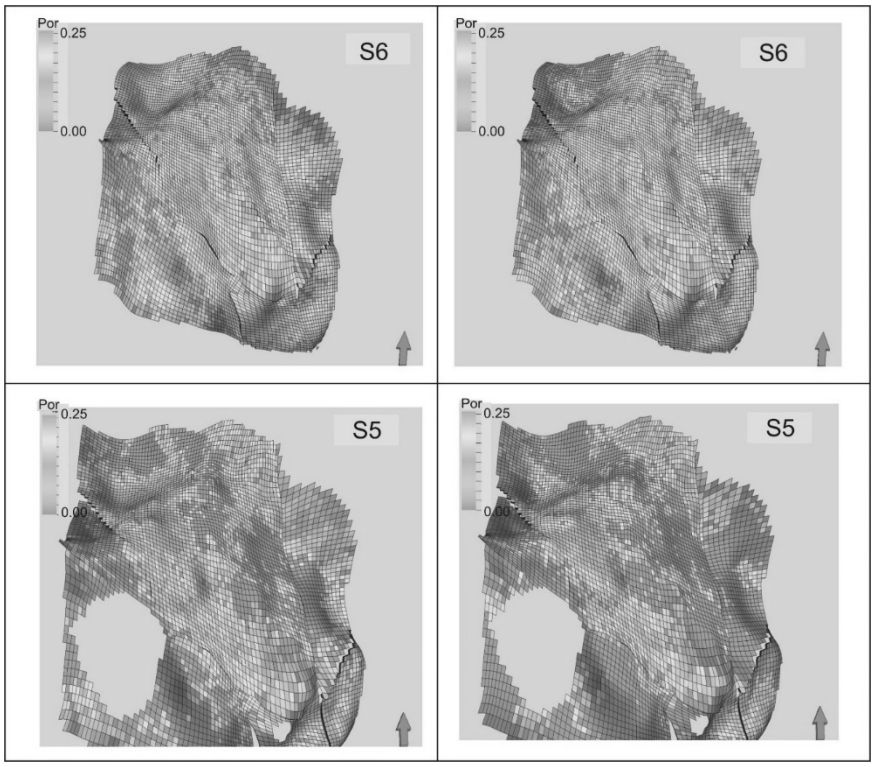

***Figure 4**: Different realizations obtained by Sequential Gaussian Simulations*

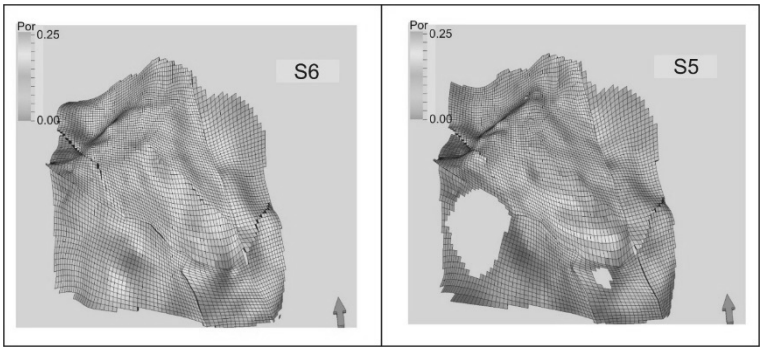

***Figure 5**: Porosity distribution obtained by Ordinary Kriging*

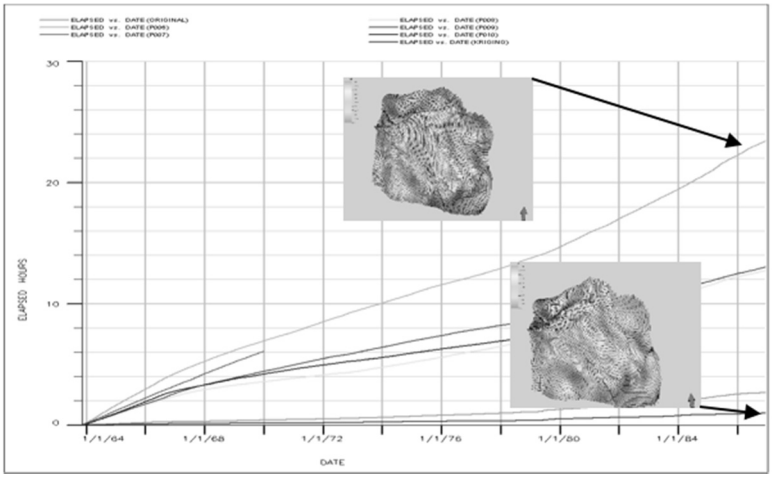

***Figure 6**: Simulation time (SGS realizations 1-5 and Kriging)*

4. CONCLUSION

Input data set used for geological model construction comprised of well log data, quantitative log analysis, core data and previous geological model. Structural model was defined with 21 zones. Correction for overburden pressure and depth correlation of log analyses and coring data was performed. After variogram analysis for each reservoir different geostatistical methods of porosity distribution were examined. 10 realizations of Sequential Gaussian Simulations were performed, which enabled clear insight into the reservoirs uncertainty. Areas with the highest uncertainty were caused by lack of data. Realizations obtained by Sequential Gaussian Simulations had significant differences between neighbour cell values, which caused many problems in numerical simulation, e.g. simulation time drastically increased. Porosity distribution obtained by Ordinary Kriging was more acceptable in numerical modelling, since the transition between neighbour cells was very smooth (the OK cannot follow the local heterogenity). In the reservoirs recognized as channel bodies higher porosities are located in the channel centre, while toward channel borders porosities decrease. Higher porosity values could represent pure sandstones. Porosity decreasing toward channel borders points to sandstones with more marly component, i.e. to marly sandstones and sandy marls.

6. REFERENCES

de WIJS, H.J. (1951): Statistics of ore distribution. Part I: frequency distribution of assay values. Journal of the Royal Netherlands Geological and Mining Society, 13, 365-375.

DEUTSCH, C. and JOURNEL, A.G. (1998): GSLIB: Geostatistical Software Library and User's GuideSecond Edition. Oxford, University Press, New York. 340 p.

DUBRUBLE, O. (1998): Geostatistics in Petroleum Geology. AAPG Education Course Note, Series #38, AAPG and Geological Society Publishing House, Tulsa, 210 p.

GEIGER, J. (2006): The behavior of Sequential Gaussian Simulation in the limits. Xth congress of Hungarian geomathematics, May 18-20 2006, Morahalom.

GÓMEZ-HERNÁNDEZ, J. and SRIVASTAVA, R. (1990): 'ISIM3D: An ANSI-C three-dimensional multiple indicator conditional simulation program', Computers & Geosciences, 16(4), 395–440.

GOOVAERTS, P. (1997): Geostatistics for natural resources evaluation. Oxford University Press, New York. 483 p.

HOHN, M.E. (1988): Geostatistics and petroleum geology. Van Nostrand Reinhold, New York, 264 p.

ISAAKS, E.H. (1990): The application of Monte Carlo methods to the analysis of spatially correlated data. Ph.D. Dissertation, Stanford Universit

ISAAKS, E. & SRIVASTAVA, R. (1989): An Introduction to Applied Geostatistics. Oxford University Press Inc., New York, 580 p.

KRIGE, D. G. (1951): A Statistical Approach to Some Basic Mine Valuation Problems on the Witwatersrand. Journal of the Chemical, Metallurgical and Mining Society of South Africa, 52, 119-139.

MALVIĆ, T. (2008): Primjena geostatistike u analizi geoloških podataka. INA-Industrija nafte, Zagreb, 103 p.

MALVIĆ, T., CVETKOVIĆ, M. & BALIĆ, D. (2008): Geomatematički rječnik. Hrvatsko geološko društvo, Zagreb, 74 p.

MATHERON, G. (1965): Les Variables Regionalisees et leur estimation:une application de la theorie des functions aleatoires aux sciences de la mature. Masson, Paris, 306 p.

Trend analysis of mean and high river flows from stations in karstic Kupa catchment

Krešimir Pavlić[1], Zoran Kovač[1]

[1]University of Zagreb, Faculty of Mining, Geology and Petroleum Engineering, Pierottijeva 6, 10000 Zagreb, Croatia, kresimir.pavlic@rgn.hr

Trends of mean and high river flows from three hydrological stations on watercourses of the Kupa River (Kupari, Kamanje), tributary Čabranka (Zamost 2) and one meteorological station (Parg) were analysed. The paper focuses on five indicators: annual mean flow, seasonal mean flows (winter and summer mean flows), instantaneous annual maximum flow and annual precipitation. Analysed time series range from 1951 to 2013, and the fixed period ranges from 1984 to 2013. Time series of each indicator was scaled to standardized flow anomaly and was analysed using the Mann-Kendall Z test for monotonic trend, after which it is smoothed using LOESS algorithm. The analysis was conducted for each indicator for full record, e.g. 1951-2013, then 1952-2013 and so on until 1984-2013. Thus, the sample size varies from 63 to 30 years. The smoothed standardized flow anomaly, expressed in standard deviations per year, is easily comparable among different hydrologic stations. The standardized flow anomaly on all analysed stations shows undisrupted periodicity of annual mean flow, instantaneous annual maximum flow and annual precipitation up until the mid-80s, after which the periodicity was disrupted. Further analysis of summer and winter seasonal mean flows revealed different deviation from long-term annual flow average. Negative trends of certain indicators were proven using Mann-Kendall Z test, by plotting Z values for each iteration of start year (1951 to 1984).

Key words: *climate change, Mann-Kendall, precipitation, river flows, trend*

1. INTRODUCTION

The evidence of human impact on the increase of greenhouse gases, which affects the global water cycle over the last 50 years increased dramatically in the last 10 years (Gedney et al., 2006; Huntington, 2006; IPCC, 2007; Barnett et al., 2008; Murphy et al., 2013). This is usually shown by increase of annual

runoff, change in frequency of maximum and minimum annual flows and in regime change of precipitation during a year (Milly et al., 2005; Groisman et al., 2005; Dai et al., 2004; Pavlić, 2016). However, there are ambiguous research results, since there is debate about on the subject (Labat et al., 2004; Legates et al., 2005). However, the very first step of this kind of analysis is trend analysis of flow and precipitation data and its significance (Ziegler et al., 2005; Wilby, 2006; Murphy et al., 2013).

Žugaj (1995) discovered that in the Croatian karstic region in 1980's a dryer period began. Data from three hydrological- and one meteorological stations from karstic Kupa catchment were considered: hydrological stations Kupari and Kamanje on Kupa River and Zamost 2 on tributary Čabranka and meteorological station Parg near Čabar. Human impact, such as land-use, urbanization and water storage on the data from these stations is negligible.

2. RESEARCH AREA

Selected stations are located in Gorski kotar, in the mountainous area of Croatian karst. The length of Kupa River downstream to Karlovac is 160 km, and size of catchment area to the hydrological profile Kamanje is 2,340 km^2 (**Figure 1**). The whole catchment area is located in the karst. Springs of Kupa and Čabranka Rivers are situated in high mountainous area of specific karst regime. Further, watercourse of the Kupa River comes into karst plateau, so called shallow karst.

According to Köppens climate classification, this area belongs to climate denoted as *Cfb* (maritime temperate climate). More precisely, the area of hydrological stations Kupari at Kupa and Zamost 2 at Čabranka belongs to climate denoted as *Cfsbx*. This particular area stands out with deviation of amount of precipitation (area of Kupari has large amount and area of Zamost 2 quite smaller amount of precipitation, Žugaj et al., 2011). The greatest amount of precipitation at station Parg is 1,849 mm. Downstream Kupa River to Kamanje hydrological station, climate is the same, *Cfb*, but with some different properties, *Cfwbx* (Šegota and Filipčić, 2003).

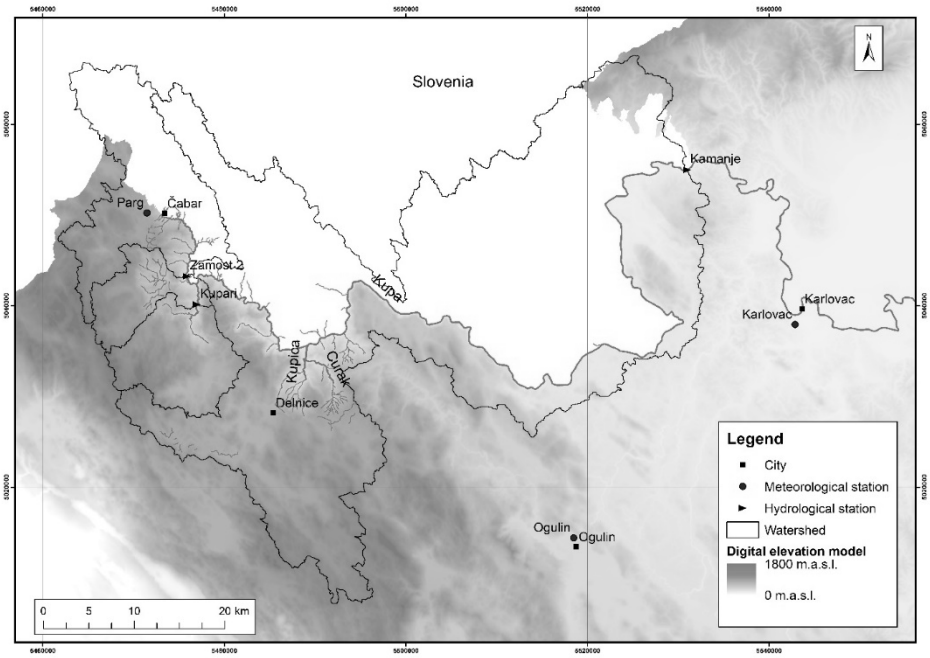

Figure 13: *Karstic Kupa catchment. Three hydrological stations (Zamost 2, Kupari and Kamanje) and one meteorological station (Parg), main watercourses and tributaries are marked.*

3. MATERIALS AND METHODS

Trend analysis was conducted on five indicators: annual mean flow, seasonal mean flows (winter and summer mean flows), instantaneous annual maximum flow and annual precipitation using time series from 1951 to 2013. Each indicator is presented as standardized flow and precipitation anomaly and smoothed using Local Polynomial Regression Fitting (LOESS) algorithm. Trend persistence is tested using Mann-Kendall Z test for each iteration of start year (1951 to 2013, 1952 to 2013 and so on until 1984 to 2013, which is fixed period of analysis).

Trend analysis focuses on five indicators that describes changes in high and mean flows:

- annual mean flow (Q_{mean}),
- seasonal mean flows (Q_{meanw}, Q_{means}),
- instantaneous annual maximum flow (Q_{max}),
- annual precipitation (P).

All flow indicators were calculated in m^3 s^{-1}, while precipitation is in mm. Analysed time series ranges from 1951 to 2013 and fixed period ranges from 1984 to 2013. Two years of annual mean flows (1996 and 1997) were missing

at Kamanje station, and they were interpolated using correlation with upstream hydrological station Metlika.

Murphy et al. (2013) propose trend analysis and study approach procedure as follows. Time series of each indicator was scaled to standardized flow anomaly (SFA), proposed by Déry et al. (2005):

$$SFA = \left(\frac{Q_i - \overline{Q}}{\sigma_Q} \right) \tag{1}$$

where Q_i is river flow ($m^3\ s^{-1}$) or precipitation (mm) value for *i*-th year, $\overline{Q}$ is the mean flow or mean precipitation for the selected time period and σ_Q is standard deviation of *Q* parameter. Sign of *SFA* represents higher or lower values of average value of considered indicator. Obtained *SFA* of each indicator were smoothed using LOESS algorithm with smoothing parameter set to 0.25. Detailed description of this method can be found in Déry et al. (2005) and Stahl et al. (2010).

Trend analysis of each indicator as *SFA* is then analysed using Mann-Kendall (MK) test for monotonic trend (Kendall, 1975). A two-tailed MK test is chosen with 5% significance level. Null hypothesis of no trend is rejected if $|Z| > 1.96$.

Trend magnitudes were estimated using slope of the Theil-Sen Approach (*TSA*) (Theil, 1950; Sen, 1968), and slopes were calculated using time series of the *SFA*. Mann-Kendall test and slope of *TSA* were calculated using MAKESENS Microsoft© Excel template application (Salmi et al., 2002).

The analysis consists of two steps. First is related to the determination of the fixed period 1984-2013. This allows comparison of trend data between considered hydrological and meteorological stations. Second, the persistence of trends was inspected by systematically reducing the start year of analysis, starting from 1951 to 2013, then 1952 to 2013 and so on until 1984 to 2013, which represents the fix period of 30 years (Wilby, 2006). For each iteration MK Z statistics test was calculated, for full record 1951-2013, then 1952-2013 and so on until 1984-2013, so the sampling size varies from 63 to 30 years. By plotting obtained Z values for each iteration of start years, trend persistence and evolution through a given period can be achieved (Murphy et al., 2013).

4. RESULTS AND DISCUSSION

Figure 2 shows regular oscillation of annual mean flows around zero value before 1984.

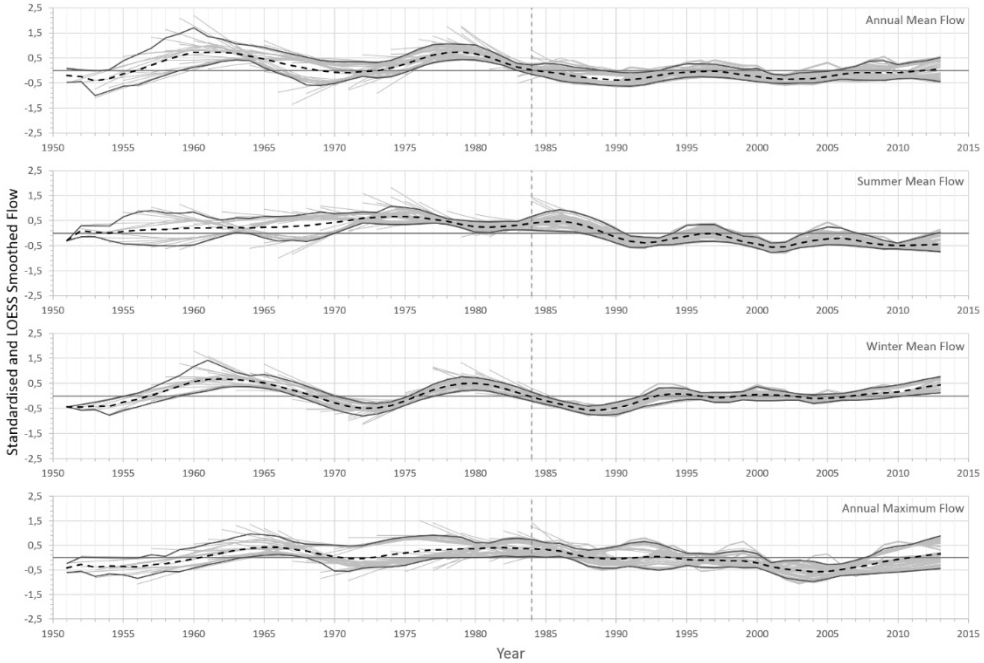

Figure 14: *Standardised and LOESS smoothed annual mean flows and annual maximum flows for hydrological stations Zamost 2, Kupari and. Grey lines reprsents smoothed SFA of each time record, red lines are the 5th and 95th percentile of standardised and LOESS smoothed series and dashed line is the mean of data set. Vertical dashed line represents the start of fixed period 1984-2013.*

After 1984, this oscillation is disrupted and mean values of annual flows are lower than long-term averages. This statement is consistent with the results obtained by Žugaj (1995) and Pavlić (2016). However, summer mean flows do not show similar oscillation before 1984, but after 1984 they do, together with lower mean values than long-term averages. Winter mean flows oscillates around long-term mean value almost through entire period with some minor discrepancy. Maximum annual flows do not have regular oscillation like winter mean flows and do not deviate so much around long-term average. Same approach was applied on annual precipitation data and is shown on **Figure 3**.

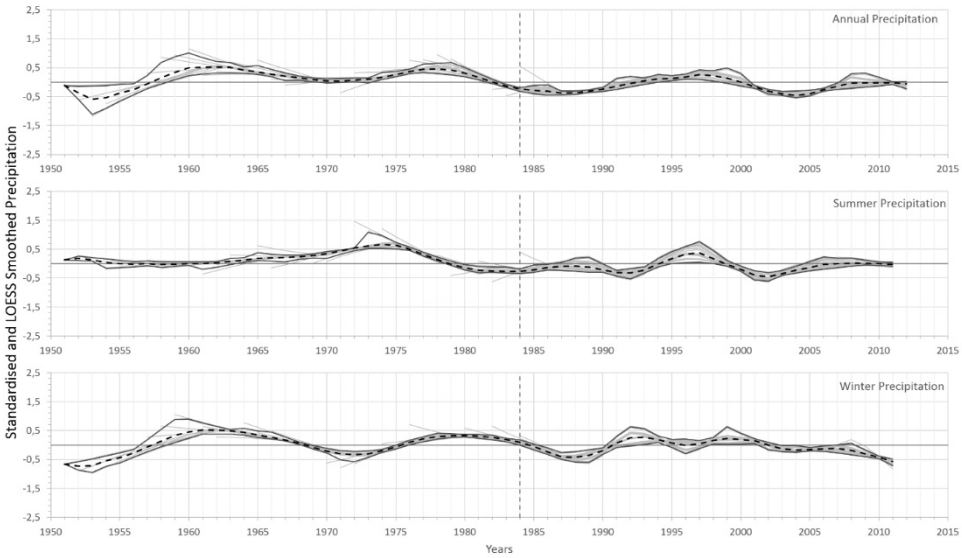

Figure 15: *Standardised and LOESS smoothed precipitation on meteorological station Parg. Grey lines reprsents smoothed SFA of each time record, red lines are the 5th and 95th percentile of standardised and LOESS smoothed series of individual station and dashed line is the mean of data set. Vertical dashed line represents the start of fixed period 1984-2013.*

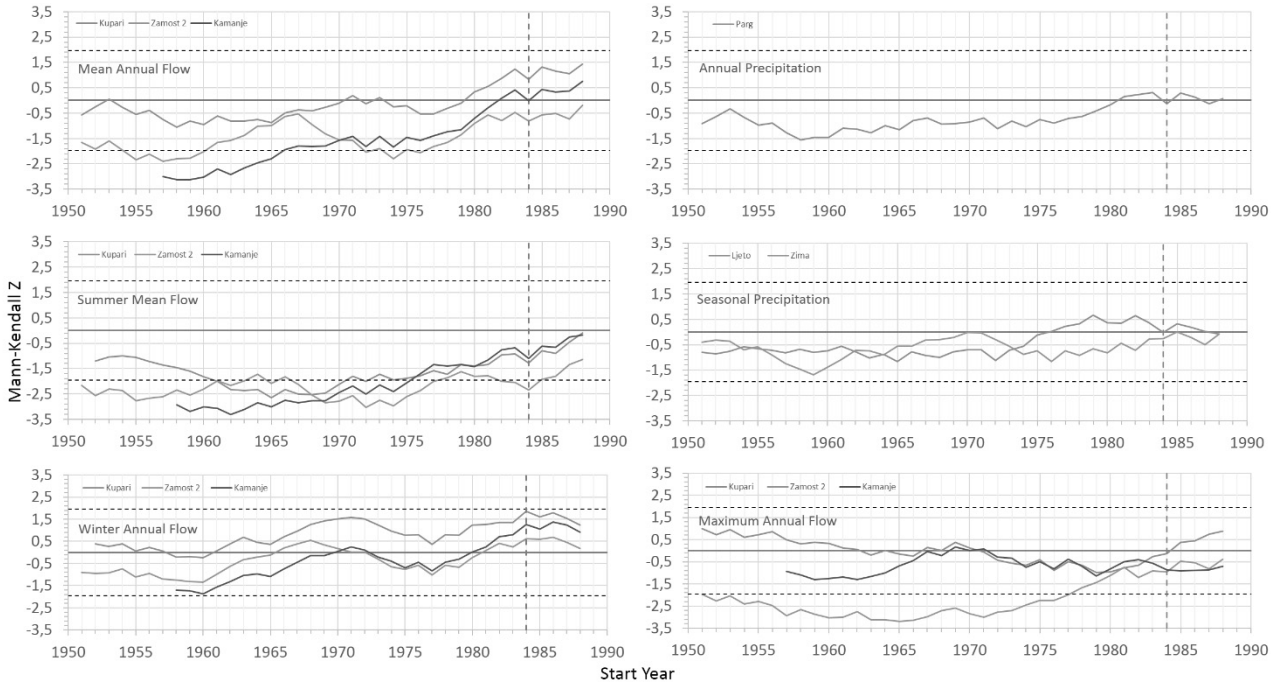

Figure 16: *Persistence plots for mean annual, seasonal and maximum annual flows, annual and seasonal precipitation ending in 2013. Solid lines represents MK Z statistics for each station, dashed horizontal lines represents threshold for significant trends at 5% significance level. Vertical dashed line represents the start of fixed period 1984-2013.*

The same can be concluded with precipitation data. In the mid-1980s, mean annual precipitation tends to be lower than long-term average.

Persistence of trends is shown on **Figure 4**. Mann-Kendall Z test is conducted for mean annual and seasonal flows, maximum annual flows, annual and seasonal precipitation.

5. CONCLUSION

Preliminary analysis of mean annual flows and annual precipitation showed that in the mid-1980s an arid period started. Further analysis pointed that summer annual flows were lower than long-term averages and winter annual flows remained close to long-term average. However, the oscillation that was pronounced in period before 1984 was disrupted in period 1984-2013 in all analysed indicators.

Trend analysis showed that mean annual flows tend to have negative trends ($Z<0$), but with significant negative trend only on Kamanje station starting in late-1950s until 1966. Zamost 2 station showed partially negative significant trend in 1950s and 1970s. Summer mean flows had predominantly significant negative trends on all three hydrological stations while winter annual flows showed no significant trend. No significant trend is found in annual nor seasonal precipitation. Maximum annual flows showed significant negative trend only on Kamanje station until late-1970s.

These results suggest a regime change of runoff on the karst basin of the river Kupa.

6. REFERENCES

BARNETT, T.P., PIERCE, D.W., HIDALGO, H.G., BONFILS, C., SANTER, B.D., DAS, T., BALA, G., WOOD, A.W., NOZAWA, T., MIRIN, A.A., CAYAN, D.R., DETTINGER, M.D. (2008): Human-Induced Changes in the Hydrology of the Western United States. Science, 319, 5866, 1080-1083.

DAI, A., TRENBERTH, K.E., QIAN, T. (2004): A global data set of Palmer drought severity index for 1870-2002: relationship with soil moisture and effects of surface warming. Journal of Hydrometeorology, 5, 1117-1130.

DÉRY, S.J., STIEGLITZ, M., MCKENNA, E.C., WOOD, E.F. (2005): Characteristics and Trends of River Discharge into Hudson, James, and Ungava Bays, 1964-2000. Journal of Climate, 18, 2540-2557.

GEDNEY, N., COX, P.M., BETTS, R.A., BOUCHER, O., HUNTINGFORD, C., STOTT, P.A. (2006): Detection of a Direct Carbon Dioxide Effect in Continental River Runoff Records. Nature, 439, 835-838.

GROISMAN, P.Y., KNIGHT, R.W., EASTERLING, D.R., KARL, T.R., HEGERL, G.C., RAZUVAEV, V.N. (2005): Trends in Intense Precipitation in the Climate Record. Journal of Climate, 18, 1326-1350.

HUNTINGTON, T.G. (2006): Evidence for intensification of the global water cycle: Review and synthesis. Journal of Hydrology, 319, 1-4, 83-95.

IPCC (Intergovernmental Panel on Climate Change), Solomon, S., Qin, D., Manning, M., Chen, Z., Marquis, M., Averyt, K.B., Tignor, M., Miller, H.L. (eds.) (2007): Climate Change 2007: The Physical Science Basis. Contribution of Working Group I to the Fourth Assessment Report of the Intergovernmental Panel on Climate Change. Cambridge University Press, Cambridge, United Kingdom and New York, NY, USA, 996 p.

KENDALL, M.G. (1975): Rank correlation methods. 4th Edition. London: Charles Griffin.

LABAT, D., GODDÉRIS, Y., PROBST, J.L., GUYOT, J.L. (2004): Evidence for global runoff increase related to climate warming. Advances in Water Resources, 27, 6, 631-642.

LEGATES, D.R., LINS, H.F., MCCABE, G.J. (2005): Comments on ''Evidence for global runoff increase related to climate warming'' by Labat et al. Advances in Water Resources, 28, 1310-1315.

MILLY, P.C.D., DUNNE, K.A., VECCHIA, A.V. (2005): Global pattern of trends in streamflow and water availability in a changing climate. Nature, 438, 17, 347-350.

MURPHY, C., HARRIGAN, S., HALL, J., WILBY, R.L. (2013): Climate-driven trends in mean and high flows from a network of reference stations in Ireland. Hydrological Sciences Journal, 58, 4, 755-772.

PAVLIĆ, K., (2016): Regional Hydrological Analysis of the Kupa Karstic Basin. Unpub. PhD Thesis, Faculty of Mining, Geology and Petroleum Engineering, University of Zagreb, Zagreb, 143 p.

SALMI, T., MÄÄTÄ, A., ANTTILA, P., RUOHO-AIROLA, T., AMNELL, T. (2002): Detecting trends of annual values of atmospheric pollutants by the Mann-Kendall test and Sen's slope estimates –the Excel template application MAKESENS. Finnish Meteorological Institute, Air Quality Research, Helsinki, Finland, 35 p.

SEN, P.K. (1968): Estimates of the regression coefficient based on Kendall's tau. Journal of the American Statistical Association, 63, 1379-1389.

STAHL, K., HISDAL, H., HANNAFORD, J., TALLAKSEN, L.M., van LANEN, H.A.J., SAUQUET, E., DEMUTH, S., FENDEKOVA, M., JÓDAR, J. (2010): Streamflow trends in Europe: evidence from a dataset of near-natural catchments. Hydrology and Earth System Sciences, 14, 12, 2367–2382.

ŠEGOTA, T., FILIPČIĆ, A. (2003): Köppenova podjela klima i hrvatsko nazivlje. Geoadria, 8, 1, 17-37.

THEIL, H. (1950): A rank-invariant method of linear and polynomial regression analysis, Part 1. Proceedings of the Royal Netherlands Academy of Sciences, 53, 386-392.

WILBY, R.L. (2006): When and where might climate change be detectable in UK river flows?. Geophysical research Letters, 33, L19407, doi: 10.1029/2006GL027552.

ZIEGLER, A.D., MAURER, E.P., SHEFFIELD, J., NIJSSEN, B., WOOD, E.F., LETTENMAIER, D.P. (2005): Detection Time for Plausible Changes in Annual Precipitation, Evapotranspiration, and Streamflow in Three Mississippi River Sub-

Basins. Climate Change, 72, 17-36.

ŽUGAJ, R. (1995): Regionalna hidrološka analiza u kršu Hrvatske, Monography of Croatian hydrological Society, Zagreb, 139 p.

ŽUGAJ, R., ANDREIĆ, Ž., PAVLIĆ, K., FUŠTAR, L. (2011): Flow duration curves. Građevinar, 63, 12, 1061-1068.

New approach in depositional environment reconstruction – Environmental Coefficient (C_e)

Luka Prša[1], Mirela Ferenčak[2]

[1]INA d.d., Exploration Sector, Šubićeva 29, 10000 Zagreb, Croatia, luka.prsa@ina.hr

[2]INA d.d., Field Development Sector, Šubićeva 29, 10000 Zagreb, Croatia, mirela.ferencak@ina.hr

Study area is located in the south-western part of the Pannonian Basin System, Sava Depression. Data set included 3 seismic horizons, well logs, lithology columns and gas shows for 96 wells from Pliocene sedimentary succession (Lonja Formation). The idea behind the study was to define a method to bypass a well to well correlation and to quantify depositional environments recognized on well data. Environmental coefficient (C_e) was calculated on all 96 wells, for two Pliocene zones separately. It is defined as sand fraction multiplied by average sand layer thickness (t_{avg}). Obtained values were interpolated to generate depositional environment maps. Results implied 3 groups of depositional environments: 1. Low energy/isolated areas, 2. Medium energy/medium depth areas and 3. Higher energy/distributary flow areas.

Key words: *Sava Depression, depositional environment, environmental coefficient*

1. INTRODUCTION

Study area is located in the south-western part of the Pannonian Basin System, Sava Depression. Late Pontian, Pliocene, Pleistocene and Holocene were the intervals during which most of the basin was uplifted. The subaqueous environment was greatly reduced, with dominant depositional settings being lacustrine, marshes and river alluvia (Malvić, 2012).

Data set included 3 seismic horizons, well logs, lithology columns and gas shows for 96 wells from Pliocene sediment succession (Lonja Formation) (Well Dossier, INA d.d., Zagreb). The idea behind the study was to define a method to bypass a well to well correlation and to quantify depositional environments recognized on well data.

2. METHODOLOGY

Environmental coefficient (C_e) is defined as sand fraction multiplied by average sand layer thickness (t_{avg}) (Eq. 1).

$$C_e = \text{sand fraction} \times t_{avg} \qquad \text{Eq. 1}$$

C_e concept enables us to describe certain depositional setting with just one number value, and to interpolate those values. This will result in maps representing synchronous depositional environments, with a fair mathematical background. This method will clearly differentiate wells with same sand fraction value (**Figure 1,** Well-2 and Well-3), which would have been equalized on often used sand fraction maps.

First step in the workflow was interpretation of three visible seismic horizons, Pal1, Pal2 and Pal3. When overlapped with well data, those horizons appeared to match with obvious boundaries on SP logs and lithology columns (**Figure 2**). Even though depositional settings and corresponding lithology changed laterally, this boundaries were traceable on most of the 96 wells.

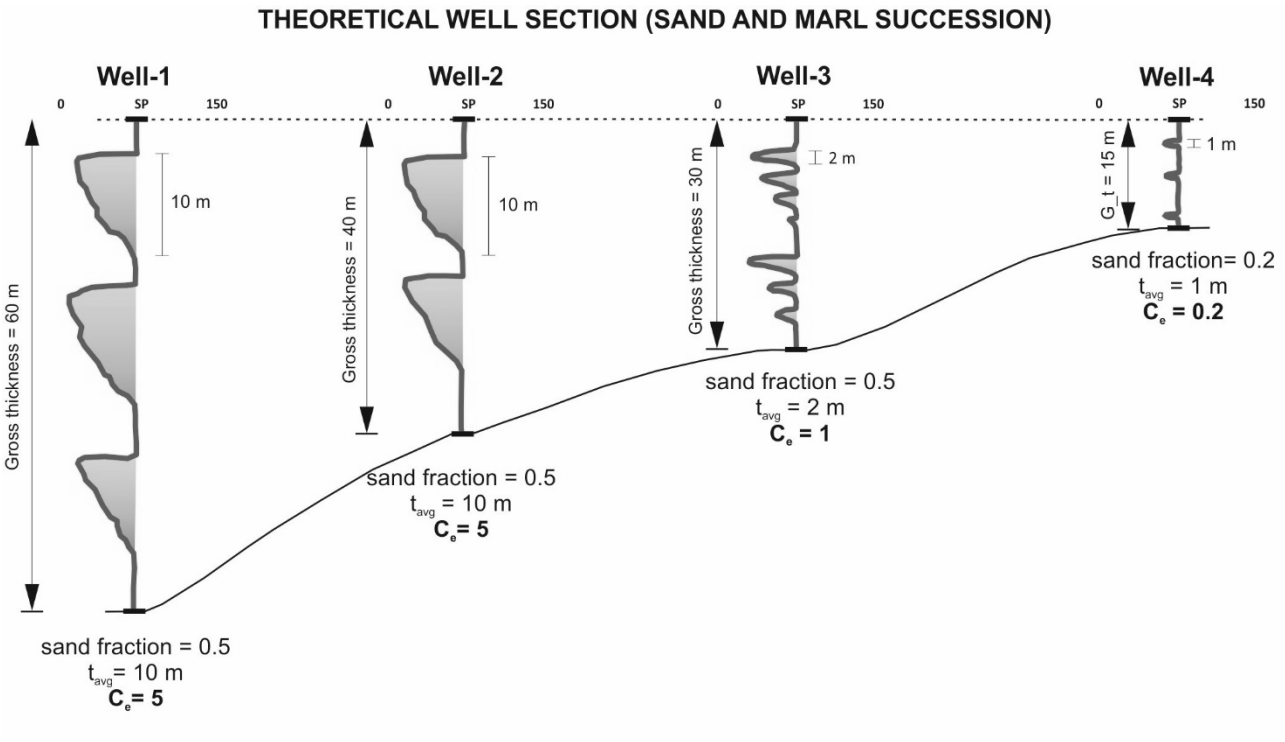

Figure 1: *Theoretical well section used for method explanation*

After defining zones of interest (Zone 1 and Zone 2), statistical lithology analysis was carried out. It included calculation of sand fraction and sand thickness, coal fraction and coal thickness, number of sand layers per zone and sand layer average thickness per zone. Results for three wells (A, B and C) are shown in **Table 1**.

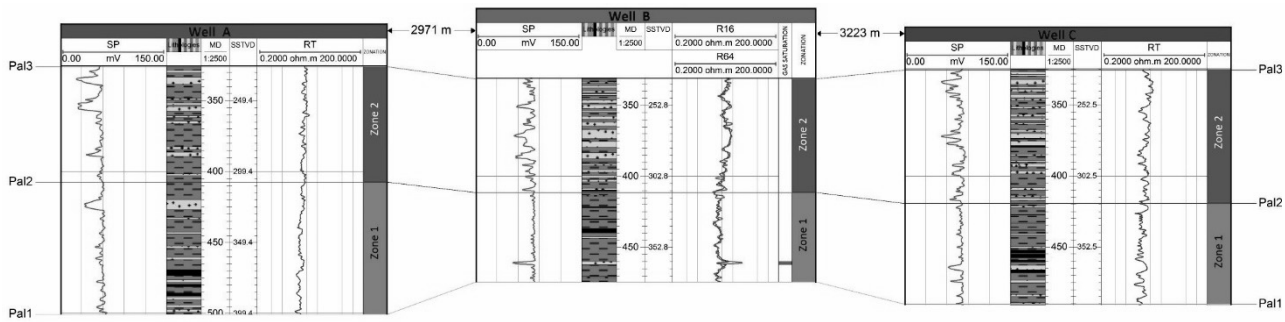

Figure 2: *Well section showing two interpreted zones*

Based on statistical lithology analysis, environmental coefficient was calculated on all 96 wells for two Pliocene zones separately. Obtained values were

interpolated to generate depositional environment maps (**Figure 3** and **Figure 4**). Apart from coefficient values, maps include zone base structural maps, gas shows and coal thickness on well location.

Table 1. *Statistical lithology analysis results for 3 correlated wells*

Well	Zone	Zone top (m)	Zone bottom (m)	Sand (fraction)	Sand (m)	Coal (fraction)	Coal (m)	Sand layers number	Sand layer average thickness	C_e
A	Zone 2	326.1	407.4	0.26	20.91	0.00	0.00	10	2.09	0.54
A	Zone 1	407.4	500.5	0.21	19.11	0.08	7.90	9	2.12	0.44
B	Zone 2	331.3	411.4	0.46	36.76	0.03	2.21	18	2.04	0.94
B	Zone 1	411.4	474.4	0.05	3.45	0.09	5.78	3	1.15	0.06
C	Zone 2	325.3	419.3	0.40	37.48	0.03	2.43	24	1.56	0.62
C	Zone 1	419.3	490.3	0.16	11.04	0.13	8.92	10	1.10	0.17

3. RESULTS

After qualitative well log interpretation and correlation with environmental coefficient values, 3 groups of depositional settings were defined:

1. Low energy/isolated areas:
   - sand percentage less than 20%
   - coal presence
   - 0.0 - 0.4 C_e

2. Medium energy/medium depth areas:
   - sand percentage between 20 and 40 %
   - favorable environment for sand lenses formation
   - 0.4 - 0.8 C_e

3. Higher energy/distributary-flow areas:
   - more than 40 % sand percentage
   - maximum sand layer thickness up to 20 m
   - > 0.8 C_e

Gray sections of the maps are representing depositional settings that could be interpreted as isolated, marsh areas. Water energy was very low, enabling organic material to be preserved (maximum coal thickness drilled).

Brown portions of the maps imply medium energy areas, depositional environments closer to sediment source, with higher water energy. Those are favorable settings for sand lenses formation, interesting in the terms of biogenic gas accumulation.
Yellow parts of the maps could be distributary flow areas, high energy parts of the basin. Maximum sand layer thickness in those areas goes up to 20 meters, confirming the concept.

Accuracy of the interpolation procedure is declining in the areas with low well control. For that reason, maps were overlapped with zone base structural maps. Considering that II. transpressional phase started in late Pontian (Cvetković, 2013), it is fair to assume that current structural relationships outline paleostuctural ones and that those structural maps could represent lake base in the time of late Pliocene sediment deposition.

During the sedimentation of Zone 1 sediments, lake surface was reduced and 3 marsh areas developed on north-west and south-east. Lake conditions remained only in the central, deepest part of basin. In general, this zone can be compared with lithostratigraphic member Ravneš, defined by Cvetković, 2013. Zone 2 represents period of lake expansion and intense sedimentation in restored basin conditions, resulting with high C_e values (distributary flow zone) in the central part of the map. Based on the results, it can be assumed that clastic material was prograding from the north-east. This zone is similar to lithostratigraphic member Oborovo described by Cvetković, 2013.

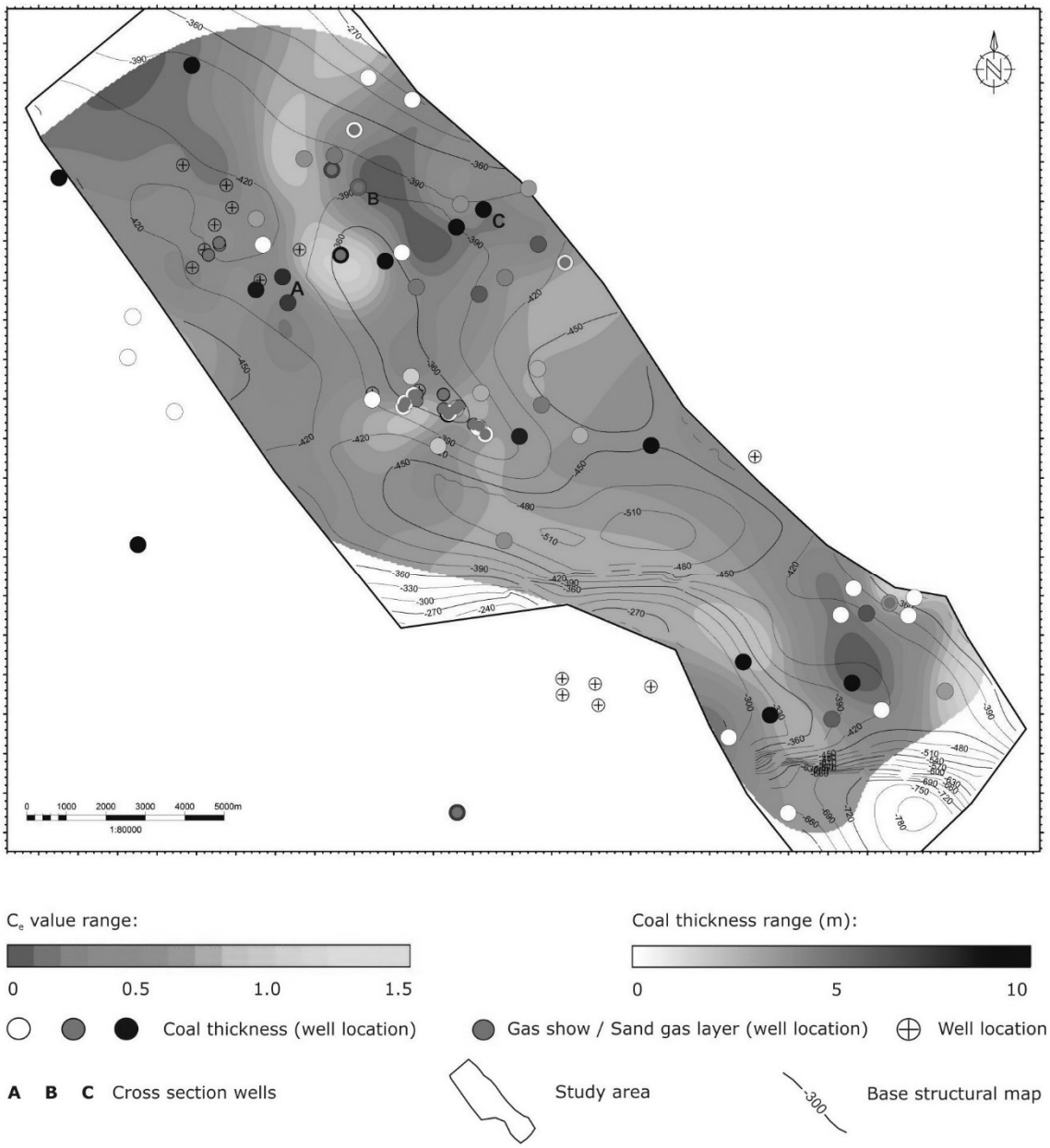

Figure 3: *Zone 1 depositional environment map overlapped with zone base structural map*

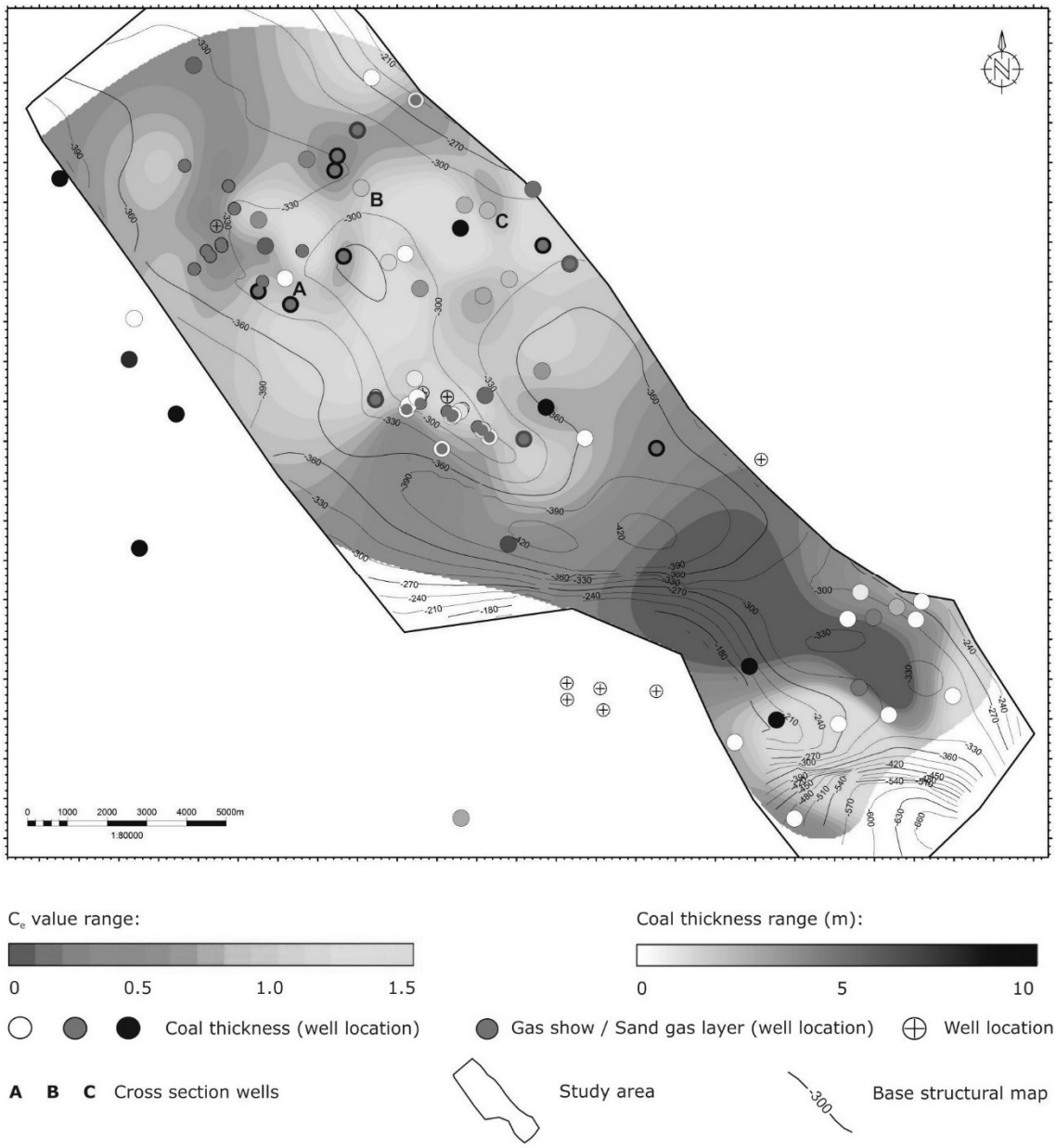

Figure 4: *Zone 2 depositional environment map overlapped with zone base structural map*

4. REFERENCES

CVETKOVIĆ, M. (2013): Lithostratigraphic units of the third Neogene-Quaternary megacycle in the Sava depression and their petroleum potential. – Faculty of Mining, Geology and Petroleum Engineering, University of Zagreb, Zagreb, 179-185.

MALVIĆ, T. (2012): Review of Miocene shallow marine and lacustrine depositional environments in Northern Croatia. - Geological quarterly. 56, 3; 493-504.

UNPUBLISHED PAPERS:

WELL DOSSIER, INA d.d., Zagreb

Neotectonic active faults in the Eastern part of Sava Depression: Implications to tectonic evolution based on 2D seismic data and 3D subsurface structural modelling

Rukavina, D.[1*], Matoš, B.[1], Tomljenović, B.[1], Saftić, B.[1]

[1]Faculty of Mining, Geology and Petroleum Engineering, Department of Geology and Geological Engineering, University of Zagreb, Pierottijeva 6, 10000 Zagreb, Croatia, david.rukavina@rgn.hr

The neotectonic fault analysis in the Eastern part of Sava Depression (ESD) is obtained by structural interpretation of 24 seismic sections and 15 wells. This enabled construction of a 3D subsurface structural model and determination of geometry, kinematics and arrangement of neotectonically active faults, using *Petrel™ Seismic to Simulation* software. The model consists of 12 fault planes and 3 seismic horizons that correspond to the three regional unconformities, i.e. the major stratigraphic boundaries in tectono-sedimentary evolution in the Croatian part of the Pannonian Basin. Tectonic evolution of the ESD commenced with Early to Middle Miocene extension along WNW-ESE striking normal faults that accommodated stretching estimated to ca. 3.2%, allowing the formation of two NW-SE striking synclines that generally correspond to the main depocenteres. Extension was followed by the Middle to Late Miocene phase of thermal subsidence that enabled deposition of more than 1600 m thick pile of sediments. This subsidence was only locally accommodated by normal faults inherited from the previous phase. The last tectonic phase is recognized along the northern edge of the ESD, characterized by reverse faulting (more than 1200 m of vertical displacement) and several pop-up structures formed during the Late Miocene to Quaternary.

Key words: *Sava Depression, Neogene, Quaternary, seismic interpretation, structural model*

1. INTRODUCTION

Novel neotectonic research of the Eastern part of Sava Depression (ESD) in the SW Pannonian Basin presented in this work is based on 24 seismic sections and 15 exploration wells, supplemented with surface geological data. It resulted in construction of structural model of the ESD, which comprise 12 fault planes and 3 stratigraphic horizons. After an overview on the ESD tectonics and geological setting, we present used methodology and results of structural analysis that includes structure contour maps and interpreted seismic cross sections.

2. Tectonic and geologic setting

The study area covers eastern part of the Sava River valley in the southern part of the Pannonian basin system (PBS), with surrounding Slavonian Mountains (Psunj, Požeška gora and Dilj Mts.) in the north, and Prosara and Motajica Mts. in the south. From the Early to Late Miocene times (c. 26-11.5 Ma), PBS evolved as a back-arc basin, the extension of which was driven by subduction roll-back of the Carpathian slab (Royden et al., 1983; Fodor et al., 1998; Schmid et al., 2008;). At the end of Middle Miocene (c. 13.0-11.6 Ma) locally within the SW marginal part of PBS syn-rift extension was shortly replaced by tectonic inversion (Horváth, 1995; Fodor et al., 1999; Horváth and Tari 1999; Tomljenović and Csontos, 2001), which yielded local erosion of pre-Pannonian deposits. Late Miocene to early Pliocene was characterized by overall thermal subsidence throughout the PBS that in the SW marginal part resulted in widening and deepening of accommodation space filled by a thick pile (≤2000 m) of contemporaneous sediments (Lučić et al., 2001; Velić et al., 2002; Saftić et al., 2003). Regional movements of Adria Microplate and changes of boundary conditions around the PBS during Pliocene and Quaternary, caused change of stress field from extension to compression (Horváth and Tari, 1999; Bada et al., 1998, 2001). In the SW PBS, this change of stress is manifested by shortening and inversion evidenced by newly formed reverse faults, folds and pop-up structures and by numerous inverted normal faults (Prelogović et al., 1998; Fodor et al., 1999; Tomljenović and Csontos, 2001; Matoš, 2014, and references therein).

3. Methods

Primary input dataset consisted of seismic and well data provided by Croatian oil company INA-d.d. Zagreb (24 2D seismic reflection sections and 15 wells). Well dataset encompassed total depths of drilled stratigraphic horizons and measured TWT-Depth relations. Beside subsurface data, geological surface data presented on geological maps in a scale 1:100 000 were used to the structural interpretation corrections. The analysis of neotectonic activity in the ESD involved in first, interpretation of the base Neogene, base Pannonian and base

Pliocene-Quaternary stratigraphic horizons, and interpretation of active fault traces. In the SW PBS, these stratigraphic horizons correspond with the major unconformities that are well recognized on well data (Velić et al., 2002; Saftić et al, 2003).

Seismic interpretation included interpretation of stratigraphic horizons and fault traces, but also cross-correlation with surface geological data. Interprated data was then used to construct geological model of study area. Modelling procedure included construction of the preliminary structural framework model and the final subsurface model with detailed fault pillar gridding, and definition of viable geological relations between identified fault planes and mapped horizon surfaces. Since, the structural modelling processes were performed in time domain, constructed subsurface model was T-D converted based on the available velocity data i.e., velocity model. In that purpose, velocity model was constructed using $V=V_0=V_{int}$ equation where the model velocity (V) is assumed as a constant value through each model zone, whereas $V_0=V_{int}$ correspond to the surveyed velocity values, i.e., well surface time-depth relations (TDR).

4. Results

Model comprises 12 fault planes and three regional stratigraphic horizons (base Neogene, base Pannonian and base Plio-Quaternary). The structure contour maps of these horizons and interpreted seismic sections are used to evaluate neotectonic activity along delineated faults in the study area. Spatial location of interpreted seismic cross sections is shown in **Figure 1**, while the seismogeological interpretation of these sections is presented in **Figure 2**.

Interpreted sections A-A' and B-B' (**Figures 2a** and **2b**) show reverse faulting in both Neogene fill and pre-Neogene basement in northern part of Sava depression. An example of the prominent inversion pop-up structures are seen in the central part of sections A-A' and B-B'. This structure was formed by reactivation along earlier normal fault, as indicated by different thickness of Miocene sequences in hanging wall and footwall of this fault.

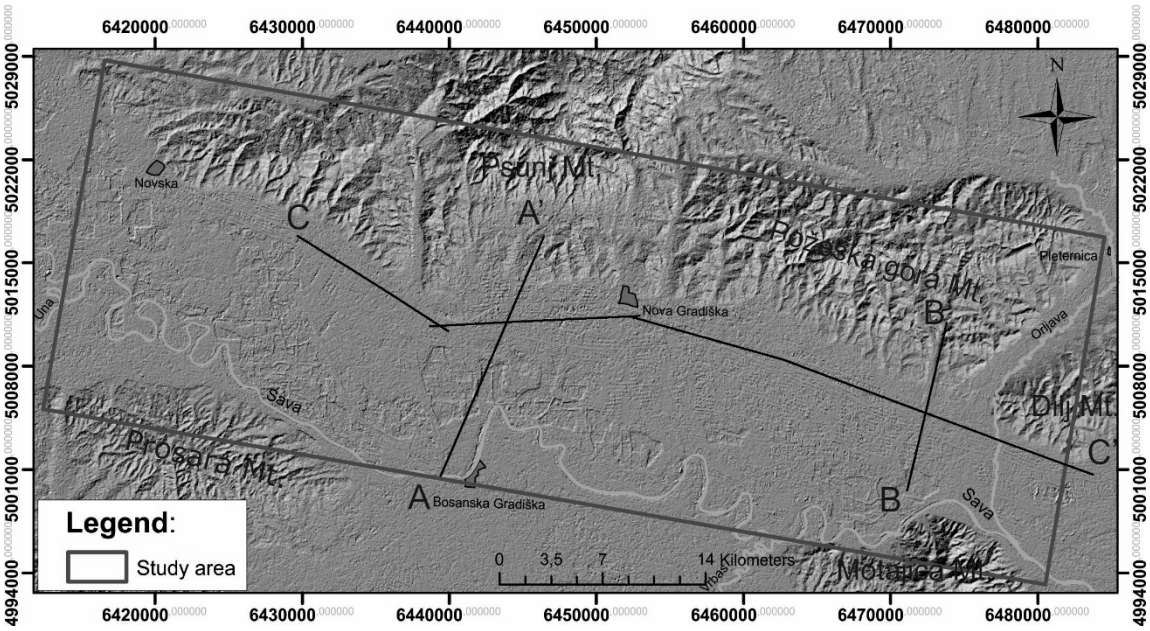

Figure 1: *Location map of interpreted seismic lines shown in Figure 2.*

Section C-C′ (**Figure 2c**) is used for observation of thicknesses variation of Miocene and Plio-Quaternary sediments along the strike of ESD studied area. It showed that Lower to Middle Miocene syn-rift sediments are the thinnest, whereas Upper Miocene sediments are the thickest Neogene sequence, locally up to 1600 m.

The base Neogene structure contour map (**Figure 3a**) indicates two main NW-SE striking synclines that generally correspond to the main depocentres that reach up to 2800 m depth along the southern margin of the Slavonian Mts. Northern limbs of both synclines are faulted with a pair of two inverted normal faults, which uplifted the base Neogene for more than 1200 m south of Psunj Mt. where the uplift is the largest and makes northern border of ESD towards the Slavonian Mts. Southern limbs are also faulted, but with NE-dipping normal faults (**Figure 3a**). In the central part of study area couple of NW-SE striking pop-up structures were interpreted. Structures delineated by the base Pannonian structure contour map (**Figure 3b**) are similar to those identified on the base Neogene structure contour map. Relative vertical displacements along the ESD boundary faults are the biggest south of the Mt. Psunj (**Figure 3b**). The base Pannonian structure contour map also shows that axes of both synclines are shifted towards the south with their troughs at depths of 2200 m. The base Plio-Quaternary structure contour map (**Figure 3c**) also shows map-scale

structures similar to those delineated on above described maps. On this map both syncline troughs are depth of more than 900 m and shifted further south. The northern limbs of both synclines are similarly faulted as on the two deeper horizons. Vertical displacements along mapped normal faults are in range of 50 m to 100 m, whereas for faults with reverse character is from 50 up to 700 m with respect to the base Neogene horizon. Vertical displacements for base Pannonian horizon for normal faults is about 50 m and for faults with reverse character is from 50 up to around 400 m.

5. Discussion and Conclusions

Number of inverted normal faults in study area of Sava depression implies strong inversion which occurred during Pliocene and Quaternary. At least some of these normal faults were active during the syn-rift stage in the ESD, and enabled opening of depositional space (**Figure 3a**) during extensional phase in Early and Middle Miocene. Palinsplastic restoration made for section B-B' provides insights into three stages of ESD evolution (**Figure 2d**). Reconstruction shows that evolution of the ESD commenced with Early to Middle Miocene extension along WNW-ESE striking normal faults that accommodated stretching estimated to ca. 3.2%. Thermal subsidence during Late Miocene enabled sedimentation of thick pile of contemporaneous sediments (**Figures 3b** and **3c**), while normal faults were at least locally still active but with lower offsets (50 m; **Figure 2d**). Inversion of most of earlier normal faults took place during the Plio-Quaternary and is particularly prominent along the northern margin of ESD where vertical cumulative displacement of the base Neogene reaches more than 1200 m.

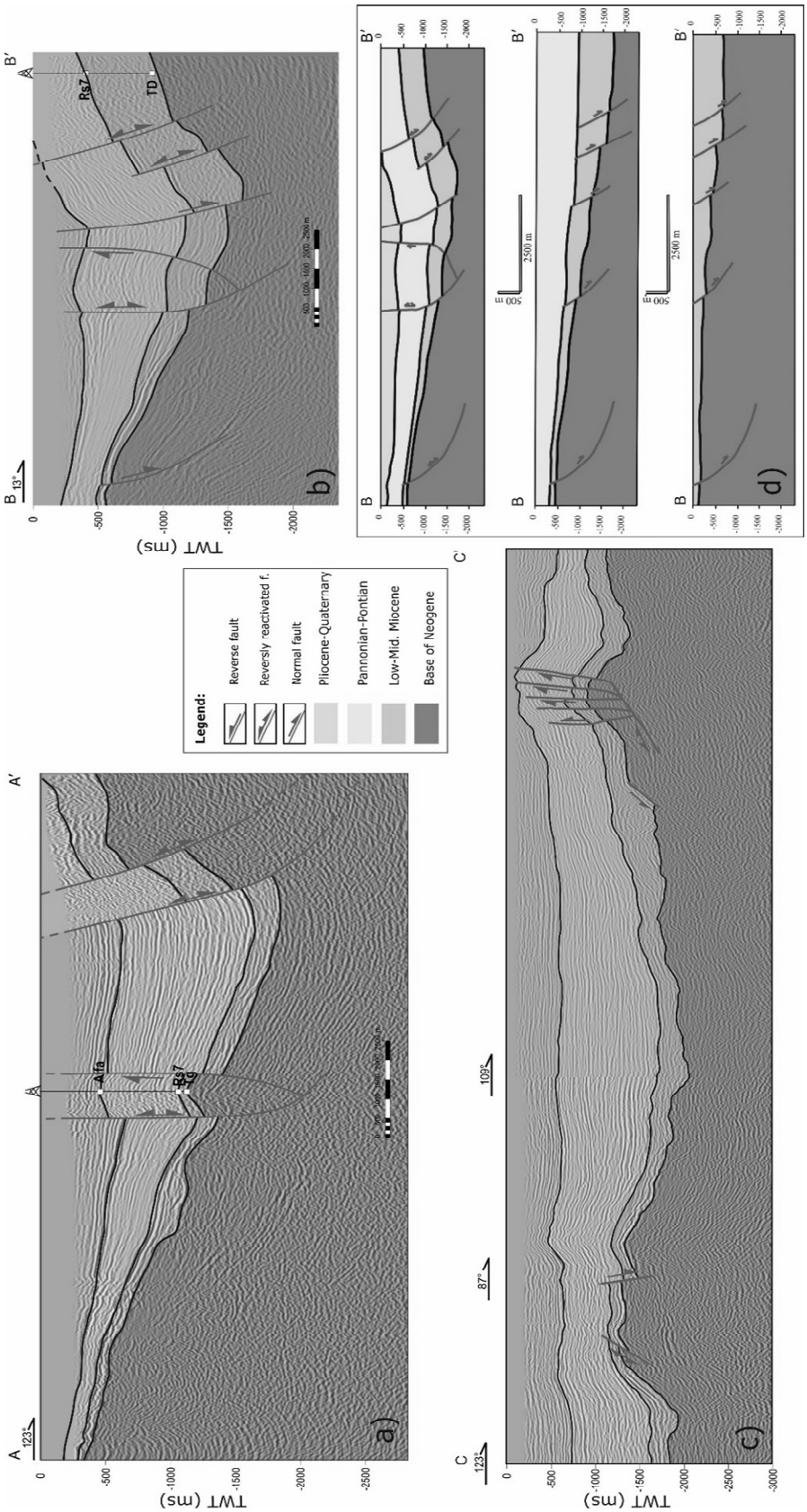

***Figure 2**: a), b) and c) seismogeological sections; 3 d) palinsplastic reconstruction of B-B′ section.*

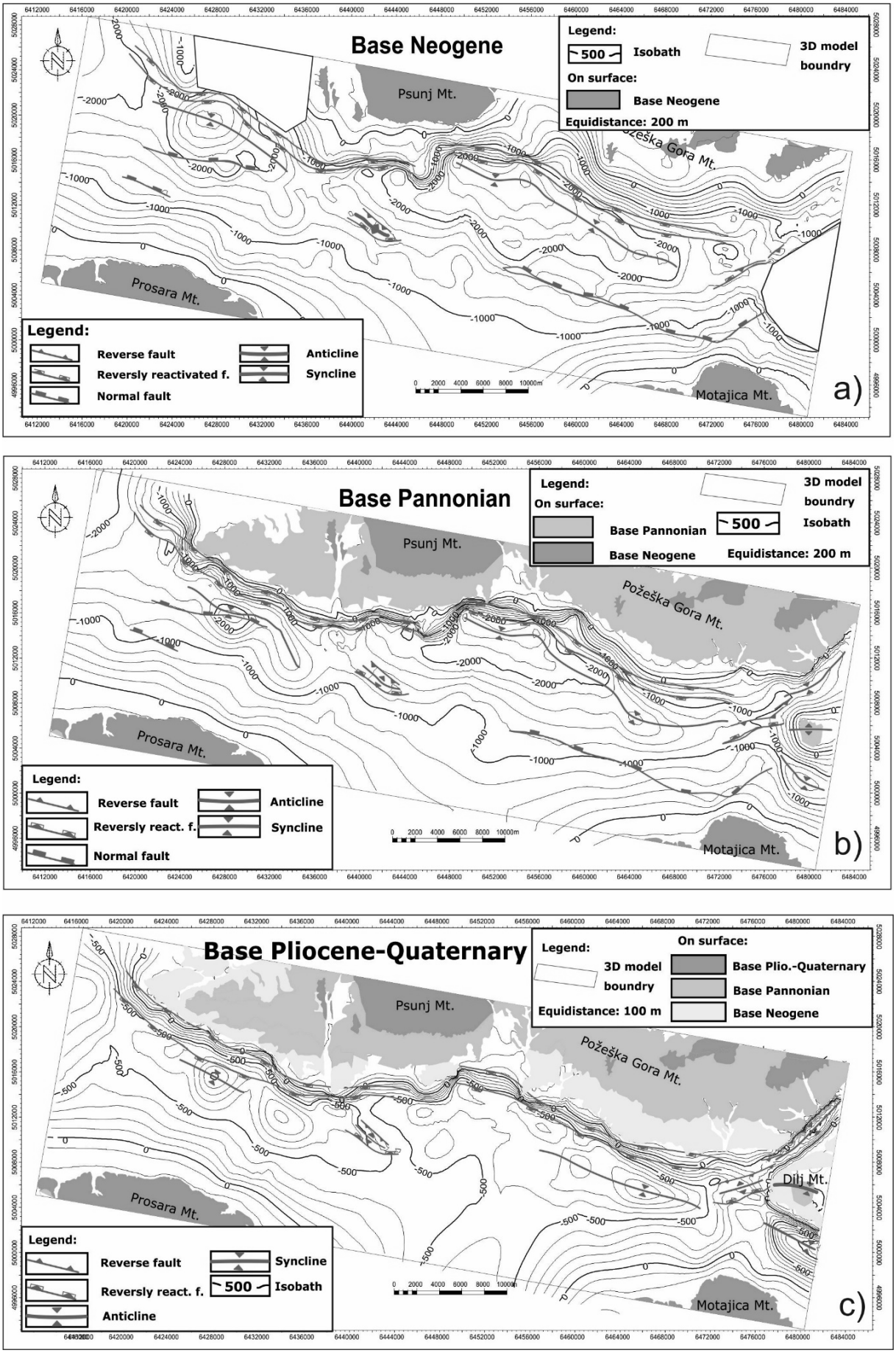

Figure 3: *a), b) and c) structure contour maps created in constructed 3D model.*

6. REFERENCES

FODOR, L., JELEN, B., MÁRTON, E., SKABERNE, D., ČAR, J., VRABEC, M. (1998): Miocene-Pliocene tectonic evolution of the Slovenian Periadriatic fault: implications of Alpine-Carpathian extrusion models. Tectonics 17, 690-709.

FODOR, L., CSONTOS, L., BADA, G., GYÖRFI, I., BENKOVICS, L. (1999): Tertiary tectonic evolution of the Pannonian basin system and neighbouring orogens: a new synthesis of paleostress data. The Mediterranean Basins: Tertiary extension within the Alpine Orogen. Geological Society of London, Special Publications, 156, 295-334.

HORVÁTH, F. (1995): Phases of compression during the evolution of the Pannonian Basin and its bearing on hydrocarbon exploration. Marine and Petroleum Geology, 12, 837-844.

HORVÁTH, F., TARI, G. (1999) IBS Pannonian Basin project: a review of the main results and their bearings on hydrocarbon exploration. Special Publication of Geological Society in London, 156, 195–213.

LUČIĆ, D., SAFTIĆ, B., KRIZMANIĆ, K., PRELOGOVIĆ, E., BRITVIĆ, V., MESIĆ, I., TADEJ, J. (2001): The Neogene evolution and hydrocarbon potential of the Pannonian Basin in Croatia. Marine and Petroleum Geology, 18, 133-147.

MATOŠ, B. (2014): Neotectonic and recently active faults in Bilogora Mountain area and assessment of their seismogenic potential. Ph.D. Thesis, University of Zagreb, Faculty of Mining, Geology and Petroleum Engineering, Zagreb.

PRELOGOVIĆ, E., SAFTIĆ, B., KUK, V., VELIĆ, J., DRAGAŠ, M., LUČIĆ, D., 1998. Tectonic activity in the Croatian part of the Pannonian basin. Tectonophysics, 297, 283-293.

ROYDEN, L.H., HORVÁTH, F., RUMPLER, J. (1983): Evolution of the Pannonian basin system, 1. Tectonics. Tectonics 2, 63-90.

SAFTIĆ, B., VELIĆ, J., SZTANÓ, O., JUHÁSZ, G., IVKOVIĆ, Ž. (2003) Tertiary Subsurface Facies, Source Rocks and Hydrocrbon Resevoirs in the SW Part of the Pannonian Basin (Northern Croatia and South-Western Hungary). Geologia Croatica, 56/1, 101-122.

SCHMID, S. M., BERNOULLI, D., FÜGENSCHUH, B., MATENCO, L., SCHEFER, S., SCHUSTER, R., TISCHLER, M., USTASZEWSKI, K. (2008): The Alpine-Carpathian-Dinaridic orogenic system: correlation and evolution of tectonic units. Swiss Journal of Geosciences, 101, 1, 139-183.

TOMLJENOVIĆ, B., CSONTOS, L. (2001): Neogene-Quaternary structures in the border zone between Alps, Dinarides and Pannonian Basin (Hrvatsko zagorje and Karlovac Basin, Croatia). International Journal of Earth Sciences (Geologische Rundschau), 90, 560-578.

VELIĆ, J., WEISSER, M., SAFTIĆ, B., VRBANAC, B., IVKOVIĆ, Ž. (2002): Petroleum-geological characteristics and exploration level of the three Neogene depositional megacycles in the Croatian part of the Pannonian basin. Nafta, 53/6–7, 239–249.

Siliciclastic coasts- Problems and possible solutions related to modeling of these extreme heterogenic environments

Case Study

Viktor Volford

University of Szeged, Dept. of Geology and Paleontology

Szeged, Egyetem utca 2-4 viktor.volford2@gmail.com

The actual stratigraphic records of a coastal environment are the results of several physical processes and their complex interactions acting along the coasts. The internal sedimentary parameters and organic contributions to the deposited sediments are influenced by these forces and processes. Sediment characteristics are significant in the interpretation of the vertical relationship of the sedimentary facieses and in identifying the lateral distribution of sedimentary sub-environments. This study essays to combine the theoretical and practical issues in order to delineate the particular facieses in the function of the available dataset.

The target field is composed of basal conglomerates and form a part of the lower pannonian sequence. Four genetic lithotypes were identified in the subsidence from cores: (1) grain supported conglomerates (2) mud supported conglomerates (3) aleuritic fine-sandstone (4) medium grain size sandstone with mica. Based on their sedimentary characteristics the following depositional mechanisms could be considered: (1) debris flow (2) wave induced abrasion (3) rip/longshore currents. The available well logs do not allow the separation of these lithotypes consistently due to their similar response. However logs capable to divide into units with different reservoir qualities. That fact, one of the most important factor in the control of sediment distribution on coastal environment is the paleo relief, the expected occurrence of the better quality reservoir rock connected to smaller relief and worse properties incorporated with higher relief.

The modeled geometry and their incidence probability incorporated with the paleo basement morphology were totally capable to join these units into the desirable facies types.

Key words: *paleo basement morphology, Co-simulation, clastic coasts, vertical proportional curves*

1. INTRODUCTION

The purpose of this is study tracing a practical and common used workflow including handling diverse types of information which represent different volume support. Problem arises if there are not suitable well logs for consistent lithology differentiation. It is more pronounced in the case of a shoreline conglomerates which insight heterogeneity is complex and the lateral distribution of the different lithofacieses hardly understandable. Although they have really good reservoir properties due to non-directivity and missing of small - scale stratification besides they storage gas. That was the main reason why the industrial "rock typing", accurately their simplest form was chose. It is based on cutoff-values regularly connected to water saturation, permeability and porosity. In this study two rock types were separated based on their permeability cutoff approach (1mD) values determined from capillary and pore throat size distribution curves.

According to the literature (Bérczi, 1985) the basal sequence consists of two types of conglomerates genetically based on the rock texture: (1) abrasive origin – matrix supported (2) debris flow origin – mud supported.

The first type occurs in the structural high position contrary to the second which deposited towards the basin as the results of debris-flow. The transition between them is gradual rather than abrupt. Obviously other lithotypes also occur in the strata such as pebbly sandstone and aleurolite. These clear separations cannot be solved because they are embedded, stacked and their measurable petrophysical properties from logs concur with the enclosing strata. Nevertheless some statement could be done refers to lateral changes from the shoreline to the basin: (1) the average grain-size needs to decrease (2) the shale contents increasing (3) the sorting reducing. These changes also reflected in the context of average porosity-permeability-water saturations. To inherit this multivariate lateral trend into the final model the sequential Gaussian co-simulation with Markoc-type extension were used for porosity-permeability modelling constrained by the rock types (Ntg) model.

2. USED WORKFLOW

Pieces of the standard industrial workflow were used in the modelling process. Broadly includes the following steps: (1) structural modelling, (2) gridding and upscaling, (3) facies/Ntg modelling, (4) petrophysical modelling, (5) volume calculations, (6) sensitivity analysis.

This study is not intended to give hydrocarbon initially in place calculations. That is why the last two steps were ignored.

The Ntg/rock-types log derived from capillary curves. These delineated vertically the effective and not effective parts of the reservoir. Two seismic horizons from 3D seismic as top and base were the inputs for structural modelling. After the gridding and well log upscaling into the 3D grid resolution Ntg model was evolved with sequential indicator simulation. In order to preserve the Ntg proportions in each grid layer in the model, vertical proportional curve (VPC) was used as a vertical 1D trend calculated from wells.

The obtained Ntg model served as a constraint for the petrophysical modelling. It is quite important because the petrophysical continuity thus the variogram ranges are different in the different rock types. One individual Ntg realization connected to one petrophysical output realization. There were 100 realizations produced.

The algorithm was the before mentioned sequential Gaussian co-simulation with Markov-type extension. It does not require the Linear Model of Coregionalization (LMC) like the full sequential Gaussian co-simulation only the semivariogram model of the primary variable $\gamma_{pp}(h)$ and $\gamma_{ps}(h)$ by the correlation coefficient $\rho_{ps}(0)$ needs to describe. (Geiger, 2015).

Comparison between the results and the main assumptions were well coincident and also the well data were correctly captures and reproduces statistically.

3. RESULTS

3.1. Measurements on rock samples

Seventeen capillary pressure curves were available from Hg invasion for cutoff permeability determination. The related pore throat size distributional curves were also obtained (**Figure 1**).

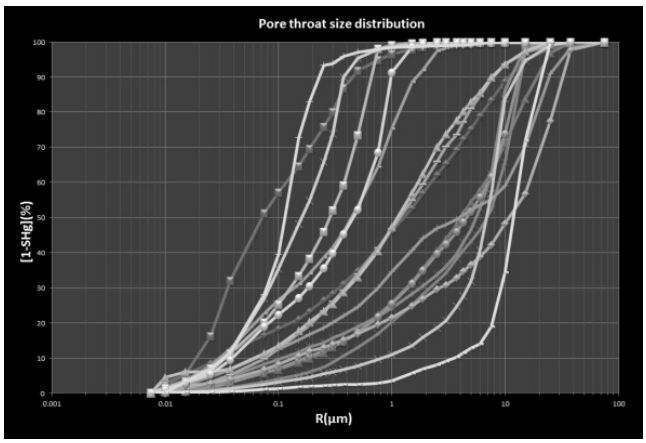

Figure 1: *Pore throat size distribution curves plot*

Figure 2 shows the pore throat radii corresponding to a mercury saturation of 50% (R50) versus measured permeability in millidarcy. Well known fact, that the permeability is the function of pore throat size distribution rather than porosity. If (R50) pore throat radii were increased the permeability was increased exponentially. In oil saturated reservoir the effective pore throat sizes are above 2 microns because it requires two-phase fluid flow. Consider that the present reservoir are saturated with gas the cutoff radii was much lower due to the lower viscosity. Actually 1 mD belonged to 0.2 microns could be justified.

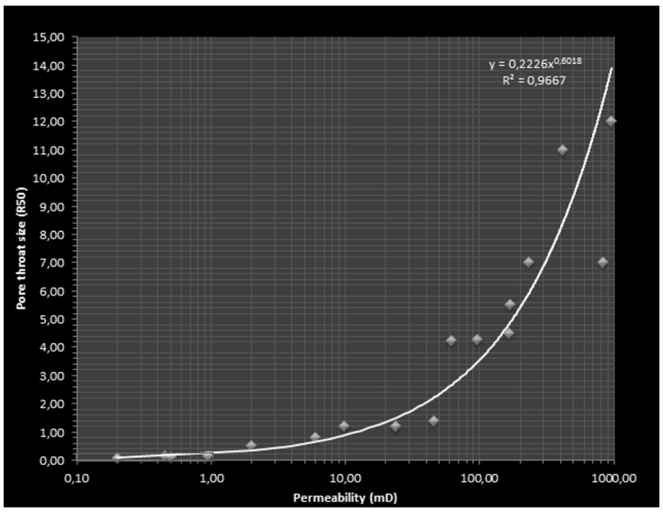

Figure 2: *Cutoff permeability determination plot*

Such high effectivity is typical in conglomerates if diagenetic alteration does not take place in the pore structure. None relationship can be discovered on Co_3 versus vertical and horizontal permeability scatter.

The medium-high Co_3 content is due to carbonate particles, which means that the pores have not been affected by carbonate cementation. This high non-effective/effective ratio was also evidenced from vertical and horizontal permeability cross plot measured on almost 120 samples. Such high correlation indicated lack of small-scale layering or bedding.

3.2. Plug measurements and quantitative well log interpretations

The distribution of a variable is scale dependent. However comparison the dataset coming from direct measurements from core plugs and well logs provide a good method to check the quality of quantitative log interpretation.

Por-perm from plugs and por-perm from interpreted well logs represented similar trends with different standard deviations. Lower por-perm values were under represented from plug measurements because the coring focused on better quality intervals. Practically, similar trend enabled to use the correlation coefficient from quantitative well logs for petrophysical modelling (**Figure 3**).

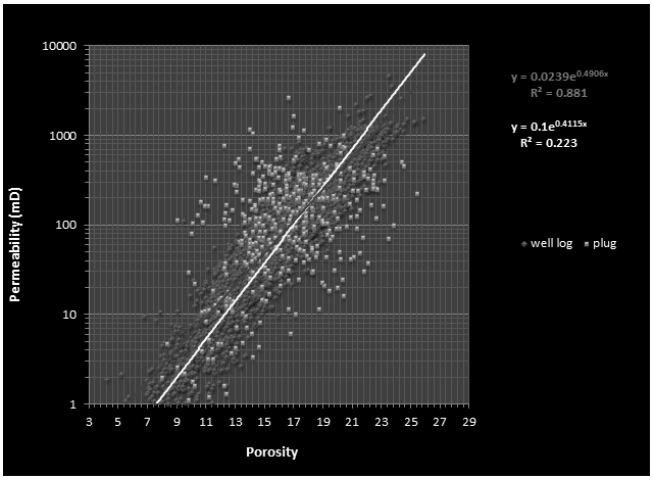

Figure 3: *Porosity and permeability plot from well logs and plugs with trends*

3.3. Structural models and gross thickness

The reservoir is located above a structural height. The basement strike is NW-SE. Except from the SE side the conglomerate pinched out on the basement.

There were also two parts in the centre where the reservoir is not present. The reservoir can be followed on 3D seismic on the SE side, but it was skipped out at this study.

Highest gross thickness was concentrated around the structural hight due to the highest sedimentation rate. (**Figure 4**)

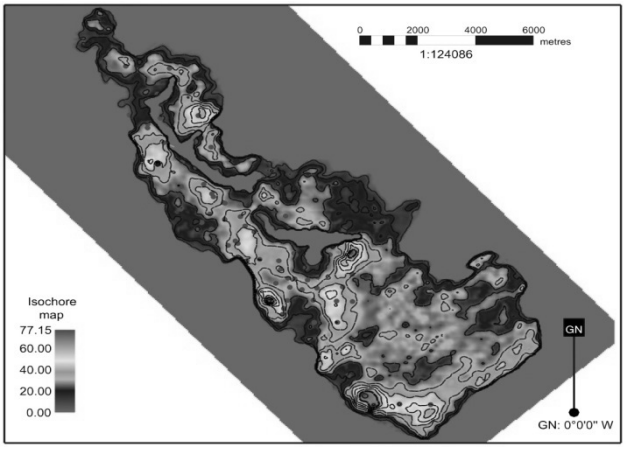

Figure 4: *Gross thickness map*

3.4. Petrophysical models

The expected porosity and permeability values in the model were truncated into different ranges represented by codes to emphasize the mentioned lateral changes and lead the visual quality control of the model. Intersections from permeability model parallel and perpendicular the main axis of the reservoir clearly suggested that transition. (**Figure 5 and 6)**

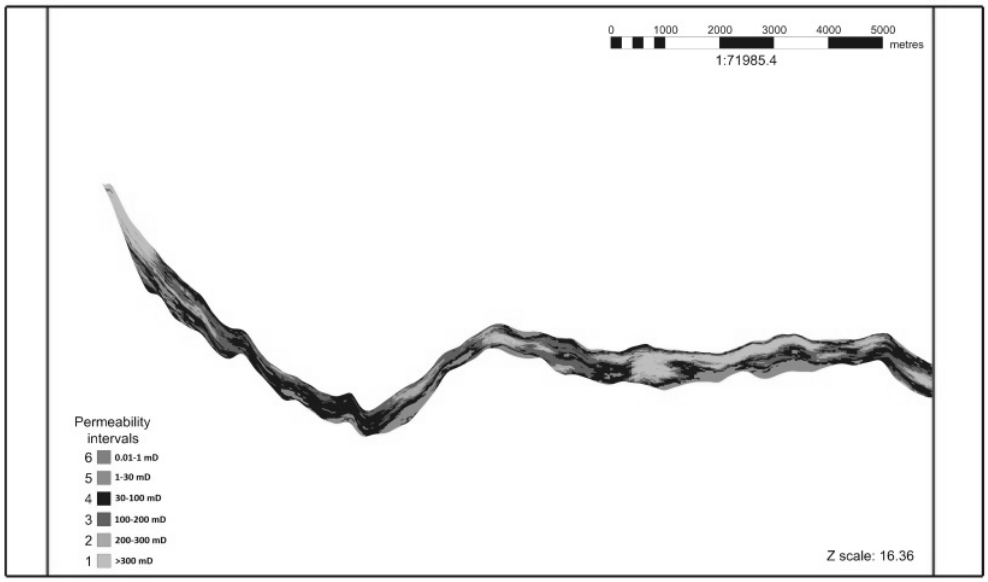

Figure 5: *Itersection from permeability model (NW-SE)*

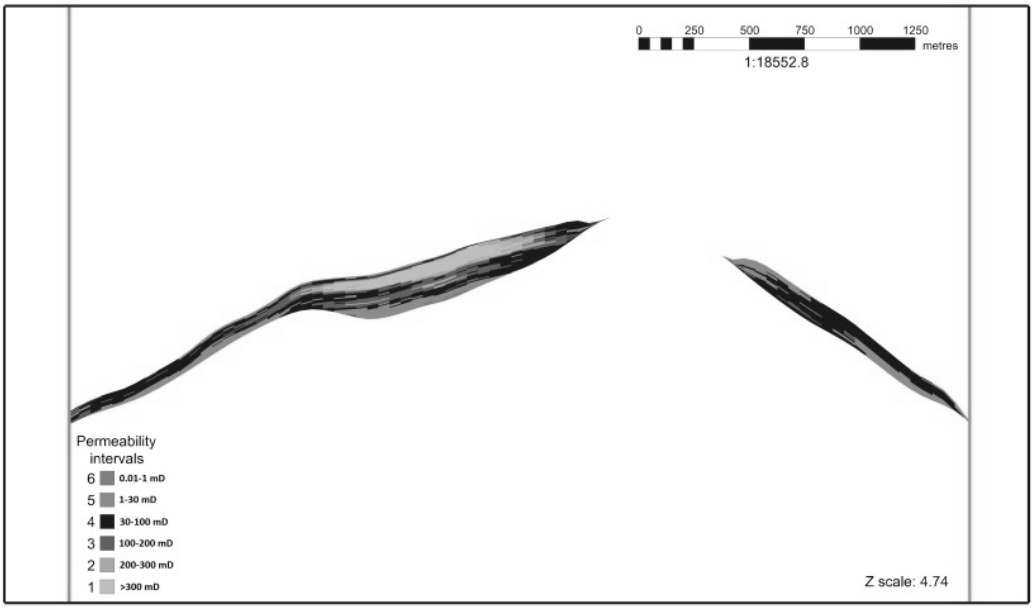

Figure 6: *SW-NE intersection from permeability model*

It is quite evident that the reservoir property is controlled by the basement morphology. The actual structural position definitely has changed for the deposition due to the uplifting but the surface morphology could remain the same. Fault presence was verified neither on 3D seismic nor on well tests. And if we agree this statement we also agree that reservoir the quality is understandable through the present slope conditions.

The assumption was also confirmed by the Heff*HPor and Heff*HPerm maps. (**Figure 7**)

High values on the thickness weighted permeability and porosity maps were most likely to concentrate to parts with low surface dip. (**Figure 8**)

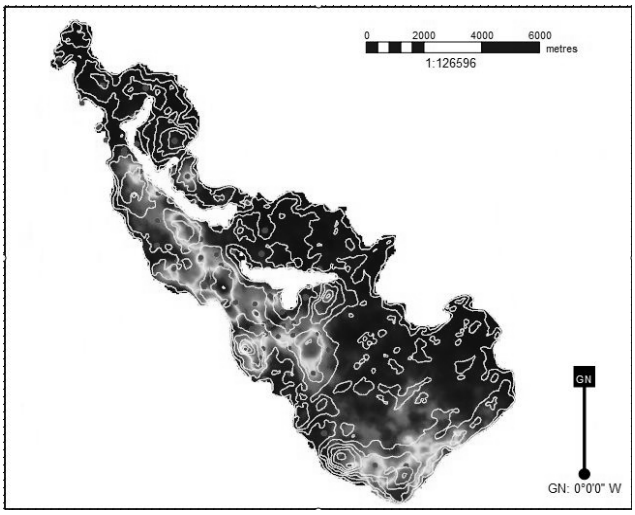

Figure 7: *Heff * HPerm map with thickness contours*

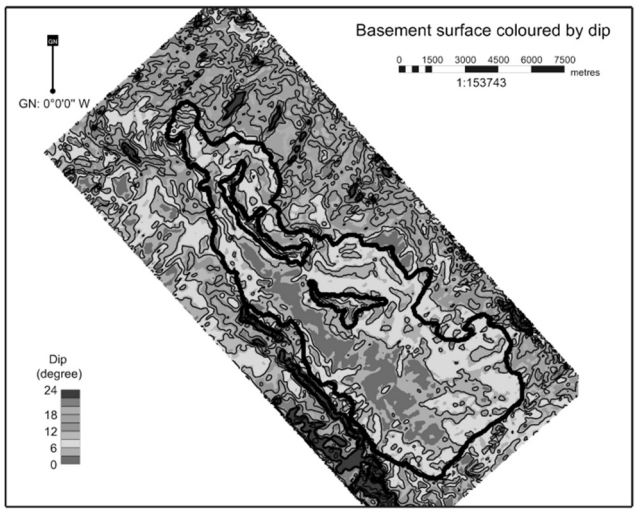

Figure 8: *Basement surface coloured by dip*

4. DISCUSSION AND CONCLUSION

A comprehensive and realistic reservoir model was elaborated. The model consistency could be confirmed by theoretical point of view. The most porous, highest permeable parts represented by elongate shapes corresponding to the wave induced abrasion conglomerates around the structural height. The upper shoreface and lower foreshore which strongly affected by waves sediment tend to be free from suspension and coarse grained sediments deposited. Those sediments are characterized by large initial porosity and permeability and also by the high average pore throat sizes. In normal circumstances the lower shoreface and offshore zones where fine grained sediments subside from suspension and reworked by organisms. The size of transitions between the different shoreline subenvironments tightly depends on the basement relief. (Reading, 1996) This transitions can be traced clearly from the petrophysical models and more pronounced where the dip of the surface decidedly changing. It followed that the occurrence probability of the debris flows increasing from the upper shoreface to the offshore-transition. These approximately linear elements were also noticeable from the results with significantly lower permeabilities.

5. REFERENCES

BÉRZCI, I. (1985): A szénhidrogén prognózis szedimentológiai háttere. Földtani közlöny, Bull. Of the Hungarian Geol. Soc. 105p.

GEIGER, J. (2015): Some applications of Markov-Type sequential Gaussian co-simulations - In Conference Book of 6th Croatian-Hungarian and 17th Hungarian geomathematical congress, "Geomathematics - from theory to practise", Opatija, Croatia, 8 p.

READING, H.G. (1996): Sedimentary environments: Processes, Facies and Stratigraphy - Department of Earth Sciences., University of Oxford, Oxford, 180p.